Environmental and Economic Impacts of Small-Scale Biomass Gasification

A THESIS
SUBMITTED TO THE FACULTY OF
UNIVERSITY OF MINNESOTA
BY

Matthew Ries

IN PARTIAL FULFILLMENT OF THE REQUIREMENTS
FOR THE DEGREE OF
MASTER OF SCIENCE

Dr. William Northrop

June 2017

Acknowledgements

I would like to thank Professor William Northrop and Darrick Zarling for their constant guidance as this project progressed. I would also like to thank undergraduate student Omar Ahmed for his help in running the Power Pallet and other day to day activities. Funding for this project was provided by the Minnesota Environment and Natural Resources Trust Fund as recommended by the Legislative-Citizen-Commission on Minnesota Resources (LCCMR). The Trust Fund is a permanent fund constitutionally established by the citizens of Minnesota to assist in the protection, conservation, preservation, and enhancement of the state's air, water, land, fish, wildlife, and other natural resources.

Abstract

Biomass is one of the most abundant, easily accessible energy resources on the planet. However, much of the world's available biomass is not fully utilized because it is distributed and is often left to rot or burn in open piles. Therefore, this material is not deemed economically worthwhile to transport to a large energy facility. Unused biomass emits large quantities of greenhouse gases and health hazards into the surrounding environment. One potential use for this wasted biomass is small-scale gasification, which can produce heat and electricity while simultaneously reducing harmful pollutants and reduce operating costs compared to commercial plants.

The Power Pallet, a small-scale gasifier-generator system produced by All Power Labs (Berkeley, CA), is designed to produce up to 20kWe of electricity and can be easily transported due to its compact design. The purpose of this research is to quantify emissions factors of CO_2, CO, C_xH_y, NO_x, and PM from the Power Pallet system and compare them to current biomass usage methods. Results indicate that the Power Pallet significantly reduces CO_2 compared to ordinary combustion processes because of the high carbon content stored in the biochar created as a byproduct of the gasification process. CO and PM emissions are also reduced compared to open burning and wood fired stoves due to a more carefully controlled combustion process. The net greenhouse effect of the gasifier was found to be lower than the other methods. However, large-scale biomass plants still emit lower CO, NO_x, and PM emissions than distributed systems like the Power Pallet because of the additional exhaust cleaning technologies found on these plants. Additionally, it became clear over the course of testing that several improvements need to be made to increase efficiency, further reduce emissions, and increase ease of use to help this technology can realistically compete with existing technologies on a widespread scale.

Table of Contents

List of Figures

List of Tables

1 Introduction

While fossil fuels remain the top source of global energy production, greenhouse gas emissions from their combustion are a well-established cause of anthropogenic climate forcing. The Paris Agreement, which was signed by 196 countries in December 2015, aims to curb GHG emissions by 2030 to limit global temperature rise to within 2 °C of preindustrial levels. Because global energy usage will increase as rural areas develop, renewable energy sources including hydro, solar, wind, and biomass must see large growth in the coming decades to make up for the targeted decrease in fossil fuel usage. Of these renewable resources, biomass is perhaps the most divisive in how it should be used. The debate over biomass largely depends on whether biomass is truly carbon neutral, with proponents arguing that harvested biomass' carbon is reabsorbed during new plant regrowth and opponents suggesting that encouraging biomass harvesting can lead to a decrease in diversity and losses in soil carbon content (Cornwall, 2017). The term biomass hereafter refers to plants and trees that can be used as fuel.

It is estimated that there is 100 EJ of sustainable energy available annually from biomass sources worldwide; if this was fully utilized, it would be able to account for up to 30% of global energy usage (Parikka, 2004). While a significant portion of the world's biomass is already utilized in the form of lumber or fuel, there is still a huge portion that is left unused, wasted, or used inefficiently. Even after a region has been logged, there is often a large amount of forest residue leftover (or produced as a waste product) that would not be suitable as lumber and/or is not worthwhile to collect and transport to a large facility. This waste biomass is left to rot, burned in open piles, or used in simple wood burning appliances

like furnaces or boilers. These biomass consumption methods produce undesirable emissions in the form of greenhouse gases like CO_2 and methane, and health hazards like particulates, nitrogen oxides (NO_X), and CO.

Recently, an emerging method of forest residue utilization is to use waste biomass in localized, small-scale gasification systems to produce heat and electricity. Small-scale gasification offers a middle ground between large commercial operations and letting nature take its course. For small-scale gasification to be a viable alternative in the long term, there are a few criteria that must be met. First and foremost, any new energy technology must release fewer harmful emissions than what it will be replacing; this includes both gases that are damaging to the environment and/or are known health hazards. In this case, gasification would directly replace the emissions from open burning, decomposition, or residential use. Second, the system needs to be able to provide all of this at a competitive cost to become widely adopted.

While there has been a significant amount of research regarding the emissions from open burning, decomposition, largescale power generation using biomass, and even primitive cook stoves, there has been very little research to characterize exhaust emissions of gasification systems within the 10-100 kWe scale. The goal of this study is to quantify the primary emissions from these small-scale systems and compare them to waste biomass disposal techniques and large scale power facilities. The Power Pallet, a commercial small-scale (20 kWe) gasification-generator system developed by All Power Labs (Berkeley, CA), was used to conduct this research. In addition to characterizing the emissions from the gasifier-generator system, emissions associated with the supply chain of organized

biomass usage are considered to more fully understand the feedstock's lifecycle when used in such a system.

2 Background

2.1 Overview of Biomass Emissions and Their Processes

Biomass is a crucial component in regulating the global environment. Trees and plants remove gases from the atmosphere (CO_2) and nutrients from the soil (N, K, P) during growth and release them back into the environment during their destruction. The way that biomass is destroyed can have a large effect on the chemical compounds formed and released into the environment. Thus, it is important to understand the emissions from individual biomass destruction processes like decomposition, complete combustion, incomplete combustion, gasification, and any combination of these.

All biomass is primarily made up of four elements: Carbon, Hydrogen, Oxygen, and Nitrogen. The emitted gases must be composed of these as well, and so the composition of the biomass is an important factor. The chemical makeup of several plants often used as fuel is given in Table 1.

Source	Material	C wt %	H wt %	O wt %	N wt %	Ash wt %
(Miles et al, 1995)	Switchgrass	46.68	5.82	37.38	0.77	8.97
(Evans et al, 1988)	Corn stover	46.50	5.81	39.67	0.56	7.35
(Gaur et al, 1998)	Softwood (Douglas Fir)	52.30	6.30	40.50	0.10	0.80
(Feldmann et al, 1988)	Hardwood (Red Oak)	49.34	5.93	41.74	0.07	2.76

Table 1: Composition of several biomass feedstocks on a dry basis

As shown in Table 1, woody biomass has higher carbon and hydrogen contents and much lower ash content. Ash is an umbrella term that includes inorganic elements, most notably

potassium (K), calcium (Ca), sodium (Na) and phosphorus (P). Sulfur is an additional element not shown in Table 1. Though the sulfur content is typically much less than 0.5% in biomass derived fuels, it is a source of sulfur dioxide (SO_2) emissions, which are a component of acid rain. Coal, by comparison, contains a much higher sulfur content; as high as 10% by weight.

Because ash content is low and is minimally reactive, the emissions associated with C, H, O, and N are the most crucial. The most energetically preferential decay reaction for these four elements (C, H, O, N) when exposed to atmospheric oxygen is complete oxidation. The global reaction is given by Equation 1

$$\text{Biomass} + O_2 \rightarrow CO_2 + H_2O + N_2 + \text{Ash} \quad (1)$$

where the carbon in the fuel is converted to CO_2, all the hydrogen to H_2O, and the nitrogen remains inert. If all biomass was completely combusted, it would be a perfectly clean energy source; the CO_2, H_2O, and ash would all be reabsorbed during the growth of new biomass leading to zero net emissions. In actuality, complete combustion is not a valid assumption. Variances in local oxygen levels, temperatures, and elements available can lead to incomplete oxidization, which creates other emissions such as CO, methane, and particulates. Some of these emissions can be harmful both to people and the environment. An overview of these impacts is briefly discussed in Sections 2.1.1-2.1.7 below for the most prevalent emissions. Except for N_2O, these are also the emissions that are measured for the small-scale gasification system in this experiment.

2.1.1 Carbon Dioxide (CO_2)

As mentioned above, carbon dioxide is the product of complete oxidation of carbon present in biomass. There are two primary paths for CO_2 formation: aerobic decomposition (discussed more in Section 2.2.2) and combustion. Assuming clean burning with 100% combustion efficiency, all the carbon present in biomass would be converted to CO_2. In Table 1, it is worth noting that Douglas fir would emit 12.5% more CO_2 than the same mass of corn stover due to their differing carbon contents. Lower combustion efficiency allows carbon to be stored in other compounds such as soot, CO, and CH_4; all products of incomplete oxidation. Because the carbon available in biomass is fixed, lower combustion efficiencies inevitably lead to reductions in CO_2 emissions as well.

In the US, CO_2 accounts for an estimated 81% of the GHG emissions every year and it is the leading GHG emission worldwide (United States EPA, 2016). CO_2 equivalent (or CO_2e) is a standard used for comparing the relative effects of other greenhouse gases compared to CO_2. The weighting of other greenhouse gases is accomplished by assigning each gas a global warming potential (GWP), which is a measure of how large of an impact 1 kg of the selected gas would cause over a 100-year period when compared to 1 kg of CO_2. Because CO_2 is the standard that other gases are compared to, it is defined as having a GWP value of 1.

2.1.2 Carbon Monoxide (CO)

Carbon monoxide is a product of incomplete oxidation, and thus, lower combustion efficiencies lead to higher CO emissions. CO has well established adverse health effects, and is a regulated emission around the world. The recommended standard for CO

concentrations is 9 ppm for ambient air and 25-50 ppm for occupational exposure (Raub, Mathieu-Nolf, Hampson, & Thom, 2000). At nonlethal concentrations, CO can cause headaches, disorientation, fatigue, and vomiting. High concentrations can be lethal, and is the leading cause of death by poisoning worldwide (Raub et al., 2000). In sufficient levels, it reduces the oxygen carrying capacity of the blood by bonding with hemoglobin and it ultimately leads to oxygen deprivation.

While CO is not widely considered a greenhouse gas alone, it does influence overall warming potential. In the atmosphere, CO's lifespan is around one month, as it is eventually oxidized into CO_2, usually through reaction with the hydroxyl (OH) radical (Lashof & Ahuja, 1990). Due to oxidization alone, CO has an effective GWP of at least 1.57, as 1 kg of CO creates 44/28 (the ratio of their molecular weights) kg of CO_2. Additionally, the hydroxyl radical happens to be the primary radical responsible for decomposing methane in the atmosphere which means that CO concentrations reduce the amount of OH available in the atmosphere, leading to less methane destruction and ultimately more CH_4 in the atmosphere. While it is indirect and the actual GWP depends on the environment, the relationship between CO and CH_4 leads to carbon monoxide having an effective GWP of somewhere between 1.57-5 (Lashof & Ahuja, 1990).

2.1.3 Methane (CH_4)

Like CO, methane is a product of incomplete combustion, but is also created during anaerobic decomposition (see Section 2.2.2). CH_4 is a much more potent GHG than CO_2. According to the Intergovernmental Panel on Climate Change (IPCC), methane has a GWP of 25 (IPCC, 2007). In the same EPA estimate discussed earlier, methane is the second

leading greenhouse gas, as it is responsible for 11% of the US' CO_2e emissions each year (United States EPA, 2016). Higher order hydrocarbons (C_2H_6 and higher) are also present in mixtures created by incomplete combustion in lower concentrations, but have effective GWPs between 0.5-5.5 and their combined greenhouse contribution is much less than that of methane (IPCC, 2007).

2.1.4 Nitrous Oxide (N_2O)

Nitrous oxide emissions are caused by both aerobic and anaerobic decomposition, as well as combustion. In decomposition, N_2O is created from either incomplete denitrification of the biomass under anaerobic decomposition or incomplete ammonium oxidation in aerobic conditions and is primarily affected by nitrogen content (Wihersaari, 2005). Agricultural land is the primary natural source of N_2O emissions worldwide because of high nitrogen contents available in fertilized soil.

During combustion, N_2O is an intermediate product that quickly dissociates at high temperatures (> 500 C) (Hayhurst, A.N. and Lawrence, 1992). Because of this temperature dependence, N_2O emissions can be as low as < 1 ppm from combustion sources but will be higher for lower temperature processes. Measurable nitrous oxide has also been observed to be byproduct of systems that use a catalytic converter for NO_x reduction (Hayhurst, A.N. and Lawrence, 1992).

While nitrous oxide is not directly caused by incomplete combustion, it is an indicator due to its temperature dependence; complete combustion results in higher temperatures that lead to less N_2O. In all cases, nitrous oxide only accounts for a small fraction of the original

nitrogen content because much of the nitrogen remains inert in the form of N_2 or remains bound in a solid (Christian et al., 2003; Wihersaari, 2005).

While there is some debate as to whether nitrous oxide can be dangerous for human consumption under repeat exposure to high concentrations, it is still used in medicine as an anesthetic (laughing gas) and high concentrations for low periods of time are considered safe (Weimann, 2003). The primary concern associated with nitrous oxide is that it is one of the more potent greenhouse gases, as it has a GWP of 298 (IPCC, 2007) and is responsible for approximately 6% of US CO_2e emissions (United States EPA, 2016).

2.1.5 Nitrogen Oxides (NO_x)

NO_x emissions include NO and NO_2, and these compounds can form any time oxygen and nitrogen are exposed to high temperatures. Thus, NO_x is almost entirely a function of temperature in air-fueled combustion. NO is created through the extended Zeldovich mechanism reactions, seen below, that rely on oxygen and nitrogen dissociation at high temperatures.

$$N_2 + O \rightarrow NO + N \quad (2)$$

$$N + O_2 \rightarrow NO + O \quad (3)$$

$$N + OH \rightarrow NO + H \quad (4)$$

At standard atmospheric conditions, the nitric oxide (NO) will react with oxygen over time and decay into nitrogen dioxide (NO_2). NO_2 can also react with atmospheric air to create ozone. Nitric oxide is considered safe, but the health effects of NO_2 include nose and throat irritation and an increased risk of respiratory infections; the indirectly increased concentrations of ozone can also lead to lung inflammation (Kampa & Castanas, 2008).

Like CO, NO_x's contribution to the greenhouse effect is indirect. There is no universally accepted GWP value, but it has been linked to reducing CH_4 concentrations and increasing ozone (O_3) concentrations. NO_x emitted near the ground is estimated to have a weakly negative GWP due to more effective methane destruction, but it has been linked to an overall GWP of 100 or more due to ozone creation when emitted at high altitudes from aircraft (IPCC, 2007). As biomass burning occurs near the ground, NO_x concentrations are likely insufficient to have a noticeable climate impact when compared to the other major greenhouse gases: CO_2, CH_4, or N_2O.

One additional environmental concern with NO_x emission is acid rain. A portion of NO_x can become a component in nitric acid (HNO_3) in the atmosphere. Acid rain is a pressing concern because it has been linked to increased nutrient loss from affected ecosystems and has been known to damage man-made structures (Johnson, Turner, & Kelly, 1982). Acid rain is also known to directly impact wildlife, particularly in waterways where the acidity is most concentrated. In the 1970s, acid rain was determined to be a driving factor behind widespread fish kill events when waterways reach the critical acidity of pH less than 4.5 (Likens & Bormann, 1974).

2.1.6 Particulate Matter and Soot

Particulate matter was among the first air pollutants known to be a health threat. While particulate matter can be from a variety of sources, the type emitted from biomass burning is referred to as soot. Soot is a byproduct of incomplete combustion and is composed of particles with a carbon rich core that readily absorbs condensable compounds like tars, sulfates, and nitrates from the surrounding atmosphere. As different size particles affect

the body in different ways, particulates have been sorted into different subsections as shown in Table 2 below. Of these, $PM_{2.5}$ and PM_{10} are the most commonly used standards.

Classification	Particle Size (μm)
Ultrafine	< 0.1
Fine	< 1
Coarse	> 1
$PM_{2.5}$	< 2.5
PM_{10}	< 10

Table 2: Particulate matter classifications (Kampa & Castanas, 2008)

The health effects of soot are typically respiratory system related and are influenced by the particle's size. Carbon nanoparticles are a known carcinogen, and have been linked primarily to lung cancer (Donaldson et al., 2005). Additionally, the carbon core of soot particles readily absorb harmful compounds that are normally filtered out in the lungs and carry them deeper into the body before releasing them (Harrison & Yin, 2000). Small particles, notably those classified as ultrafine, are theorized to penetrate deeper into the respiratory system, and potentially into the circulatory system where particulates can cause irritation and possible infection. In general, it has been estimated that for every 10 $\mu g/m^3$ increase in ambient PM_{10} concentration, daily mortality increases by about 1% (Harrison & Yin, 2000).

Climate impacts from airborne particulates work in both directions. Particles that have low albedo, like those that form clouds, reflect sunlight back into space and cool the atmosphere, while darker particles will exhibit significant absorption of energy and warm the atmosphere. As of 2005, all atmospheric aerosols were estimated to be responsible for

a net -1 to -2 W/m^2 cooling effect compared to +2.4 W/m^2 warming effect from greenhouse gases (Pöschl, 2005). However, the net forcing is likely higher for particulates emitted from biomass sources due to the high black carbon contents. Black carbon has been associated with warming rates of between 0.23 and 0.6 W/m^2 in the arctic, where the albedo of the surroundings is most heavily impacted (Liu, Goodrick, & Heilman, 2014).

2.1.7 Charcoal/Bio-Char

Charcoal is the remaining solid leftover after biomass is combusted. In the case of complete combustion, 100% of the carbon in the biomass would have been converted into CO_2 and only unreacted ash would remain. However, during a gasification process or other source subject to incomplete combustion, there is a carbon/ash mixture remaining that is usually very carbon rich; when created specifically from a gasification process, this byproduct is referred to as biochar.

Charcoal, whether from natural or artificial processes, often ends up in the ground, where it has been found to have effects on the soil chemistry. The most immediate impact of charcoal on the carbon cycle is carbon sequestration. The carbon remaining in charcoal is the most stable, because the highly reactive carbon has already been combusted. Because of this, charcoal is very resilient to decomposition and can therefore effectively sequester carbon from the atmosphere altogether. From a gasification study, it was found that about 97% of the carbon in biochar is not readily bioavailable and can sequester carbon, if undisturbed, for hundreds of years (Wang, Xiong, & Kuzyakov, 2016).

Charcoal is also an ideal lattice for holding nutrients in the soils due to its absorptive properties. Especially in sandy soils, charcoal can absorb nutrients that would normally wash away which leads to more fertile soils. 'Terra Preta' soil, a soil type that was historically used to greatly increase agricultural productivity by native populations in otherwise infertile regions of the Amazon, is a well-documented example of the effects that charcoal amendment can have (Glaser, Haumaier, Guggenberger, & Zech, 2001).

The effect that charcoal has on other greenhouse gas emissions is more complicated. On one hand, charcoal amendment into soils has been shown to reduce naturally occurring N_2O emissions (Harter et al., 2014). Conversely, charcoal laden soils have been linked to increased rates of decomposition for non-charcoal biomass (soil organic matter, or SOM) present in sandy soils, including the increased CH_4 and CO_2 release that goes along with that; in darker soils, mixed results of SOM decomposition have been observed with biochar addition and there is no clear understanding of the exact mechanisms behind this (Wang et al., 2016). What can be inferred is that the changes in CH_4 and CO_2 emissions from the soil are due to changes in the soil chemistry (which lead to changes in the levels of biological activity). Sandy soils become much more fertile after biochar addition and, the increase in decomposition should be offset by increased plant growth in the area in the future. Because of this, biochar amendment can lead to a positive GWP initially (due to an immediate increase in SOM decomposition rates) but will provide a net negative GWP after the system has stabilized (due to N_2O reduction). The GWP is further reduced because of the carbon sequestered directly in the biochar.

2.1.8 Carbon Neutrality Assumption

Biomass is often called a carbon-neutral fuel, but it is important to understand what is needed for this assumption to be valid. Looking at an immediate timescale, biomass' carbon emissions are comparable to that of coal by volume of CO_2 released. The carbon neutral assumption requires that the amount of biomass removed from an area is regrown – this means that it can take up to 50 years from harvest to regrowth for a cycle to be truly carbon neutral (Zanchi, Pena, & Bird, 2011).

When a tree is growing, the carbon stored to fuel that growth is removed from atmospheric CO_2 as a part of the photosynthetic reaction given below.

$$6CO_2 + 12H_2O + light \rightarrow C_6H_{12}O_6\ (glucose) + 6O_2 + 6H_2O \qquad (5)$$

When this tree is ultimately burned for fuel, it re-emits this absorbed CO_2. If fresh trees are not planted to replace those that were removed, then all the carbon that would have been stored as a solid in the tree will remain in the atmosphere, thereby increasing the atmospheric CO_2 concentration.

Additionally, the carbon neutral assumption is more uncertain when additional GHG emissions are considered. Due to their higher GWPs per mass of carbon, methane and carbon monoxide can lead to an increase in overall greenhouse effect if they are emitted in significant concentrations. At the same time, biochar's resistance to decomposition can isolate carbon from re-entering the atmosphere while simultaneously stimulating new plant growth. Whether a biomass system is truly carbon neutral will vary on based on the magnitude of these emissions and the environment they are entering.

2.2 Biomass Usage Paths

To motivate implementation of biomass gasification for small scale electricity production, it is necessary to understand how it compares to other method of biomass usage paths from both an economic and environmental standpoint. Four alternate biomass use paths are discussed in the following sections: open burning, decomposition, residential use, and large-scale use.

2.2.1 Wildfires and Open Burning

Wildfires have been around for hundreds of millions of years wherever carbonaceous biomass is found in sufficient quantity. Recent trends indicate that wildfires, particularly in the northern boreal forests (which contain about 30% of the global forested area), will become more common in the future as temperatures continue to rise (A. L. Westerling, H. G. Hidalgo, D. R. Cayan, 2006; Goode et al., 2000).

Over the past several hundred years, human disturbance has had significant impact on the amount and severity of wildfires. While the magnitude of human disturbance differs around the world, the United States' forestry management practices are a good example of the way these fires have been viewed over the last hundred years. In the early 1900s, wildfires were often allowed to freely burn through a region because there were fewer firefighting resources available and a smaller population to protect. Frequent burns kept the amount of burnable biomass available at any given time low. High burn frequency also meant that a limited amount of biomass had time to regrow before the next fire, which helped keep the severity of wildfires low. The mid-1900s – headed by "Smokey the Bear's" introduction in 1944 – signaled a shift in forestry practices as emerging firefighting technologies led to

wildfires being put out quickly or prevented altogether. Instead of burning off biomass in small chunks frequently, the biomass could accumulate. When a fire goes through these unburned forests, more available fuel leads to a more severe fire.

It has been estimated that although there was only 1/10 as much area burned in the US at the end of the 20th century compared to the beginning, the carbon emissions were as high as 1/3 of the early 20th century's indicating an average of over 3 times higher emission density (Mouillot, Narasimha, Balkanski, Lamarque, & Field, 2006). It is now commonplace to manage the amount of biomass in high risk areas by periodically removing dead, dry biomass from the area to reduce the chances of a major wildfire. The plant matter is often burned in open piles as a cost-effective means of clearing the land without needing to haul the biomass out of the area. Similarly, some farmers use controlled burns to fertilize and clear land prior to planting their crops; this is most common in third world countries that are experiencing rapid deforestation.

The emissions from open burning can vary widely depending on several variables, but of these the most important is moisture content. In wood burning, moisture contents between 20% and 30% have been found to be the most effective at allowing high combustion efficiencies (Simoneit, 2002). Moisture contents that are too high take so much energy to vaporize the water that the heating value is significantly reduced and the combustion can get suppressed. Moisture contents that are too low can burn too quickly and lead to oxygen deficiencies in the immediate vicinity of the burn that cause incomplete combustion. Forests often consist of a mixture, ranging from live biomass (> 40% MC) to long dead

biomass (< 20% MC) and because of this tend to have a significant amount of the incompletely oxidized emissions discussed above.

As opposed to smaller point sources of emissions, it is also important that wildfire emissions can have significant effects across large regions due to the size of the burned area. Plumes of soot and carbon monoxide from large wildfires can be carried long distances by the prevailing weather systems without sufficient dissipation, and can trigger air quality warnings hundreds of miles from the source. For example, Canadian wildfires have been shown to noticeably increase CO concentrations in the southeastern US and particulates from these fires have triggered air quality warnings in Minnesota (Wotawa, 2000).

Below are a selection of emission factors from various literature sources. As expected, the values vary widely depending on the specific fire, in part due to the difficult nature of determining fuel consumed and emissions in an open system. Some report soot concentrations as both $PM_{2.5}$ and PM_{10}, but PM_{10} was used where available as it is a better measurement of total soot and thus a better comparison to the method of soot measurement used in this experiment. Akagi et al. reported several emission factors as both $PM_{2.5}$ and PM_{10}. Their study indicated that $PM_{2.5}$ is responsible for approximately half of the reported PM_{10}. Larger soot particles (2.5-10 micron) are thought to be created from regions of high temperature and low oxygen availability caused by a high intensity flame, while smaller soot particles are created from smoldering (Reid, Koppmann, Eck, & Eleuterio, 2005).

Source	Case	CO_2 (g/kg)	CO (g/kg)	CH_4 (g/kg)	NO_X (g/kg)	PM (g/kg)
(Sinha et al., 2004)	Zambia Woodland	1705	73	1.4	3.5	--
	Zambia Grassland	1759	42	0.5	2.4	--
(Akagi et al., 2011)	Tropical Forest	1643	93	5.07	2.55	18.5_b
	Savanna	1686	63	1.94	3.9	7.17_a
	Crop Residue	1585	102	5.82	3.11	6.26_a
	Pasture Maintenance	1548	135	8.71	0.75	28.9_b
	Boreal Forest	1489	127	5.96	0.9	15.3_a
	Temperate Forest	1637	89	3.92	2.51	12.7_a
	Extratropical Forest	1509	122	5.68	1.12	15_a
(Christian et al., 2003)	African Savanna	1689	71.4	2.17	3.5	--
	Indonesian Fuels	1509	137	7.46	1.17	--
(Aurell, Gullett, & Tabor, 2015)	Grass Burn	1711	78	--	--	17.5_a
	Forest Burn	1654	114.5	--	--	24.5_a
(Liu et al., 2014)	Wildfire	1564.8	120.9	5.9	8.5	16_b
(Yokelson et al., 2011)	Mexico Wildfire	1638	89.66	4.9	3.8	8.9_a
	Average:	1622	97.2	4.6	2.9	15.5

a = reported as $PM_{2.5}$
b = reported as PM_{10}
-- = no data reported

Table 3: Open burning emission factors for a range of conditions

Emission factors reported in Table 3 are not all from the same feedstock used in this experiment; therefore, they are not directly comparable due to differing carbon contents. However, the values still give a good representation of the expected ratios between emissions (such as CO/CO_2 ratio).

Considering the data presented in Table 3 in more detail, grasses tend to burn more completely due to being drier and thus they produce more NO_X and CO_2 while producing less CO and PM emissions. Conversely, wood is better at holding moisture in a natural environment and therefore has higher emissions associated with incomplete combustion (and lower temperatures). Of the emission factors reported in Table 3, the feedstock most closely related to the one used in this experiment is the temperate forest reported by Akagi et al. – despite this, the average values will be used for comparison purposes to include a wider range of studies.

2.2.2 Decomposition

Decomposition has been linked to three primary greenhouse gas emissions: CO_2, CH_4, and N_2O. The rate of production and ratio between these emissions relies on many factors of the biomass including temperature, airflow, surface area, chemical composition, and decay duration. With GWPs of 1, 25, and 298 for CO_2, CH_4, and N_2O respectively, even a small amount of methane or nitrous oxide can lead to a large increase in the overall greenhouse gas effect. Decomposition that only emits CO_2 will be referred to as 'clean decomposition' in the sections that follow.

CO_2 formation occurs in an aerobic environment, and it is the primary emission path of the carbon in the biomass. Generally, CO_2 formation occurs at the surface on biomass heaps, where there is sufficient oxygen present. Increased airflow through the decomposing biomass due to less dense packing or a larger surface-to-volume ratio will increase the amount of aerobic surface area. Anaerobic conditions are more likely to be found towards the middle of bulk storage piles, underwater, or underground.

Methane formation occurs in an anaerobic environment. A fraction of CH_4 produced will also be consumed as it rises towards the surface of the pile where oxygen is present, and converted to CO_2 (Wihersaari, 2005). More densely packed piles will lead to less oxygen permeation and therefore increased CH_4 production. Methane production also occurs in biomass buried in the soil, but is typically released slow enough to be converted to CO_2 by the time it reaches surface. Because of this, methane production from decomposition is most notably a concern in man-made piles of biomass (particularly compost piles) that are not sufficiently aerated.

N_2O can be produced in both aerobic and anaerobic conditions, and is mostly a function of nitrogen content (Wihersaari, 2005). There is no consensus concerning the volume of emissions released from decomposition because it is difficult to measure due to extended time scales and highly variable environmental factors. For heaps of biomass, some studies suggest emissions could be as high as 5% of available carbon emitted as CH_4 (indicating 95% emitted as CO_2) and as much as 2.6% of the nitrogen content emitted as N_2O (Wihersaari, 2005).

Unlike a combustion process, the release of CO_2, CH_4, and N_2O from decomposition occurs over a long period. Wihersaari et al. measured mass losses of between 0.4 and 3.6% each week in a biomass heap over their six-month storage period, and it can take many years for naturally deposited biomass to fully decompose.

Using these assumptions, Table 4 presents the percent contribution to the greenhouse effect of CO2, CH_4 and N_2O from different biomass feedstocks. The compositions of each feedstock are those given earlier in Table 1. The ‘Net Effect’ is the total greenhouse effect

after weighting the emissions by their GWP and is compared to that of clean decomposition (the calculated effect divided by the effect from clean decomposition).

Material	CO_2 (%)	CH_4 (%)	N_2O (%)	Net Effect
Switchgrass	41.4	54.4	4.2	2.30
Corn stover	41.1	54.1	4.7	2.31
Softwood (Douglas Fir)	42.9	56.4	0.7	2.21
Hardwood (Red Oak)	43.0	56.5	0.5	2.21

Table 4: Greenhouse effect contribution from decomposition emissions of a biomass heap consisting of different biomass feedstocks

As shown in Table 4, methane is the most significant greenhouse emission for all cases and N_2O, while the most potent greenhouse gas, has a much smaller impact. Despite the variance in carbon/nitrogen contents of the fuels, the net effect is nearly the same across all feedstocks at 2.2 to 2.3. The data shown apply to a standard biomass heap – fertilized land would likely have a greater N_2O contribution, and evenly distributed, well aerated biomass would be more skewed towards CO_2 emissions than CH_4.

2.2.3 Residential Use

Biomass fired stoves and fireplaces have been a primary source of heat for cooking and staying warm for tens of thousands of years. While many developed countries have switched over to more energy dense fuels such as natural gas, biomass is often used in third world countries and remote locations due to its widespread availability and lack of technological barriers.

Residential use of biomass is an umbrella term; countless devices have been created to harness biomass energy for personal use over the years. Specifically, stoves and furnaces are considered because they are the most common used today. Designs of these devices can vary widely, and similarly lead to different biomass combustion efficiencies and likewise different ratios of related emissions. Residential emissions have not gained widespread attention until the 1900s, yet the emissions from these residential devices are particularly important from a health perspective because of their proximity to people – inside their own home if no smokestack is present.

A comparison of some of the most commonly used technologies is given in Table 5 below. Traditional cook stoves are used in third world countries for cooking, and are responsible for the bulk of residential emissions in those regions. Wood stoves are used for indoor heating all over the world and are still commonplace in both developing and developed countries. Pellet heaters are the most advanced of the three; these tend to include sophisticated air controls and a highly uniform fuel, but require additional fuel processing.

Source	Setup	CO_2 (g/kg)	CO (g/kg)	HC (g/kg)	NO_x (g/kg)	Soot (g/kg)
(Bhattacharya, Albina, & Salam, 2002)	Traditional Cook Stoves (24 variations)	1560-1620	19-136	6-10[a] 6-9[b]	0.05-0.2	--
(Ozgen et al., 2014)[c]	Wood Heaters	--	89-154	5-20[b]	2-2.7	3-10
	Pellet Heaters	--	2-7	0-0.2[b]	1.2-1.4	1.2-2.2

a = Methane
b = Non-methane hydrocarbons (NMHC)
c = Data converted to g/kg dry assuming a heating value of 20 MJ/kg
-- = no data reported

Table 5: Emission factors for traditional cook stoves and wood fired furnaces

For cook stoves with little to no automated controls, emissions have been found to contain noticeably more products of incomplete combustion than open fires (Ballard-Tremeer & Jawurek, 1996). Cast iron wood stoves, even in developed countries, are some of the worst polluters because they restrict airflow by design to create a smoldering fire with low combustion efficiency that is efficient at radiating heat to its surroundings with high heating efficiency. Increasing combustion efficiency versus heating efficiency was not considered important before emissions were a cause for concern.

The emissions from residential biomass burning is especially important in devices where there is no smoke stack, such as a cook stove. A common design for a single pot cook stove is shown below in Figure 1, which uses a batch process with the flame right under the cooking area and ceramic insulation used to channel the heat.

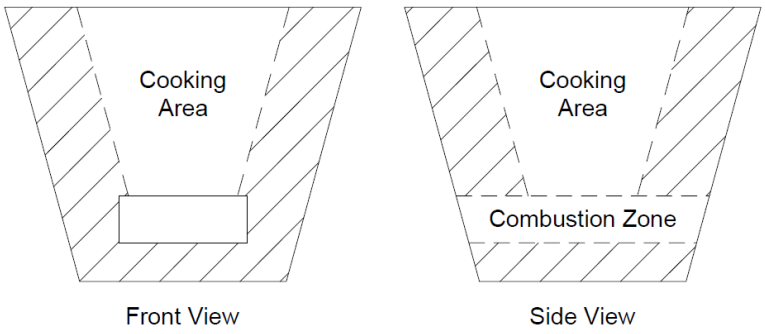

Figure 1: Simple clay cook stove common throughout Asia and Africa

The insulation is efficient at channeling heat into the pot/cooking area, but does not have adequate oxygen supply for consistent, complete combustion when the airways are obstructed. A fire with high combustion efficiency may not be desirable for residential use because the required airflow can carry away the hot gas before it has time to transfer much heat to its surroundings.

Other residential technologies, such as pellet heaters have controls in place for primary and secondary air as well as strict fuel quality control. Better control contributes to the large reductions in incomplete combustion products as reported by Ozgen et al. However, the fuel and technology required for pellet heaters is comparatively expensive and not always readily available, especially in remote locations (those that are likely to use biomass sources for heat in the first place). Furthermore, there are additional emissions associated with pelletizing biomass because of the energy used in machinery required to cut and compress the feedstock.

2.2.4 Large-Scale Power Generation:

In the US, biomass based electricity generation accounted for approximately 1.6% of the total electricity generation in 2016 (EIA, 2017). However, biomass is not being used to its full potential. When alternate energy sources are cheap, the readily available biomass sources like agricultural waste and logging residues from lumber operations are the most economical while it could prove too costly to go and harvest biomass specifically for electricity production.

Steam boiler and fluidized bed systems have historically dominated the large-scale biomass market due to their relatively low capital cost and high reliability. These traditional systems use heat from burning biomass produce steam that can be sent to a turbine, producing work. More than with other fuels, it is also common for biomass plants to recover lost heat. In 2012, 70% of biomass facilities included combined heat and power (CHP), compared to only 28% for natural gas and 5% for coal (Cai, Wang, Elgowainy, & Han, 2012). However, these biomass systems tend to be older due to a boom in their construction during the oil

crisis in the 1980s and, due to their age, tend to be higher emitters of harmful pollutants as well as significantly less efficient than modern natural gas plants.

The construction of integrated gasification combined cycle (IGCC) plants have been increasing in a push to increase efficiency and reduce emissions. An IGCC plant's core operating principles are like the small-scale gasification system studied here (more details on small-scale systems are in Section 2.3), where the feedstock is first gasified to produce a combustible gas. This combustible gas, known as syngas or producer gas, is cleaned up before being burned and run through a gas turbine. The hot exhaust from the gas turbine is then used to generate steam which powers another turbine. Obviously, this type of plant is more complicated (and costly) than a boiler-turbine system, but IGCC thermal efficiencies can be as high as 45% (without CHP), compared to 25-30% for older systems. IGCC plants also tend to have significantly reduced emissions, in part due to better emissions control systems, and in part because there are two points at which the gas stream is cleaned: both before and after the gas turbine. Despite all of this, biomass plants tend to have lower thermal efficiencies than natural gas or coal plants with similar technologies due to the higher moisture contents present in plant matter.

The EPA's AP-42 Fifth Edition Compilation of Air Pollutant Emission Factors reports compiled average emission factors from different biomass power plants that have been in operation for decades. This does not differentiate between feedstocks and the biomass composition will lead to deviation in reported emissions. Because many largescale plants use agricultural byproducts as fuels (which have a low carbon content) rather than woody

biomass, the carbon carrying emissions from this report are an underestimate of what would occur for the woodchips chips used throughout this experiment.

To supplement the EPA's data, emission factors reported in Argonne National Lab's GREET 2016 software were used to determine emissions for a feedstock more closely resembling the woody biomass used in this experiment (50.3% carbon content). Because of this, the GREET factors will be presented for comparison later in the Results/Discussion Section. More information on where these emission factors were derived can be found in Cai et al.

Source	Plant	CO_2 (g/kg)	CO (g/kg)	CH_4 (g/kg)	NO_x (g/kg)	PM (g/kg)
AP-42 Report (EPA, 2010)	All Except FB	1678	5.16	0.34-0.52	1.89-4.21	0.46-4.82
	Fluidized Bed	1678	1.36	0.34-0.52	1.89-4.21	0.46-4.82
GREET 2016 v1.3.0.13107	IGCC Plant (η = 40%)	1843	0.16	0.07	0.17	0.05
	Steam Turbine (η = 22%)	1833	5.82	0.60	1.13	2.57

Table 6: Large-scale power plant emission factors

As shown in Table 6, there is a significant decrease in almost every emission (except CO_2) in the newer IGCC plants. The increase in CO_2 simply indicates more complete combustion, which explains the lower production of CO, CH_4, and PM.

2.2.6 Processing

Emissions also occur during processing required to use biomass as a fuel. While decomposition and open burning require little to no preparation, small-scale and large-scale plants must first collect, chip, and transport biomass before it is useable.

GREET includes estimated emissions factors for preparing biomass for a 150 MW IGCC plant. Emissions factors are shown for different processing activities in Table 7, as described in Han et a1. This estimate includes collection of logging residues from a tree farm, on-site chipping, and transportation in a heavy-duty truck.

Process	CO_2 (g/kg)	CO (mg/kg)	CH_4 (mg/kg)	NOx (mg/kg)	PM (mg/kg)
Collection + On-Site Chipping	13.4	47	25.8	96.4	7.4
Transportation (per 100 miles)	40.2	36.2	44	97	1.6

Table 7: Emissions factors from biomass processing for use in an IGCC plant

As seen in Table 7, the emissions associated with collection, chipping, and transportation are small when compared to the total emissions from primary usage but not entirely insignificant. These emissions will be included in a simple lifecycle analysis model to be discussed in the results section.

2.3 Small-Scale Gasification:

Gasification is the process of heating a carbon rich material, referred to as feedstock, to high temperatures with little to no additional oxygen present. This leads to partial oxidation of the feedstock to produce large concentrations of carbon monoxide and hydrogen gases often referred to as syngas or producer gas.

2.3.1 Gasification History

Gasification as a technology is hundreds of years old. Jan van Helmont is credited with first discovering gasification in 1609 when he observed coal released gas when heated. In 1792, William Murdock was the first to commercialize gasification by heating coal in a low oxygen environment to create town gas. Town gas was first used for street lighting and industrial purposes in 1798 and eventually became the dominant source of lighting in London by 1816 (Miller, 2005). However, the discovery of natural gas reserves caused gasification to become largely obsolete as fuel prices plummeted. It wasn't until the mid-20th century that there was a resurgence in gasification interest due to the fuel shortages during World War II. During the height of the war, there were as many as 900,000 wood-fueled vehicles utilizing gasification (Rajvanshi, 1986). Similarly, the worldwide fuel shortages of the 1970's prompted the rest of the world to begin searching for alternatives to fossil fuels due to the limited nature of their supply. Since then, gasification has become an option as a simple, readily accessible method of reducing greenhouse gas emissions from heat and power generation and as a renewable source of liquid fuels through pyrolysis.

2.3.2 Gasification Basics

There are five steps to gasification: drying, pyrolysis, combustion, tar cracking, and reduction. The first step in the gasification process is drying. Before other processes can begin, the moisture stored inside the feedstock must be boiled off. Because of water's high latent heat of vaporization, higher moisture feedstocks will contain less energy per unit mass than comparatively drier feedstock. Higher moisture content feedstocks have been shown to reduce the rate of feedstock consumption and in turn the power output of the

system (Sheth & Babu, 2009). If initial moisture contents are too high (> 40 wt. % dry basis), then the gasification process may be unable to sustainably provide enough energy (without external input) to evaporate all the water and the whole process will be quenched.

The second step is pyrolysis. In pyrolysis, the feedstock becomes hot enough that it is broken up into three products: solid bio-char, condensable tars, and gaseous fuels. All plant based biomass is composed of a combination of lignin, cellulose, and hemicellulose; for woody biomass, this is approximately 23-33 wt. %, 40-50 wt. %, and 25-35 wt. % on a dry basis respectively (Mohan, Pittman, & Steele, 2006). Each of these components will be affected differently by pyrolysis. The bulk of the cellulose decomposition occurs in the narrow temperature range of 250-360 °C, hemicellulose decomposition occurs between 200-280 °C, and lignin gasification occurs slowly over the whole temperature range 200-900 °C. Both cellulose and hemicellulose gasification are efficient at converting carbon to gaseous compounds, and lignin is responsible for much of the bio-char production (Pasangulapati et al., 2012). Cellulose has also been shown to be responsible for the highest fraction of tar (higher order, condensable hydrocarbons) production from pyrolysis (Collard & Blin, 2014). The desired byproducts of pyrolysis can determine which feedstocks will work best. For example, in liquid biofuel production, it is helpful to have high cellulose and low lignin contents and in bio-char production it is best to have high lignin content.

The bulk of gaseous compounds created during pyrolysis include CO, CO_2, H_2O, H_2, CH_4, and various tars. Small-scale gasification systems like the one being used in this experiment use IC engines; these engines are not designed to handle the condensation of tars, as they

can cause the pistons to stick and/or deteriorate the seals. In these systems, tars need to be broken down to make the gas more suitable for use in an IC engine.

Downstream processes in gasification consist of combustion and tar cracking. Drying, pyrolysis, tar cracking, and reduction stages of gasification all require available energy to proceed at reasonable rates. While heat can be delivered in other ways, the simplest (and by far the most common) technique is to combust a portion of the remaining charcoal. This is achieved by allowing a small amount of an oxidizer (usually air, but steam or pure oxygen have also been used) into the combustion zone, at which point the exothermic reaction described below begins.

$$C_{charcoal} + O_2 \rightarrow CO_2 + 393.5\, kJ\ heat\ released \quad (6)$$

Ignoring intermediate reactions, tars also react with oxygen in a similar manner, albeit with varying levels of heat release.

$$Tars + O_2 \rightarrow CO_2 + H_2O + heat\ release \quad (7)$$

While combustion is complete oxidation of the charcoal and tars, tar cracking refers to those tars that are only partially reacted. In the presence of low oxygen and high temperatures, tars begin to break down into smaller hydrocarbons and ultimately CH_4, CO, and H_2 rather than the full reaction's products of CO_2 and H_2O. The temperatures in the combustion and tar cracking region are typically between 800 and 1300 °C depending on the system's design and feedstock.

The fifth and final step of gasification is reduction. This is where the CO_2 and H_2O created in the combustion and drying stages are reacted with remaining carbon in the charcoal to form higher concentrations of CO and H_2 gases. This is a primarily endothermic region and the three most prominent reduction reactions are listed below.

$$C + CO_2 + heat \Leftrightarrow 2CO \quad (8)$$

$$C + H_2O + heat \Leftrightarrow CO + H_2 \quad (9)$$

$$CO + H_2O + heat \Leftrightarrow CO_2 + H_2 \quad (10)$$

These are equilibrium reactions and the dominant reactions going from left to right each require heat, so the temperature in this region will drop. At normal operating temperatures for this region (650 °C-800 °C), these reactions favor high CO and H_2 concentrations.

2.3.3 Gasifier Types

While the gasification processes remain the same for all cases, there are many different approaches to gasifier design. Updraft, downdraft, and fluidized beds are the three most common; each of these are briefly discussed below.

Updraft:

Updraft gasifiers are the oldest gasification technology, being both simple and robust. The feedstock enters through the top of the chamber and flows down, while the oxidizer and producer gas flow up, as seen in Figure 2.

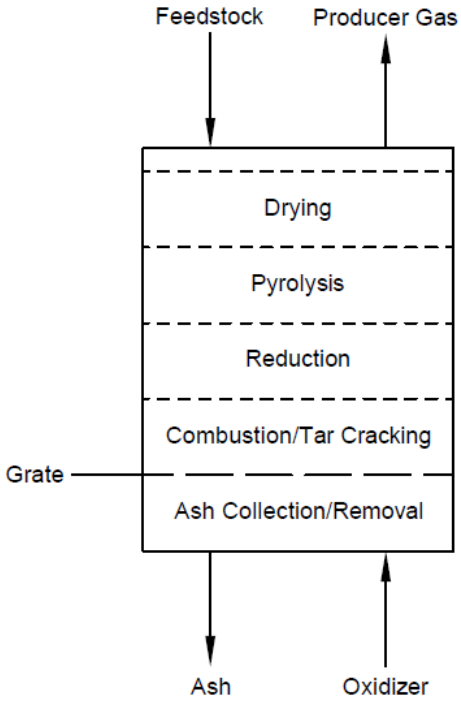

Figure 2: Updraft gasifier flow diagram

Updraft gasifiers have distinct regions where the processes discussed in Section 2.3.2 occur, starting with combustion where oxygen is available and the heat is largely dissipated upwards along with the producer gas.

The low exit temperature and long residence time of the feedstock allows for high thermal efficiency using this design. However, because some of the feedstock is affected by pyrolysis at the top of the chamber where there is not enough heat present for efficient tar cracking, updraft gasifiers have been associated with a large amount of tar production. If this producer gas were to be used in an engine or turbine, extensive gas cleanup would be required. These high tar concentrations are one of the primary barriers that have kept gasification from becoming more common (Bridgwater, 1995).

Downdraft:

Downdraft gasifiers are currently the most common design for the type of small-scale gasifier used in this experiment because they retain much of the simplicity of the updraft designs while producing significantly reduced tar concentrations in the producer gas. The feedstock enters through the top of the chamber and flows down, while the oxidizer is injected in middle. A flow diagram of a downdraft gasifier is shown in Figure 3.

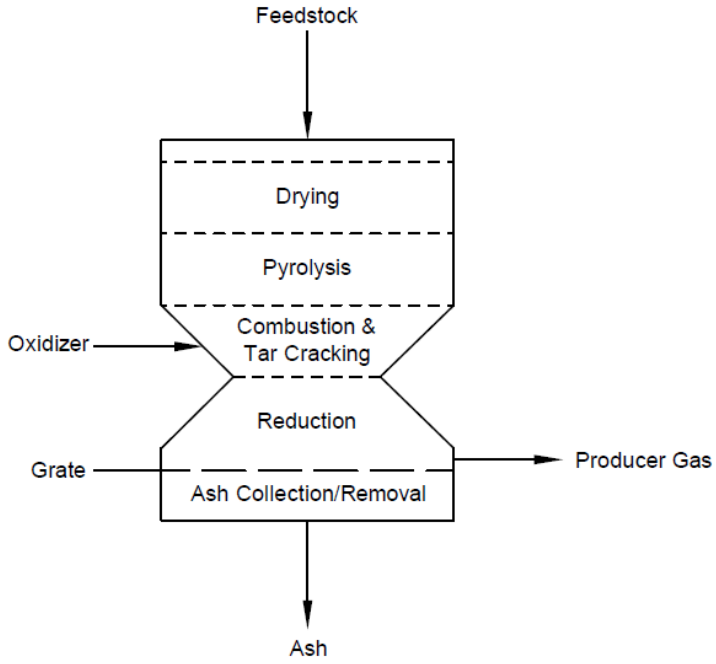

Figure 3: Downdraft gasifier flow diagram

Like updraft gasifiers, downdraft gasifiers have distinct regions where the five processes occur. In these gasifiers, combustion occurs in the middle of the chamber and the heat disperses in both directions. In an Imbert style downdraft gasifier like the one shown in Figure 3, a restriction is added to increase temperatures in the reduction region to allow for

the reduction reactions to proceed more quickly; this restriction is not required, but it is generally accepted to improve producer gas quality.

Tar formation in downdraft gasifiers is low because the pyrolysis stage is completed before the high temperatures in the combustion stage. The combustion region occurs first in the gas flow of an updraft gasifier allowing for more efficient tar cracking. One downside of the downdraft design is that heat from combustion is dissipated more than in updraft gasifiers. Further, downdraft gasifiers are more susceptible to moisture content in the feedstock and are not as robust as updraft reactors during operation (Bridgwater, 1995). Additionally, high producer gas temperatures at the exit carry more sensible enthalpy that, if not recaptured, is lost to the environment, thus lowering thermal efficiency.

Fluidized Bed:

There are a wide range of fluidized bed gasifier designs, but they all operate under the same general principles. Feedstock is injected into the side of the gasification chamber while the oxidizer flows up. The feedstock (and accompanying ash) are suspended by the oxidizer's upward flow to form a sort of bed suspended off the base, while producer gas leaves through the top of the chamber. The five processes discussed earlier all occur simultaneously near the floating bed, and once the feedstock is exhausted the ash becomes light enough to be carried away with the gas stream. In some cases, a portion of the ash that is removed along with the producer gas can be filtered out and reinjected to ensure complete gasification. A fluidized bed gasifier flow diagram is shown in Figure 4.

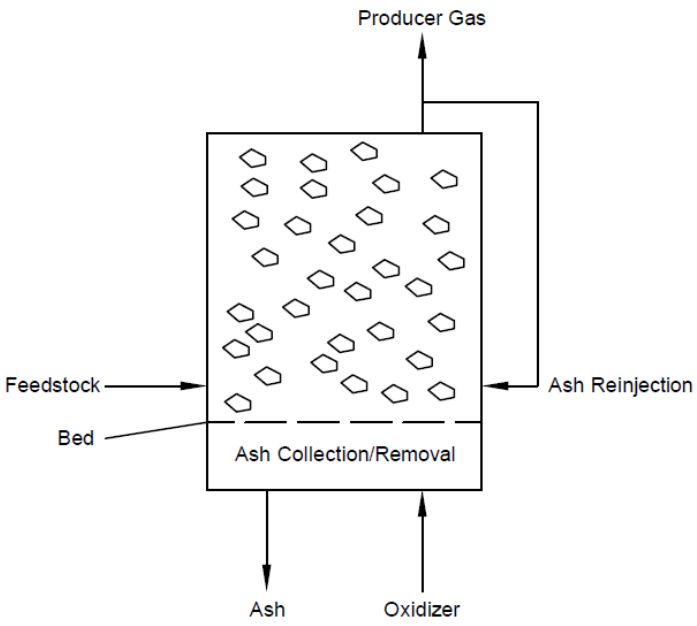

Figure 4: Fluidized bed gasifier flow diagram

Fluidized beds are most often used for large scale power plants because they can be scaled up easily while still producing much lower tar concentrations than updraft gasifiers and simultaneously maintaining high thermal efficiencies (Bridgwater, 1995).

2.3.4 Gasification Products

Producer Gas:

The resulting gas leaving the gasifier is known as producer gas. Producer gas generally has high concentrations of CO and H_2 and these are the two main combustible gases created from the process. The exact concentrations of combustible gases rely heavily on the oxidizer used for the combustion stage. In almost all cases (including the gasification system studied here), the oxidizer is atmospheric air. Some large-scale gasification systems will instead use steam or oxygen as the oxidizer, resulting in much higher H_2 and CO concentrations and increased efficiency due to the lack of nitrogen dilution; however, this

is more expensive and adds additional complication. For a downdraft gasifier like the one being studied, typical gas compositions are shown in Table 8.

Oxidizer	Gas Composition (vol. % dry basis)					HHV (MJ/m^3)
	H2	CO	CO_2	CH_4	N_2	
Air	17	21	13	1	48	5.7
Oxygen	32	48	15	2	3	10.4

Table 8: Typical downdraft gasifier producer gas concentrations (Bridgwater, 1995)

Despite the designing to minimize these, there will still be some amount of tars and soot present in the producer gas. A qualitative overview of the tar and soot creation based on the technologies discussed above is provided below in Table 9.

	Tars	Particulates	Efficiency
Updraft	Very high	Moderate	High
Downdraft	Very low	Moderate	Low
Fluidized Bed	Low	High	High

Table 9: Tar, particulate, and scaling factors for different gasifier types

Downdraft reactors are often considered the best balance between low tars and low particulates while still maintaining a simple construction for small-scale systems. However, they cannot easily be scaled up to meet high power requirements and are not used for systems above 1 MW (Bridgwater, 1995). Updraft reactors require extensive tar treatment systems that can prove costly and require increased maintenance costs. Fluidized beds are best suited for largescale production because they have high efficiency and low tar production, but are less suited at operating below full capacity.

Even with an ideal gasifier design, the tars and particulates carried by the producer gas are often too high for an IC engine or turbine downstream to handle. Maximum allowable tar and soot present in the gas for IC engines are shown below.

	Unit	IC Engine	Turbine
Particulates	mg/Nm^3	< 50	< 30
Particle Size	μm	< 10	< 5
Tars	mg/Nm^3	< 100	

Table 10: Acceptable tar and particulate levels for use in an IC engine (Milne & Evans, 1998)

Filtration is necessary, and is often done cheaply and effectively using a packed bed filter. In largescale systems, it is more common to use an electrostatic precipitator and/or a catalyst that promotes condensation. These tar removal techniques have been found to be capable of removing upwards of 95% of tars present in producer gas (Milne & Evans, 1998).

However, not all biomass plants require an engine or a turbine. Some biomass plants, such as pyrolysis plants, target high tar levels so that they can be condensed to produce bio-oil for use as renewable gasoline or diesel replacements (ethanol and biodiesel respectively). Because this project focuses on gasification to create combustible gases, pyrolysis plants will not be discussed in further detail here.

Biochar:

Biochar is the other major byproduct of gasification. The only difference between biochar and regular charcoal is the high carbon contents present (which can exceed 70% carbon content by weight, depending on the process used – similar in carbon content to coal). The

carbon remaining is difficult to gasify, so it is often a waste product of the gasification cycle, but biochar can still be used as a fuel for combustion, soil amendment, or carbon sequestration vessel as described in Section 2.1.7.

3 Materials/Methods

3.1 Power Pallet Overview

The gasifier used in this experiment is a part of a commercially available system known as the Power Pallet. The Power Pallet is a 20 kWe integrated gasifier-generator system created by All Power Labs (APL) in Berkeley, CA. A flow diagram of the system is shown in Figure 5.

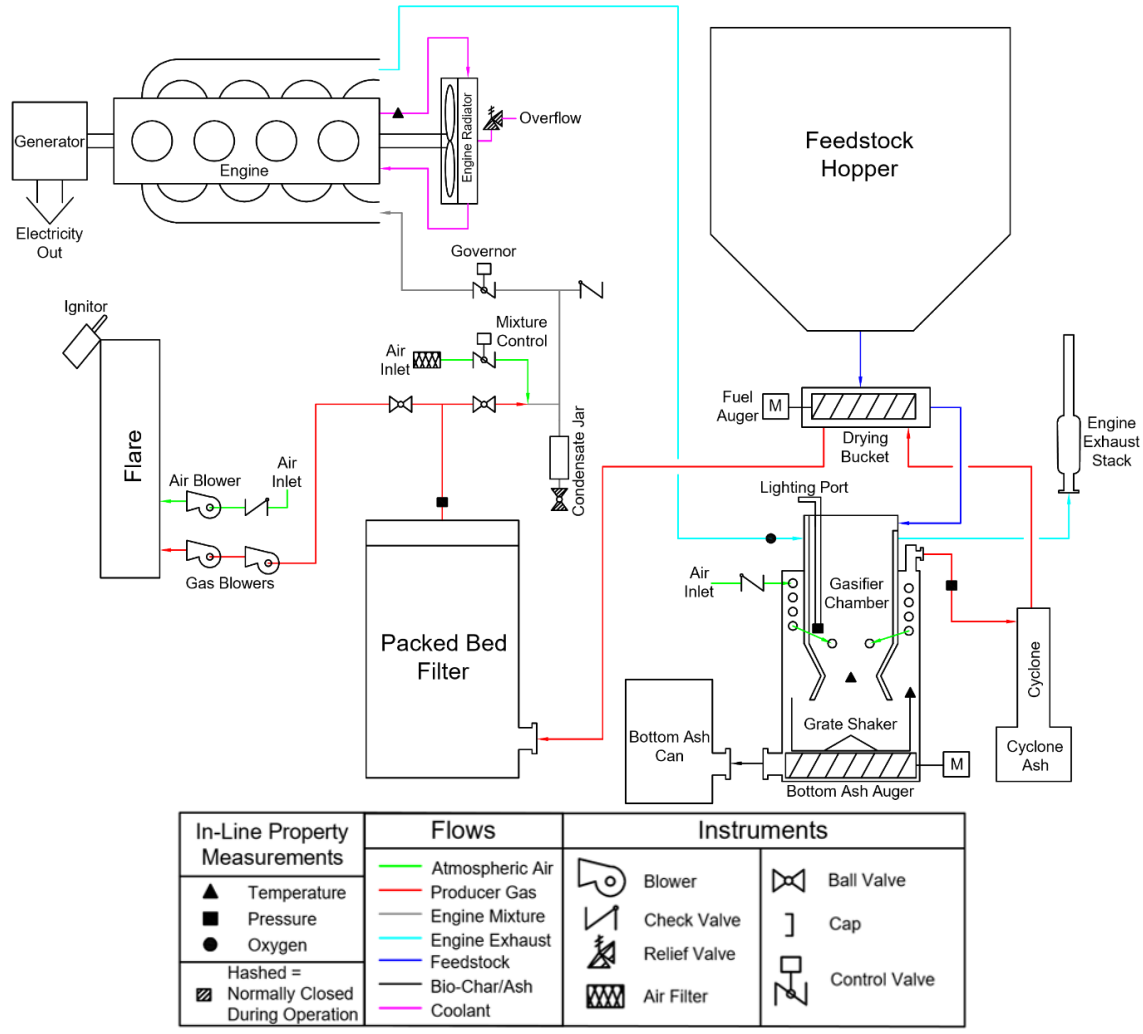

Figure 5: 20 kW Power Pallet flow diagram prior to modification

3.1.1 Gasifier Overview

The Power Pallet system uses an Imbert downdraft style reactor that is operated under a slight vacuum. Feedstock is pushed into the top of the reactor by a feed auger controlled by a level switch. The oxidizing agent is atmospheric air, which is inducted through tubes that are wrapped around the outside of the gasification chamber but inside of the producer gas sheath. This air is preheated by the producer gas before entering at the top of the restriction. The grate shaker is operated periodically to remove biochar, which is pushed into an ash bucket by a second auger to allow room for fresh feedstock.

The producer gas leaving the gasification chamber first goes through a cyclone to remove most the particulates. The hot gas is then sent through another heat exchanger at the bottom of the hopper to help dry feedstock entering the top of the gasifier. After the drying bucket heat exchanger, the producer gas is sent through a packed bed filter (composed of a combination of bio-char and feedstock) to drop out tars and any remaining particulates. After filtration, the producer gas is ready to be sent to either the flare (during the initial start-up period) where it is burned off or the engine (during normal operation) where it is used to produce power.

The engine on the Power Pallet is a GM Vortec 3.0L 4 cycle natural gas engine modified to accept producer gas as a fuel with a fixed spark timing of 42 degrees before TDC and engine speed of 1800 RPM. The engine is attached to a MeccAlte NPE32 E/4 12-wire 4-Pole generator. The fuel-air ratio in the engine is targeted at $\lambda = 1.05$ based on a predefined producer gas concentration estimate created by APL and controlled by feedback from an oxygen sensor on the exhaust.

3.1.2 Producer Gas Quality Control

The producer gas leaving the gasifier chamber requires some quality control to ensure it is suitable for an engine and has low emissions when it is burned. The three main areas of concern include the start-up period, soot, and tars.

Startup:

Because the entire system starts at room temperature, an external heat source, such as a propane torch, is required to get the reactions started. While the temperatures in the reactor begin to rise, the producer gas is routed to the flare and blower assembly. The gas blowers produce a vacuum that pulls atmospheric air in through the tubes wrapped around the reactor, which in turn is the oxidizing agent for the necessary combustion reactions. Once the combustion process has begun, the temperatures will begin to rise until the standard operating temperatures of ~700-800 °C at the restriction are reached, at which point the producer gas should be of sufficient quality to ignite in the engine. The startup period typically takes 10-15 minutes.

Filtration:

The soot and tars carried by the producer gas out of the reaction chamber are undesirable due to the environmental and operational concerns discussed earlier, and these both need to be filtered out. The Power Pallet uses a two-step filtration process consisting of the cyclone and the packed bed filter.

The cyclone is the primary soot reduction mechanism and it is the first component after the reaction chamber. It uses centripetal forces to separate heavy particles from the gas stream by requiring the producer gas to take a winding path through it. While this is sufficient to drop out the bulk of particulates, there will inevitably be some remaining further downstream.

The packed bed filter is the primary tar reduction mechanism and is composed of charcoal/biochar and feedstock as shown in Figure 6.

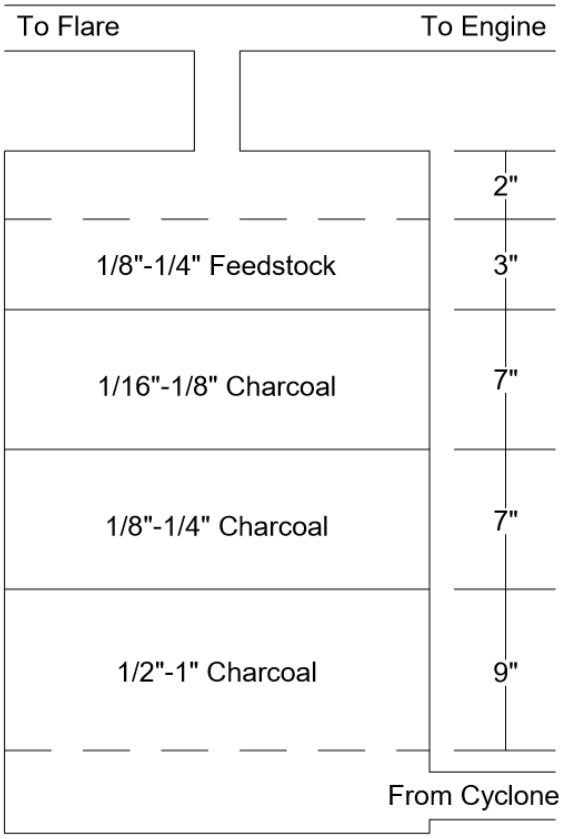

Figure 6: Power Pallet's packed bed filter with bed material specifications as recommended by APL

Like in the soil amendment scenarios discussed earlier, charcoal is an ideal bed material because it easily absorbs tars entrained in the producer gas flow. Because of the tortuous path traversed by the gas stream through the filter, further reduction in soot is achieved through impaction. An earlier iteration of this filter design was shown to collect as much as 99% of tars from the producer gas (Hamilton, 2013).

3.1.3 Power Pallet Modifications

The Power Pallet is a commercial product, not a device designed for research. Therefore, some modifications were required to allow for the desired data collection. These modifications involved adding additional temperature and pressure sensors, flow meters, access ports, and a NO_x sensor. Each of these modifications will be discussed in more depth in Section 3.3. The modified flow diagram is shown in Figure 7.

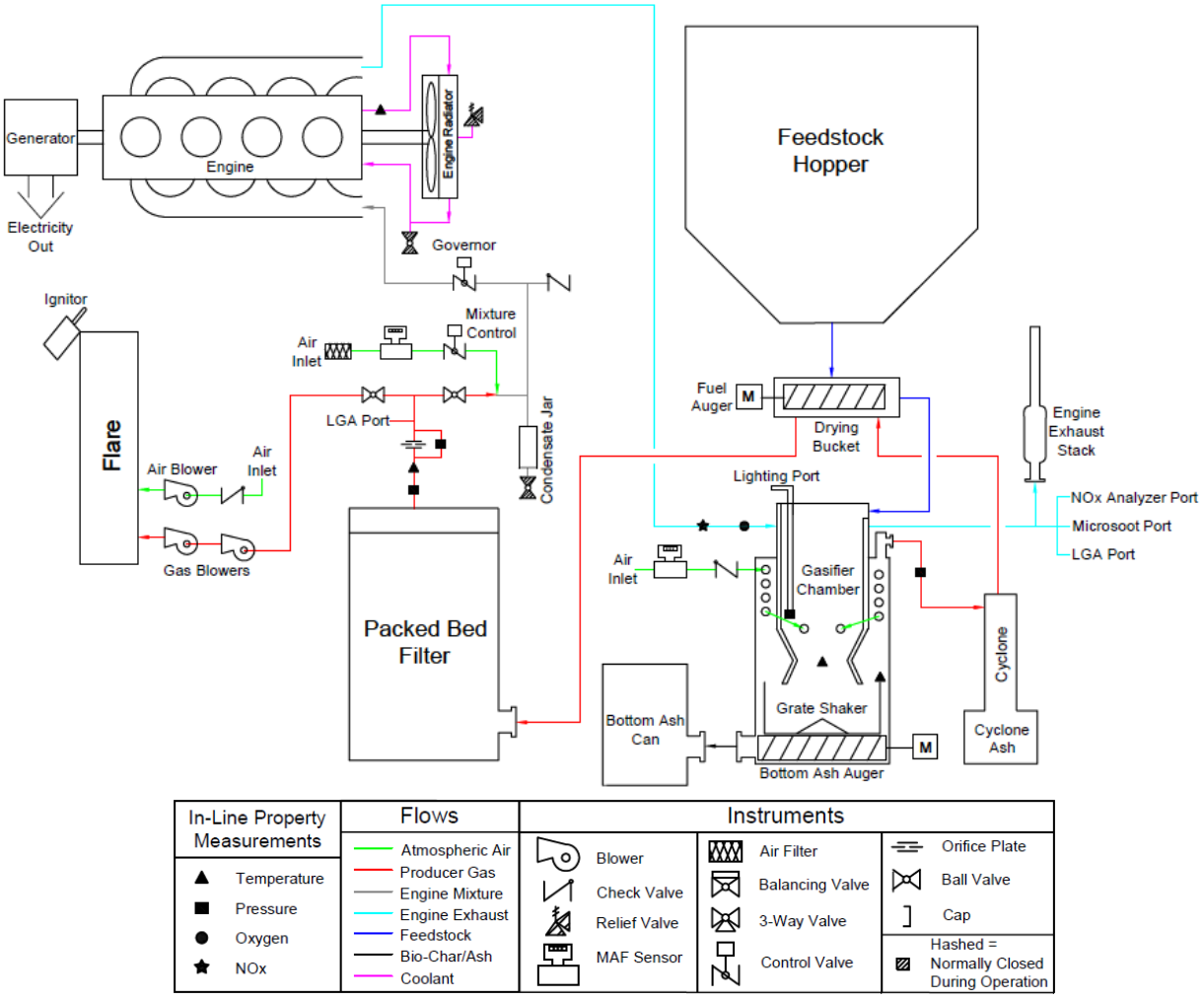

Figure 7: Power Pallet flow diagram including modifications made for the experimental study

3.2 Feedstock Requirements

Feedstock properties are very important for consistent and efficient operation of the Power Pallet. Moisture content, density, and chip size can all cause issues in the gasifier if outside of the recommended ranges. APL's feedstock requirements are shown in Table 11.

Ideal Chip Size	0.5”-1.5” (1 cm - 4 cm)
Moisture Content (% dry basis)	< 30%
Ash Content	< 5%

Table 11: Recommended feedstock properties for use in the Power Pallet

Feedstock that is too small contains a large fraction of fine particles that can clog the packed bed filter. Feedstock that is too large can cause bridging across the hopper and reactor which interrupts feedstock flow. Additionally, high moisture content in the feedstock slows reactions because it takes significant energy to evaporate which lowers the temperatures in the reactor. High ash content fuels can be damaging to the gasifier due to high levels of corrosive compounds that can be created when at high temperatures.

Feedstocks that have previously been successfully tested in the Power Pallet include coconut shells, hardwood chips, softwood chips, walnut shells, and corn cobs. For this experiment, locally collected mixed woodchips were used.

Prior to each run, an aggregate sample of feedstock was taken from several places inside the hopper, mixed together and tested for moisture content. The moisture content was measured by weighing the sample beforehand and then placing it in an oven at 105 °C for 24 hours, at which point the sample was weighed again. The moisture content calculation used is given in Equation 11.

$$MC\ (\%\ dry\ basis) = \frac{Wet\ Weight - Dry\ Weight}{Dry\ Weight} * 100 \qquad (11)$$

This moisture content calculation was used as a guideline, but a real-time moisture content calculation (based on feedstock and producer gas hydrogen concentrations) was used as well because there was significant moisture content variability throughout the feedstock. This real-time moisture correction is described in detail in the Results section, and the relevant MATLAB code is included in Appendix B.3.

3.3 Instrumentation System

3.3.1 Laser Gas Analyzer

The main instrument used for real-time emissions data was the Laser Gas Analyzer (LGA), an instrument created by Atmospheric Recovery Inc (ARI). This analyzer uses Raman spectroscopy to differentiate between gases. Raman spectroscopy relies on the fact that when a light of a specific wavelength (laser) is shined upon a certain compound, the light will be absorbed and re-emitted at a different wavelength. Each compound measured will have a different, discrete wavelength that it emits and the intensity of this discrete wavelength is directly related to the amount of the compound present (ARI, 2017).

The LGA can measure the concentration of up to 8 gases at once due to 8 different detector modules, each conditioned for a different wavelength. In this application, O_2, H_2, CO, CO_2, N_2, H_2O, NO_2, and C_xH_y were the 8 select gases measured. C_xH_y is calibrated for methane, but the LGA cannot accurately differentiate between specific hydrocarbons. Because the most common hydrocarbon is known to be methane from other peer-reviewed gasification studies, the C_xH_y reading is treated as entirely methane when doing calculations.

The sample run through the LGA was not a raw gas sample. To protect the instrument from excessive condensation, the gas was first run through a chiller that was set at 33 °F. This

dropped out much of the water vapor present in the sample, so what enters the LGA is a dry sample (with only about 1-2% water vapor remaining by volume).

The LGA pulled a sample flow rate of around 300 mL/min for all tests that used this device. The flow rate was controlled using an internal pump, an external pump, a needle valve, and a bypass line. This sampling system can be seen in Figure 8, with only the external components being shown.

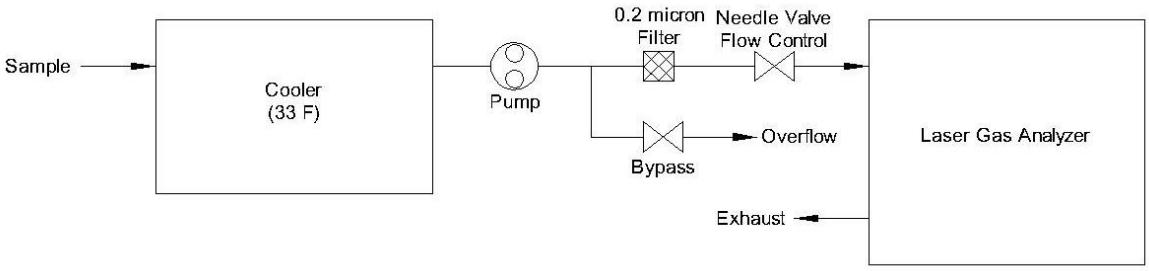

Figure 8: External components of the laser gas analyzer sampling system

Both pumps were used to regulate pressure, but the external pump had to be added as an assist to the internal pump. In both instances, leak free positive displacement pumps were used to ensure the sample was kept isolated. The needle valves were used to restrict the flow rate going into the LGA and the bypass line was added to ensure the sample did not have excessive pressure when entering the LGA and as a secondary path for the flow to go through in the case that the LGA was isolated. Just before entering the LGA, the sample went through an ARI 0.2-micron filter to ensure particulates did not foul the device.

LGA samples were taken right after the filter or just before the engine exhaust stack as was detailed in Figure 7 earlier. Data was collected and recorded on the LGA's computer at a rate of 1 Hz.

3.3.2 Micro Soot Sensor

Particle measurements were collected in real-time using the Micro Soot Sensor (MSS) produced by AVL. This sensor relies on a photoacoustic effect present when "black" particles, or those with strong light absorption, are quickly heated and cooled by a modulated laser. The expansion and contraction of the particle sends out pressure waves, which can be picked up by a sensitive microphone. The magnitude of this photoacoustic effect is correlated to the mass of black particles. As a result, this method is able to measure total soot in the exhaust, but cannot differentiate between different particle sizes (AVL, 2009).

As with the LGA, the MSS is not designed to deal with condensation while inside the measurement chamber. A chiller could not be used because the sample needs a direct line from the exhaust to the MSS to minimize particle deposition. Instead, a dilution system and bypass branch were used to increase the dew point and increase the flow through the device, respectively. AVL provides a conditioning unit used for sample dilution, but the one provided was not functioning at the time of this experiment; an external system was created instead.

The dilution system used atmospheric air pulled through a particulate filter as the diluting gas. To achieve adjustable sample to air dilution ratios on the order of 1:5, the flow needed to be adjustable accordingly. A needle valve was placed on the air inlet to adjust the diluting flow, and an orifice was placed in the line of the gas sample to ensure the gas sample flow was several times lower than the incoming air. An orifice was used here rather than a valve to minimize particle deposition. To determine flowrates, two TSI 41221 mass flowmeters

were used; one on the air inlet and one on the total flow after the sample passed through the MSS. The difference between the two flows was assumed to be the gas flow. The MSS also has two built in flowmeters for the sample flow (differential pressure flowmeter) and bypass flow (variable area flowmeter).

The bypass system is a part of the MSS itself, and is adjusted using two needle valves. The flowrate through the sensor and the bypass were each kept at around 1.9 L/min for a total flow of 3.8 L/min of diluted sample. The vacuum required to drive this flow was provided by a pump placed after the exit of the MSS, and a makeup air valve was used to ensure the pump provided a consistent suction of 4.25 psig at the MSS exit. A diagram of the whole MSS sampling system is shown below in Figure 9.

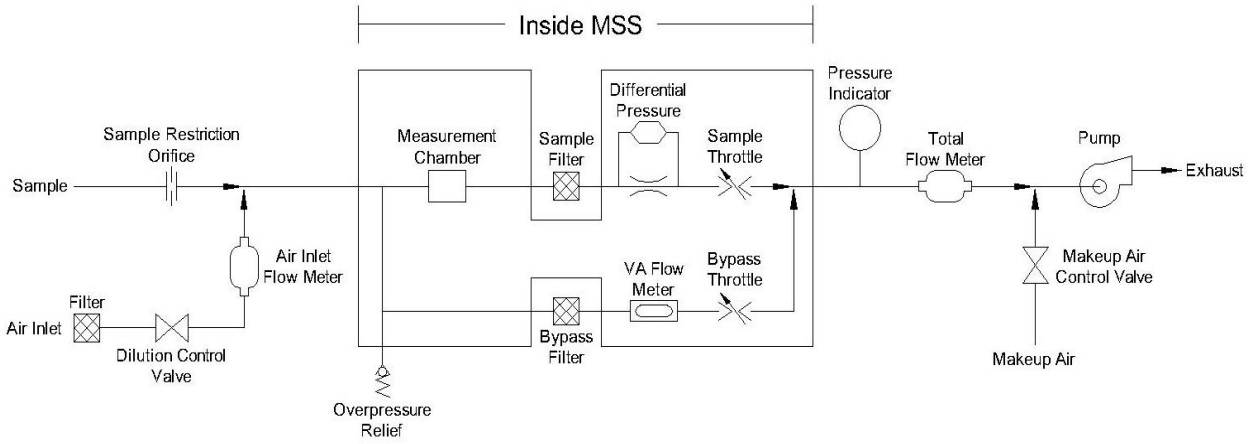

Figure 9: Micro soot sensor sampling system

The MSS features six analog outputs; the output of interest was the undiluted concentration reading because the dilution system used was external and thus not accounted for in the MSS readings. The undiluted concentration reading was combined with the readings from the two external flowmeters at a rate of 1 Hz using a cRIO-9012 controlled system described in Section 3.3.4.

3.3.3 NO_x Analyzer

Nitrogen oxides (NO_x) was one of the primary emissions of interest from the gasification system. While the LGA did record NO_2 concentrations (in % on a volume basis), the precision was not sufficient at such low concentrations. To replace this, a 600 Series CLD NO_x analyzer made by California Analytical Instruments (CAI) was used to determine more accurate values of NO and NO_2. The CAI analyzer uses the chemiluminescent reaction when NO and ozone (O_3) react to create NO_2, O_2, and light. The intensity of the light emitted from the NO reaction is directly proportional to the creation rate of NO_2 in the chamber. To determine total NO_x, the sample is first treated so the NO_2 is converted into NO and then the same chemiluminescent reaction described previously is used; this time, it measures total NO_x. The analyzer switches between NO and NO_x measurement periodically and uses the difference between the NO and NO_x measurements to give NO and NO_2 concentrations (CAI, 2017).

It was necessary to ensure the sample remained heated to reduce condensation and preserve NO/NO_2 ratio on its way to the NO_x analyzer. To accomplish this, a heated line was used and held at 90 °C and the path from the sample port to the NO_x analyzer was kept short (at less than 4 feet). Any other exposed tube/fittings were wrapped in insulation. To protect the analyzer from being fouled by particles, the sample was run through a heated bayonet filter. The sampling system of the NO_x analyzer is pictured below in Figure 10.

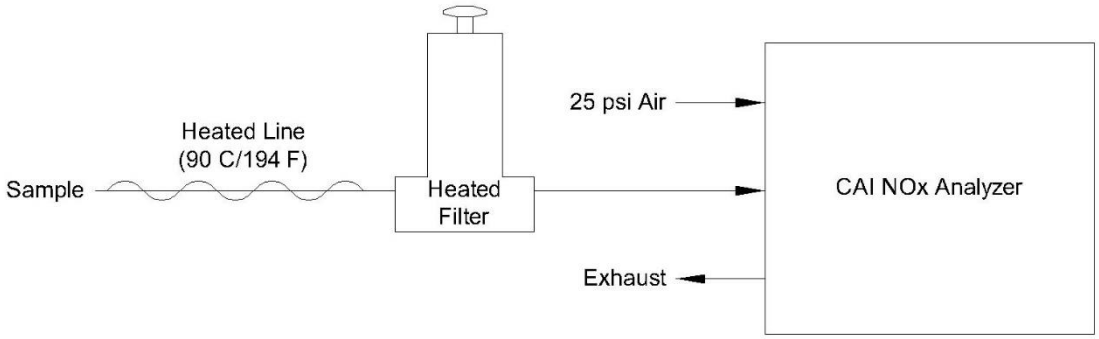

Figure 10: External components of the CAI NOx analyzer sampling system

The readings for NO and NO_2 were recorded using the NO_x analyzer's analog outputs at a rate of 1 Hz to sync with the rest of the data using the cRIO-9012 system. However, the NO_x analyzer outputs data at 1/10 Hz. Thus, the analog output would read the same value for 10 seconds before outputting a new reading. This does not affect the actual average readings, but can be seen later when comparing the NO_x analyzer to a more typical automotive NO_x sensor.

3.3.4 cRIO Controlled System

The LGA, MSS, and NO_x analyzer all read samples of gas flow either immediately after the filter or on the engine exhaust as seen in the P&ID in Figure 7. To know how the rest of the gasifier is operating, a cRIO data collection system was used. This system consisted of a ruggedized cRIO-9012 with an 8-slot chassis, a NI 9853 dual port CAN module, a NI 9209 analog input module, a NI 9211 thermocouple module, a raspberry pi 3, and an interface with the Power Pallet's Atmel ATmega1280 control board. The purpose of each component will be discussed below.

NI 9853 CAN module:

The CAN module can support up to two CAN devices, although only one port was used in this experiment. The NI 9853 module was used to communicate with a NI 9755 NO_x sensor, a standard automotive NO_x sensor like the ones used in cars all over the world; it measures total NO_x in ppm and O_2 in percent volume and this model is specifically configured to interface easily with LabVIEW. This NO_x sensor was used to provide additional data to the CAI NO_x analyzer's and as a means of comparing the performance of the two.

NI 9209 analog input module:

The NI 9209 analog input module can read up to 32 analog inputs or 16 differential analog inputs from 0-10 V. The analog input module was used for two flow rate readings, one differential pressure reading, one power reading and five differential analog inputs (3 from the MSS system and 2 from the CAI NO_x analyzer).

A differential pressure reading was taken across the orifice positioned after the packed bed filter using an Omega PX653-10D5V differential pressure transmitter to determine the flow through the gasifier at this location.

The two flow rate readings both used Green Motion hot-wire MAF sensors (an aftermarket component for a 1994 Ford Aspire) to determine airflow. One of these was placed on the air inlet into the gasification chamber, and the other was used to track additional airflow into the engine.

An analog output Load Controls model UPC adjustable capacity power sensor was used to track the power output from the Power Pallet.

The five differential analog readings were taken of the NO_x analyzer's NO and NO_2 outputs, the MSS' undiluted soot reading, and the two TSI flowmeters used for the MSS' dilution system.

NI 9211 thermocouple module:

The NI 9211 thermocouple module is a 24-bit device capable of measuring analog inputs from up to four J, K, T, E, N, B, R, or S type thermocouples at once. It was used to collect various temperature readings that were not collected through the Power Pallet's own control board. This included an ambient temperature measurement and a temperature measurement just upstream of the orifice plate. All other necessary temperatures were already being recorded on the Power Pallet's on-board Atmel ATmega1280.

Atmel ATmega1280 and Raspberry Pi 3:

The Atmel ATmega1280 is used to control all the timings and alarms present on the Power Pallet, as well as collect basic operating data. One way this data can be accessed is through a 1 Hz output USB serial string, which consists of a total of 32 readings including temperature, pressure, and current state data. Because the cRIO-9012 cannot directly interface with a USB serial output, a Raspberry Pi 3 was used to convert the USB serial stream into an RS-232 format. This RS-232 data was connected to the cRIO's onboard serial port.

cRIO-9012:

The cRIO system and all its components were powered by the same 12 V battery as the rest of the Power Pallet, and as such the system did not require external power to run. The one exception to this is the power sensor which required a small supply of 120 VAC. The cRIO was set to collect data from the serial port and all three of the modules at a frequency of 1 Hz, as that is what the preconfigured APL system output at. This data was stored locally on a USB drive.

3.4 Calibration Procedures

3.4.1 LGA

All 8 gases were calibrated by ARI shortly before starting data collection. As an additional step to ensure accurate measurements, calibrations were carried out for the several gases before each run. A warmup period of at a half hour was required for the device to get up to operating conditions, and then a zero-calibration using a 99.999% Helium mixture was performed. O_2, N_2, and CH_4 were also calibrated prior to each run using compressed air and a 10% CH4/90% Ar mixture respectively. Over the course of testing, gas concentrations of H_2, CO and CO_2 remained consistent from day to day indicating minimal calibration drift in other measurements.

3.4.2 NO_x analyzer/Sensor

The NO_x analyzer required one hour of warmup time, and was calibrated prior to each run with a 953.9 PPM NO and balance N_2 mixture. It also required a continuous supply of 25 psi compressed air throughout operation to react with the sample and purge the test cell when necessary.

A one-time calibration was also carried out to check linearity on both the CAI NO_x analyzer and the NI NO_x sensor. This was done using the same 953.9 PPM NO mixture used daily, but diluted with nitrogen using a SGD-A10 Automated Gas Divider. This allowed the same calibration gas to be diluted with additional N_2 to form 10 mixtures in 10% increments of the original. The comparison between these two devices is discussed more in Section 4.1 and the calibration graph is included in Appendix A.3.

3.4.3 Flowmeters

Both MAF flowmeters and the orifice plate were calibrated on site using a system consisting of a 2" 50MW20 Laminar Flow Element and a 2110P smart pressure gauge with a DN0020 sensor. The MAF flowmeters were calibrated under suction using room temperature air, a blower and throttled by a three-way ball valve as shown in Figure 11 below.

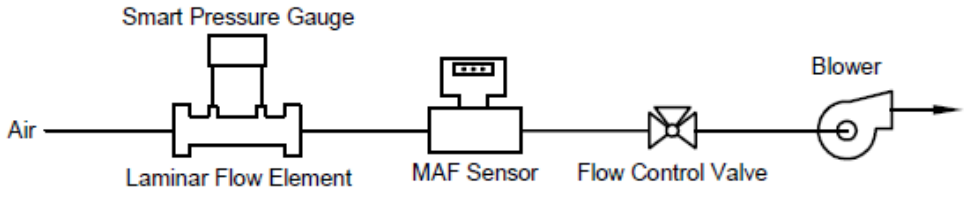

Figure 11: MAF flowmeter calibration setup for atmospheric air

Because both MAF sensors responded similarly, the same calibration curve was used for both. However, the calibration curve was split into low flow and high flow sections to ensure a better fit because the MAF sensors did not response linearly, particularly at low flows. The operating principle of MAF type flowmeters already includes density corrections due to different temperatures, as less dense gas will also transfer less heat

thereby requiring less voltage to maintain a constant temperature and thus no density correction was applied to the calibration. The calibration curve used for the MAF sensors is in Appendix A.2 and the low flow and high flow fits are given in Equation 12 and 13 respectively. V is the measured voltage.

$$Low\ Flow\ Rate\ (kg/hr) = \ 15.775\,V^2 + 3.1299\,V \tag{12}$$

$$High\ Flow\ Rate\ (kg/hr) = \ 38.097\,V^2 - 14.436\,V + 2.8358 \tag{13}$$

The orifice plate was also calibrated using room temperature air, but it had to be calibrated in the orientation that it would be used to get accurate conditions. The calibration setup used is shown in Figure 12. The calibration curve for the orifice plate can be found in Appendix A.1.

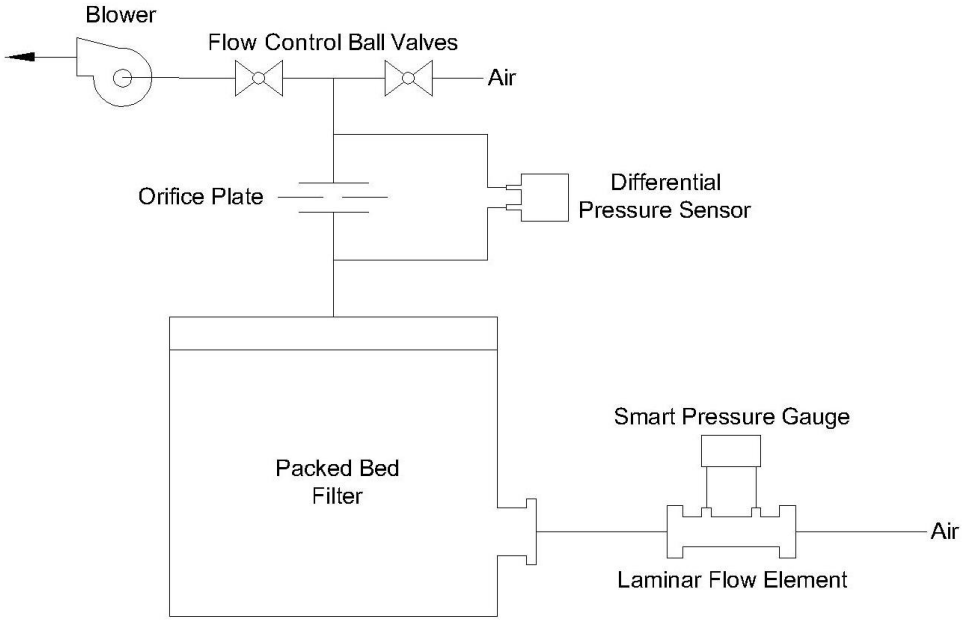

Figure 12: Orifice plate calibration setup

With orifice plates, density also plays a factor in the calibration curve as seen in Equation 14 where ρ is the density and ΔP is the pressure drop.

$$Flow \propto \sqrt{\rho * \Delta P} \quad (14)$$

The final calibration equation for the orifice is given in Equation 15. In this case, density is in kg/m^3 and pressure drop is in kPa.

$$Flow\ Rate\ (kg/hr) = 28.675 \sqrt{\rho * \Delta P} - 0.3869 \quad (15)$$

3.5 Test Plan

While transient emissions are present, especially during startup, the focus in this experiment was to determine steady state emissions because this is where a similar system would likely spend most of its time. Further, steady state testing allows for consistency between testing runs. During the experiments, the gasifier's generator was kept off-grid and was instead wired to accept up to five 208 V, 16 A heaters that acted as the electrical load. This way, the power output of the power pallet could be easily controlled by adding or removing heaters. The four power outputs measured were at 1, 2, 3, and 4 heaters (3.4, 6.8, 10.2 and 13.6 kW respectively) because the gasifier was observed to be unstable at no load (0 kW) and very high loads (15+ kW).

Daily Test Plan:

When the gasifier was first started, it ran on one heater for an extended period so that the gasifier chamber and engine block reached steady operating temperatures. Depending on factors such as moisture content in the fuel, this could take a varying amount of time, but was usually around 30 minutes. Once steady conditions were reached, data collection began.

At each load, data was collected for 30 minutes. During this time, the NO_x analyzer, NO_x sensor, and flow meters collected data continuously. The only instrument that was not constantly collecting data over this period was the LGA because it was used to measure both producer gas and exhaust concentrations. The LGA was instead placed on the producer gas port for 15 minutes (5 minutes for readings to stabilize, 10 minutes of steady state data) and then switched to the exhaust gas port for another 15 minutes.

After data for both producer gas and exhaust gas was completed for a load, then another heater was added. Whenever an additional heater was added, the system was allowed 15 minutes to stabilize and then the 30-minute data collection process was repeated. A full sweep including the 1, 2, 3, and 4 heater states was done each day for three days.

3.6 Data Analysis

The raw data were processed to account for things that the instruments themselves could not. Data processing was done using a series of MATLAB programs that can be found in Appendix B. In all data analysis done, standard deviations throughout the course of running were treated as the primary source of error and these errors were propagated through all calculations.

Water Content Correction:

Two of the major corrections necessary were the water content and density corrections when converting the LGA measurements into emission factors. The cooler in the line to the LGA led to incorrect water vapor readings in the sample gas that could not be ignored

without significantly affecting the results. The average LGA, orifice, and MAF readings at each load were combined to give more accurate measurements.

To account for the actual water content in the producer gas, a nitrogen balance on the incoming pyrolysis air and the measured concentrations in the producer gas was carried out. The amount of nitrogen brought in through the pyrolysis air port was known because the mass fraction of nitrogen present in the air is essentially fixed (varying only slightly day to day with humidity) and the MAF sensor readings did not require any sort of correction. The expected amount of nitrogen was calculated assuming nitrogen content of 75.5% in incoming air and 0.5% in feedstock on a mass basis, as seen in Equation 16.

$$Expected\ Nitrogen = 0.755 * Air\ in + 0.005 * (Orifice\ Flow - Air\ In) \qquad (16)$$

The orifice flow rate was then calculated using the average molecular weight from the LGA concentrations, which was combined with pressure and temperature readings for density and pressure drop. The LGA measurements were then converted to mass fractions (with C_xH_y treated as CH_4 as shown in Appendix B.5) and multiplied by the flow through the orifice to get the actual flow of nitrogen.

$$Actual\ Nitrogen = Nitrogen\ Mass\ Fraction * Orifice\ Flow \qquad (17)$$

Because the LGA sample did not contain water vapor, the nitrogen concentrations were inevitably measured as higher than they should be; this lead to the 'actual nitrogen' calculation being higher than the 'expected nitrogen' calculation. Comparing the actual and expected calculations resulted in the weight factor given in Equation 18.

$$Weight\ Factor = \frac{Expected\ Nitrogen}{Actual\ Nitrogen} \quad (18)$$

This weight factor was applied to all the LGA mass fractions, which would lead to a total mass fraction of something less than 1. The missing mass fraction was then assumed to be water content that was dropped out (so the water vapor fraction became 1 minus the weight factor).

This then became an iterative process because these newly weighted LGA concentrations and the added water vapor concentration changed the density, which in turn changed the calculated flow rate through the orifice and changed the ratio of actual vs expected nitrogen. This process was repeated until the calculated flow through the orifice stopped changing (with a tolerance of 0.0001 kg/hr). The code for this correction is in Appendix B.2.

A similar procedure was employed for the exhaust water content corrections, but based on the orifice flow and engine air measurements instead of the orifice flow and pyrolysis air measurements. However, the orifice flow rate and concentrations are known from the first calculation, so there is no more density dependence on the exhaust and thus this procedure was not iterative.

Feedstock Moisture:

The calculated water content was also used as a means of finding the real-time moisture content and the average moisture content at each generator load to compare to the measured bulk moisture content and see if any moisture related correlations could be found. This was

done by calculating the total flow of hydrogen through the orifice plate based on the corrected LGA measurements and comparing it to an assumed hydrogen mass content in dry feedstock. The actual mass percent of hydrogen was not measured for this feedstock specifically, but hydrogen content varies by very little regardless of the type of biomass (see Table 1); for woodchips, the hydrogen content is about 6% on a dry mass basis. The discrepancy between the dry biomass hydrogen and actual hydrogen was assumed to be moisture content. The code for this calculation is in Appendix B.3.

Ash Production:

Ash into the cyclone and bottom ash can were not measured in real time, but the total mass of ash created each day throughout each run was tracked by weighing the total amount produced. This total ash production was compared to the cumulative flows measured throughout the entire operation and used to calculate an average fraction of feedstock converted to ash. The ash production was treated as proportional to the flow rate only, although this is an oversimplification as it is likely that more ash would be created at low temperature conditions. There is also some tar accumulation that occurs in the packed bed filter itself; this tar accumulation was assumed to be insignificant compared to the total mass flow and was not tracked.

3.7 Life Cycle Modeling

A simple life cycle analysis model was created to further explore the impacts of different methods of biomass use. An illustration of the life cycle of biomass is shown in Figure 13. Resources required for growing the biomass are not included, as they are assumed to be the same across all forms of usage and thus not helpful for direct comparisons.

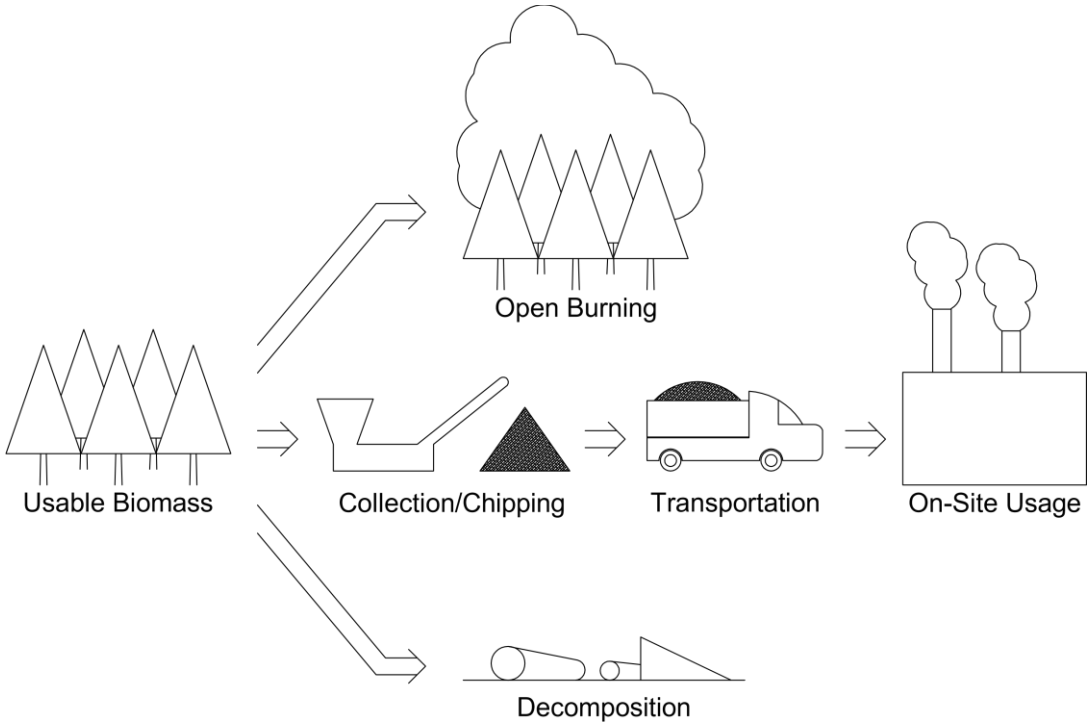

Figure 13: Simple lifecycle models of primary biomass usage pathways

As seen in Figure 13, there are three main paths for biomass to take. Even without human intervention, the biomass would either decay naturally or get consumed in a forest fire. This model considered six different possible life cycles, as described in Table 12 below. Residential usage preparation emissions are neglected because it is assumed that fuel is found locally and hand processed leading to minimal emissions. The main difference between small-scale and large-scale usage with regards to preparation are the sizes of the collection areas.

Collection/Chipping	Transportation	Usage Path
None	None	Open Burning
None	None	Decomposition
None	None	Residential Usage
Yes	10 miles	Power Pallet
Yes	100 miles	Boiler/Turbine
Yes	100 miles	IGCC Plant

Table 12: Life cycle model parameters considered when comparing the environmental impact of each method of biomass utilization

The emissions factors used in the model are those discussed earlier in Sections 2.2.5 and 2.2.6. General plant thermal efficiencies were 22% for the biomass boiler and 45% for the IGCC turbine to match those used in the GREET study that the associated emission factors are pulled from.

4 Results/Discussion

4.1 Power Pallet Emissions

Producer Gas Quality Considerations:

Before average emissions factors are presented, it is helpful to look at emissions measured over time to explain phenomena observed throughout the experiments. Figure 14 below shows one day of data collection from the LGA. The distinction between the producer gas and exhaust gas measurements is clear: high CO, H_2, and C_xH_y indicates it is a producer gas measurement and high CO_2 indicates an exhaust measurement.

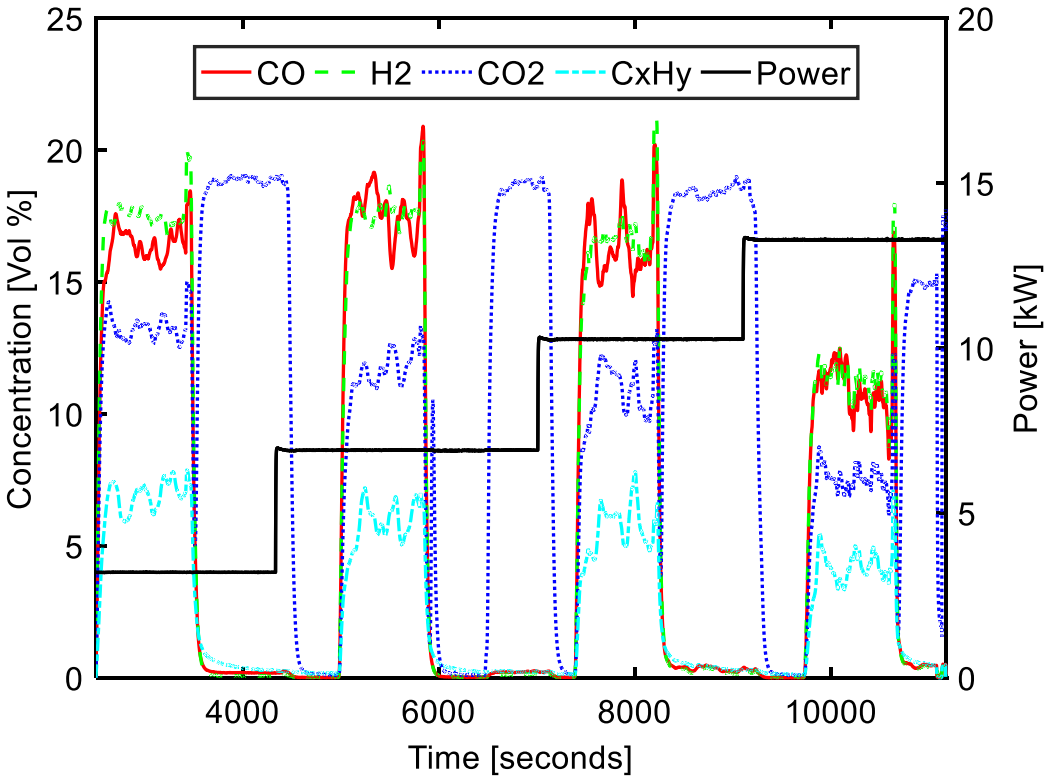

Figure 14: Real-time LGA concentration measurements for one full sweep of electrical loads

Hereafter, producer gas measurements where CO and H_2 are both above 15% will be referred to as high quality producer gas. If either concentration is less than 15%, the gas is referred to as low quality producer gas. Low quality producer gas, such as at load 4 in Figure 14, was observed to occur at either high load, when the reactor had trouble keeping up with the engine's demanded flow rate and at high moisture contents, when the reactor struggled to maintain high enough temperatures to sustain gasification reactions.

Producer gas quality also has a significant impact on the performance of the engine. High quality producer gas is more energy dense and will combust hotter and more completely (provided there is plentiful oxygen) than its lower quality counterpart. This relationship

between producer gas quality and engine performance indicates that lower quality producer gas results in higher concentrations of unburned hydrocarbons.

Emission Factors:

Emissions of CO_2, CO, hydrocarbons, NO_x, and soot were the primary emissions tracked in this experiment. For all the emission factor figures in this section, the data was averaged over the three days of data collection. Each figure reports the emission factors in two forms: mass of emission per mass of dry biomass consumed and mass of emission per kWh of electricity produced.

Some data points, particularly the emissions on a per dry feedstock basis, have large error bars associated with them. These large error bars are due to the reliance on calculated moisture contents – while the moisture contents are likely not far off from the actual values, the calculated errors associated with them became large due to the normal standard deviation of each component being carried through the complex calculations described in Section 3.6. To help make plots easier to read, emissions on a per kWh basis were visually shifted 0.25 kW to the right to avoid overlap with the corresponding per dry mass values, but they are taken at the same loads.

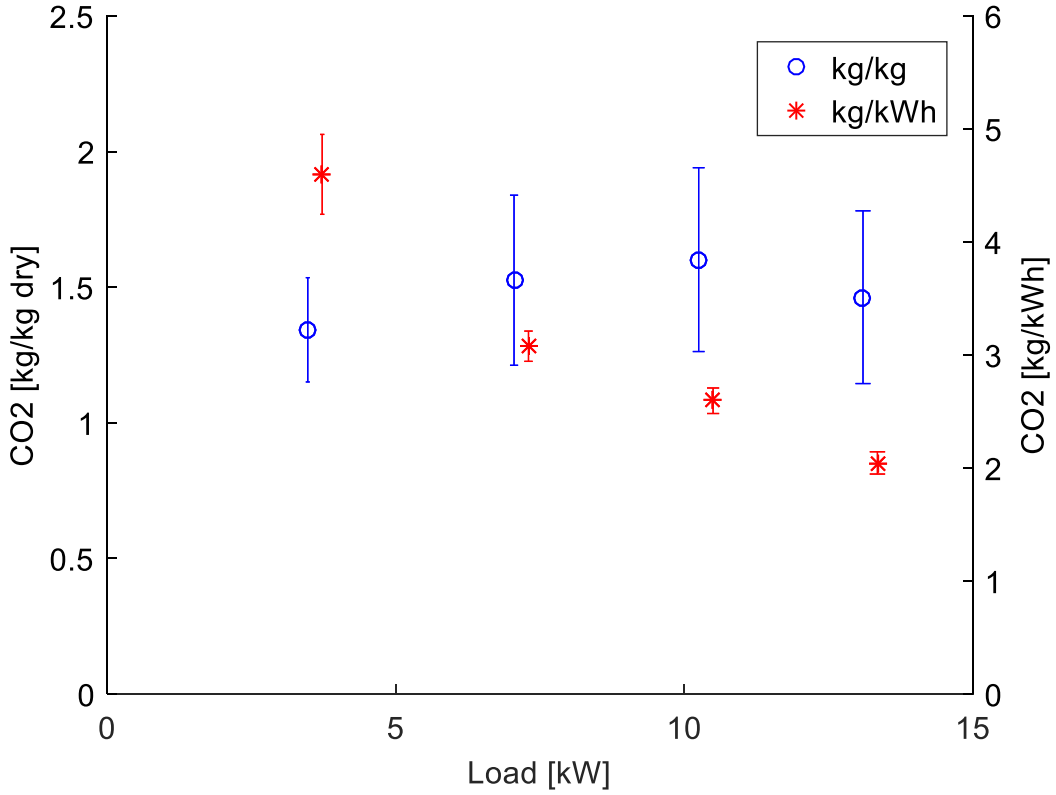

Figure 15: CO_2 emission factors for the Power Pallet per mass of feedstock and per energy produced by the generator as a function of electrical load

The primary greenhouse gas emission from gasification is carbon dioxide. As shown in Figure 15 above, the CO_2 emissions per dry biomass input does not have a clear trend with electrical load and only varies by about 15%. The lack of a clear trend is to be expected, as the biomass has a fixed carbon content regardless of load, and can only leave the system one of three ways: as solid ash, a liquid tar, or as a gas.

At low loads, the slightly lower CO_2 emissions could be attributed to lower temperatures leading to a higher fraction of the feedstock converted to biochar. The higher biochar production at low loads is probable because of the way that the Power Pallet handled its ash/biochar; the ash auger was on a fixed timer, so it removed accumulated biochar just as

quickly at low loads as it did at high loads. Another possible contributing factor to the lower CO_2 emission seen at low loads are errors in the MAF sensors; these sensors tend to be very sensitive at low flows, and thus a small deviation would have had a large impact.

The dip seen at high loads is likely due to lower producer gas quality. Figure 14 already established that high loads lead to lower quality producer gas, and this lower quality gas is less ideal for combustion in an engine. The low-quality producer gas would be expected to create more incomplete combustion emissions where carbon is emitted as CO and CH_4 instead of CO_2.

The emission of CO_2 on a per kWh basis has a clear downward trend. The observed downward trend in CO_2 produced per kWh is due to a reduction in feedstock used to produce the same amount of electricity. The amount of wood gas (defined as the amount of gasified wood present in the producer gas) required per kWh of energy produced decreases as shown in Figure 16 on the next page. The decreasing wood gas consumption indicates that thermal efficiency increases with load. Because of the fixed carbon content of the feedstock, less biomass required to produce an equal amount of electricity will lead to fewer CO_2 emissions.

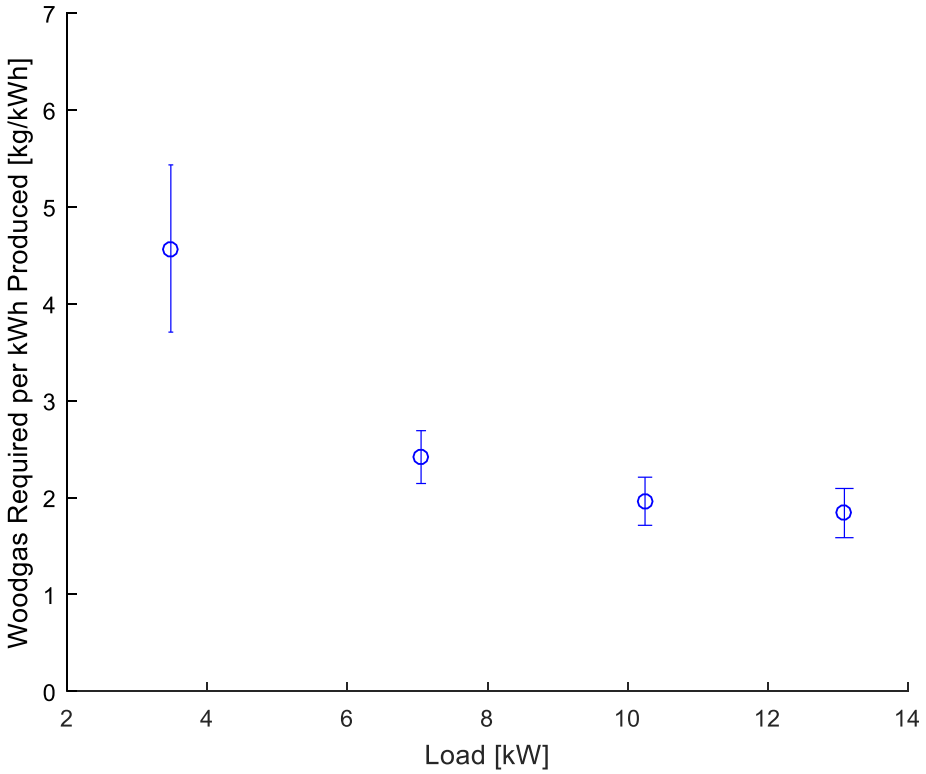

Figure 16: Mass of woodgas required per kWh of electricity produced as a function of electrical load

While the measured woodgas flow rates agree with the CO_2 emissions on a per kWh basis and are clearly the dominating factor, the biochar production and combustion efficiency discussed in the per dry biomass basis are still contributing factors.

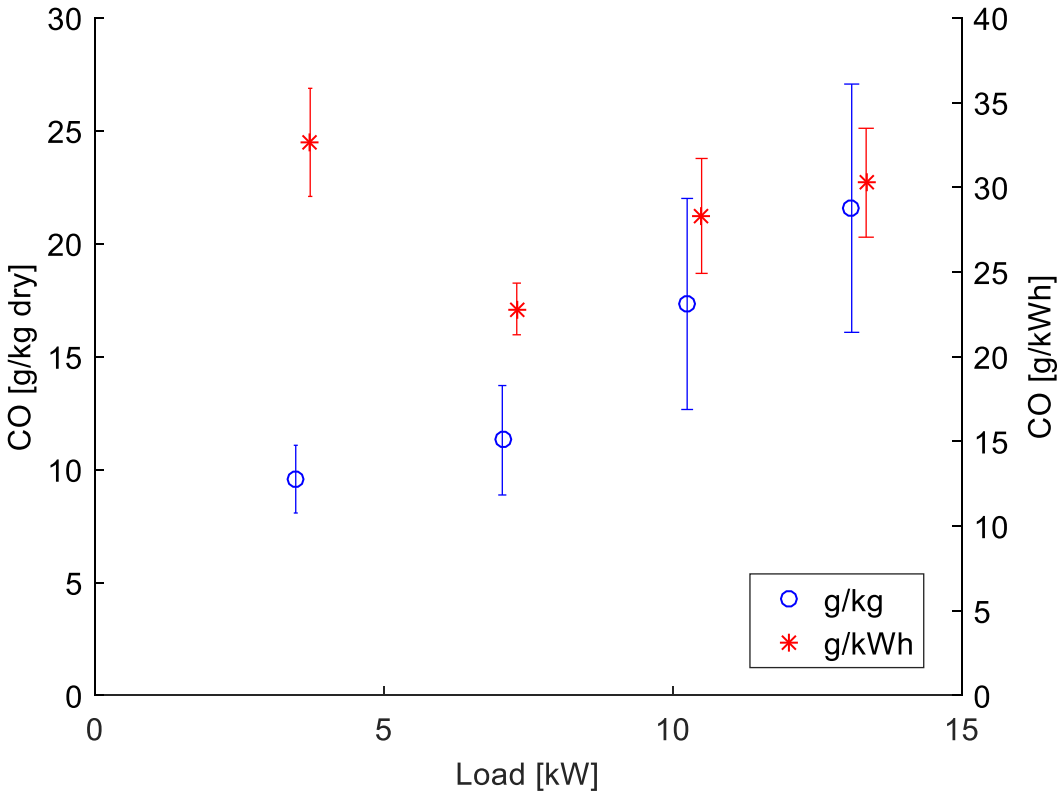

Figure 17: CO emission factors for the Power Pallet per mass of feedstock and per energy produced by the generator as a function of electrical load

Carbon monoxide emissions shown in Figure 17 exhibit very different trends than CO_2. Figure 14 establishes that producer gas quality lowers with increasing load, so it is expected that CO would increase with increasing load as it does in Figure 17. Conversely, the carbon monoxide emissions on a kWh basis initially reduce due to the sharply increasing thermal efficiency at low loads. At higher loads (above 5 kW), the reducing producer gas quality becomes more important than the increasing system efficiency, resulting in the growth at loads 3 and 4. Emissions of C_xH_y follow the same trends as CO as given in Figure 18 because both are products of incomplete engine combustion.

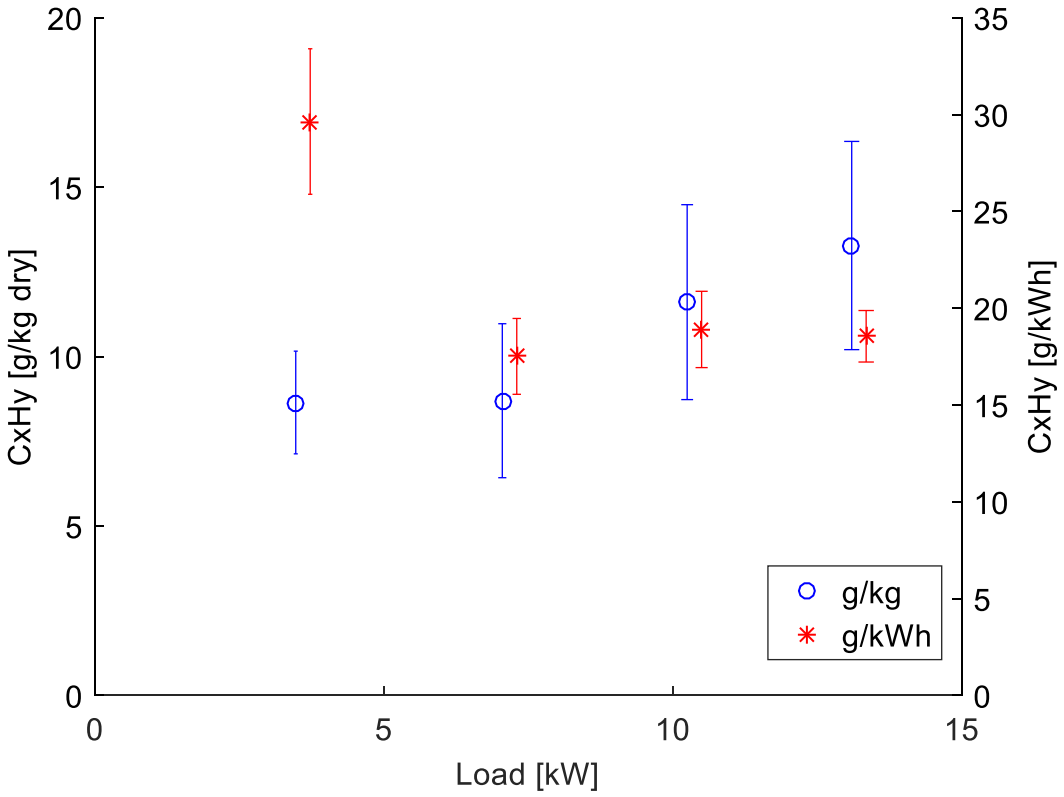

Figure 18: C_xH_y emission factors for the Power Pallet per mass of feedstock and per energy produced by the generator as a function of electrical load

One additional factor with the hydrocarbon emission factors is that because the LGA cannot clearly differentiate between different hydrocarbons, there will be some additional error due to the trace tars that may be present in the exhaust. As mentioned previously, the LGA was calibrated using methane (CH_4), and all the calculations treated C_xH_y as if it were 100% methane. Although methane is known to be the primary hydrocarbon emission from gasification systems, other higher order hydrocarbons are present in smaller concentrations and these higher order hydrocarbons tend to have a heavier weighting factor in the LGA. The actual methane emissions are likely lower than what is measured here, but a more thorough analysis of hydrocarbon emissions would be needed to quantify this. While the

other measurements would be affected by the calculated density (and thus flow rates), the amount of these hydrocarbons (<<1% by volume) is such that it would have very little effect on any of the other calculations.

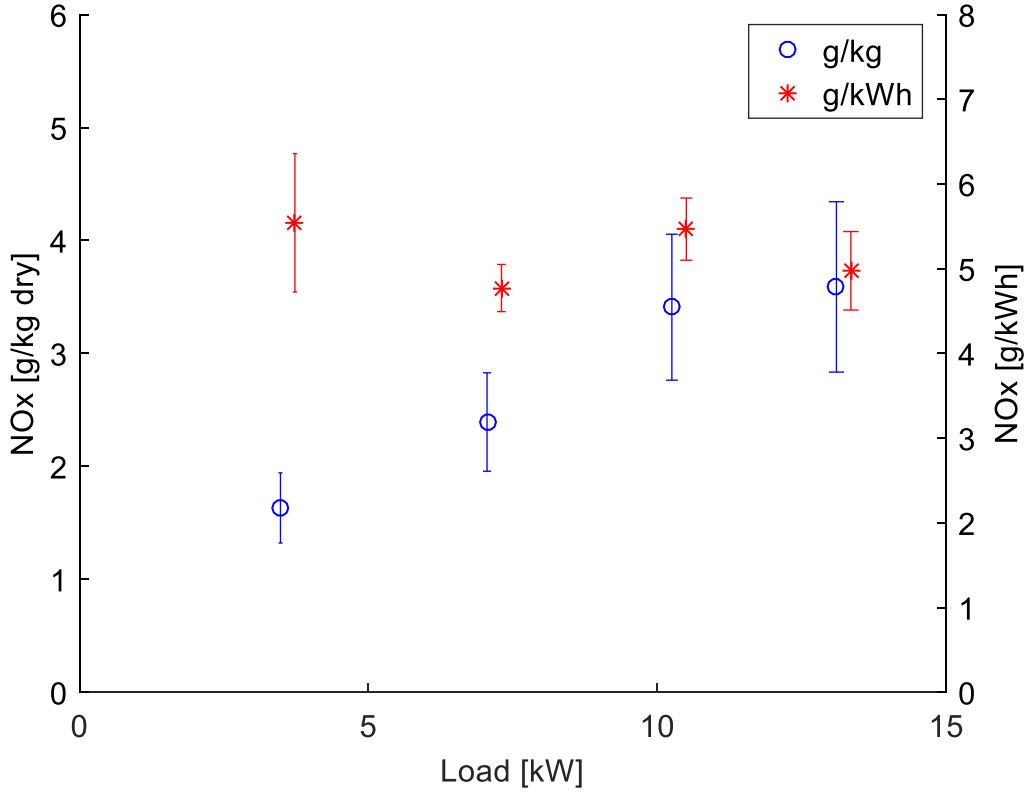

Figure 19: NO_x emission factors for the Power Pallet per mass of feedstock and per energy produced by the generator as a function of electrical load

NO_x concentrations are known to be a very strong function of temperature based on the Zel'dovich mechanism. At low loads, the engine combustion temperatures will be lowest because the resistance experienced by the engine, and thus the pressures in the cylinder, are low. As the load increases, so does the resistance (for a constant RPM engine) which causes higher in cylinder pressures and, in turn, higher in cylinder temperatures. Nearing peak load, the temperature in the engine would be expected to reduce its rate of increase

(and potentially even decrease) due to the poorer quality of the producer gas. This trend shows up as expected in the NO_x emissions on a per kg of dry biomass basis. Like previous emissions discussed, as loads increase the increasing thermal efficiency tends to push emissions down and the rising emission factor per kg of biomass tends to cause the emissions to increase. The relationship between these two factors is responsible for the inconsistent increases/decreases seen in the per kWh emission factors.

NO_x also had some very strong transient fluctuations when the engine was first started each day. One day's NO_x data is shown below in Figure 20.

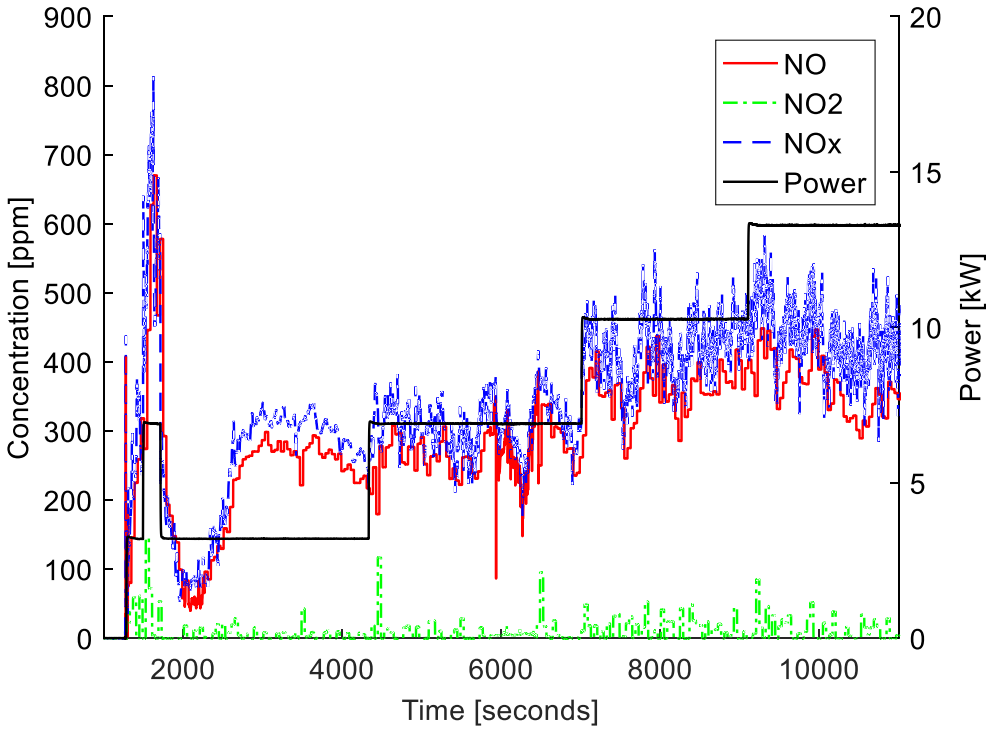

Figure 20: Real-time NO_x emissions using the CAI Analyzer (measuring NO and NO_2) and NI-9755 Sensor (measuring NO_x) over a range of electrical loads

Initially after a cold startup, the NO_x emissions were observed to have a large spike followed by a few oscillations; this spike was picked up by both the NI-9755 Smart NO_x Sensor (blue line) and the CAI NO_x Analyzer (red and green lines) at the beginning of every run and as such is unlikely to be an erroneous reading. One reason for this could be higher in cylinder pressures (and higher in cylinder temperatures) as the engine overcomes cold start frictions created from uneven thermal stresses. The temperatures then oscillate as the system overcorrects itself (high temperatures lead to smoother operation, which lowers in cylinder pressure and allows temperatures to fall back down, etc.), and ultimately settles to a stable operating condition.

Another aspect shown in Figure 20 is that the NO_x sensor was consistently reading slightly higher NO_x than the analyzer. The observed deviation is not due to differences in NO_x itself, as the controlled calibration showed much less difference between the two methods (see Appendix A.3). A more likely cause is the known cross sensitivity standard automotive NO_x sensors have with ammonia. To account for the ammonia cross sensitivity, more sophisticated NO_x control systems use ammonia correction correlations. However, no correlation for biomass burning was readily available and ammonia wasn't measured in this experiment, so no correction was done. Christian et al. have shown that ammonia can be created in small quantities from biomass combustion.

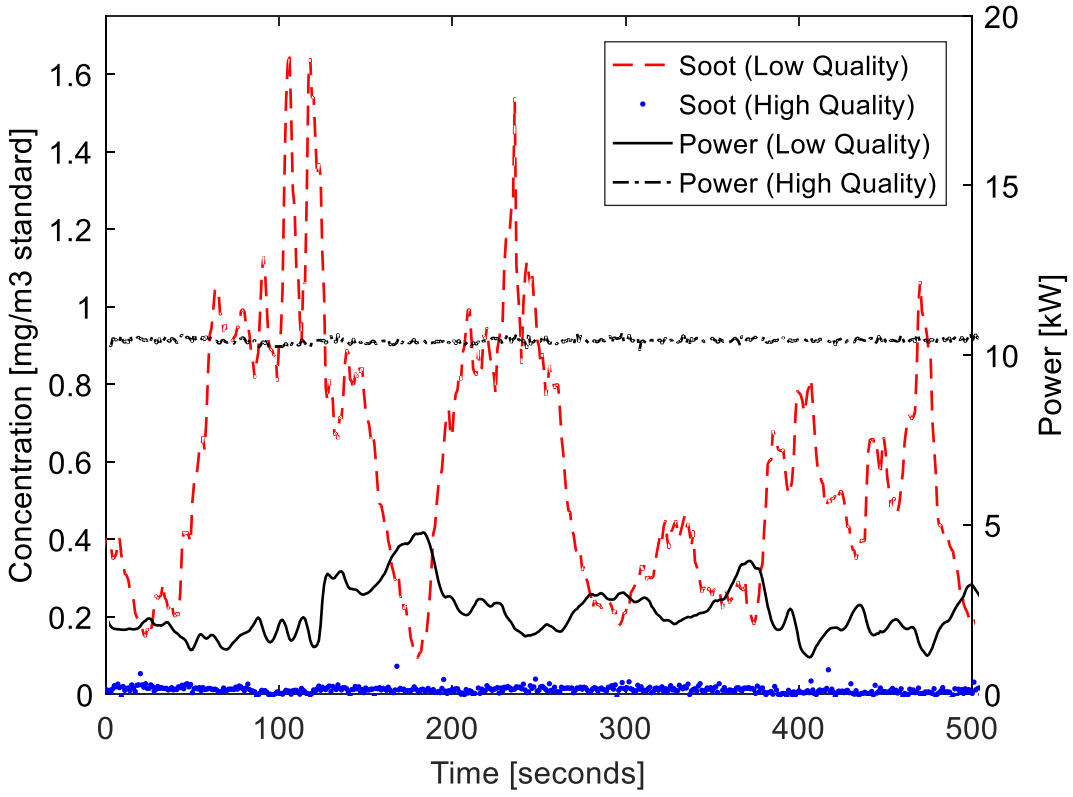

Figure 21: Example of soot emissions and associated electrical loads with high and low quality producer gas

Figure 21 includes soot emissions from two different runs plotted together on the same axis for comparison. Total soot emissions were found to be based almost exclusively on the quality of the incoming producer gas rather than as strong function of load. Average soot concentrations with high quality producer gas (and even down to CO and H_2 fractions as low as 10%) were typically below 0.02 mg/m^3 when the engine was running normally (constant power output), regardless of load. 0.02 mg/m^3 translates to 0.7-1.6 mg soot per kg of dry biomass, which is low even for largescale power plant standards. The combination of the packed bed filter and cyclone is certainly effective, but it comes at a cost of a 2-4 kPa pressure drop that gets exponentially larger with flow rate.

The soot emissions were found to be much more significant when the engine was struggling to maintain a constant power. While the Power Pallet is normally able to produce a stable power when subjected to a set electrical load (such as with Power (High Quality) in Figure 21), there can be large fluctuations in the power output if the producer gas is very low quality (CO and H_2 < 10%). Figure 21 highlights an extreme case that only happened when using very wet feedstocks, but soot spikes as high as 1.7 mg/m^3 were seen for short periods under these conditions, and the spikes tended to occur when the engine sputtered (signaled by a corresponding dip in the power output). When the engine could burn cleanly, then the power levels would rise and the soot would sharply drop.

While the spikes seen from the low-quality producer gas are nearly 100 times higher than the standard operating soot, the peak soot concentrations are still within reasonable operating limits, coming in at approximately 0.26 g/kg dry feedstock. The soot would likely be closer to the 1-2 mg/kg of dry feedstock range if good feedstock (< 30% moisture) is used.

For each of the three days, biochar formation accounted for around 2% of the initial feedstock. However, this was not a real-time measurement, and is based off the cumulative measured flow and end biochar contents.

4.2 Moisture Content Observations

While it has been mentioned previously, moisture content was one of the most significant factors in determining how the gasifier operates. While moisture content was between 20% and 30% for each load on each day, the effects are still visible in the emissions. This is a

qualitative discussion, as significantly more data would be required to get any qualitative relationships. Figure 22 shows the CO emissions for the three days along with their average moisture contents. In Figure 22, it is evident that the size of the error bars (relative to the measured value) is related to the moisture content measured for that load.

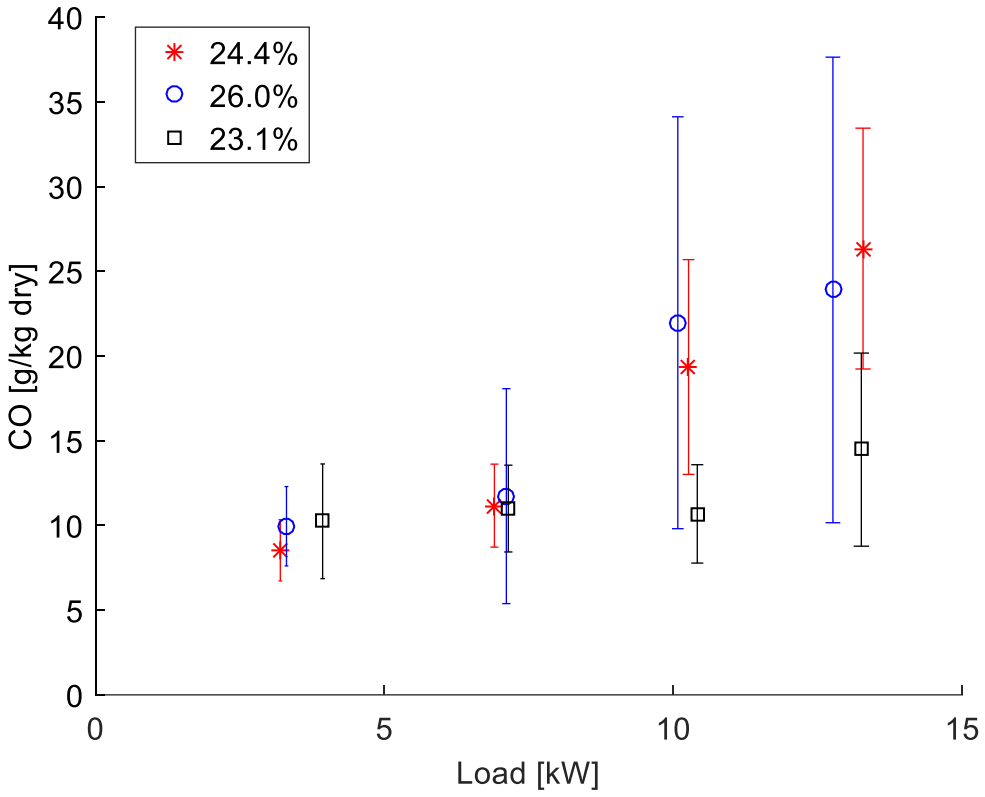

Figure 22: CO emissions on a per mass basis as a function of electrical load for different moisture content feedstocks

As shown in Figure 22, the wetter feedstock began to exhibit increasing emissions sooner. The earlier increase in emissions is likely due to the moisture reducing temperatures, which in turn reduces reaction rates, and ultimately the quality of the producer gas. In general, the Power Pallet exhibited the physical effect where the point at which the emissions begin to rise is shifted to a lower power for higher moisture content feedstocks while low moisture

feedstocks will maintain lower emissions for longer. The heavy relationship between moisture content and emissions also highlights how sensitive the system is to moisture – just a few percent difference leads to significant changes in the emissions. All Power Labs recommends feedstocks no higher than 30% moisture content for this reason.

Because of the higher temperatures caused by dryer feedstocks, NOx was also heavily influenced by moisture content. Figure 23 shows the NO_x emissions for the three days. NO_x is almost double at 23.1% moisture content what it was at 26% moisture content, and this trend would be expected to be even higher for feedstocks less than 20% moisture. For a short time, NO_x even passed 1100 ppm when an unusually dry patch of feedstock was in the reactor.

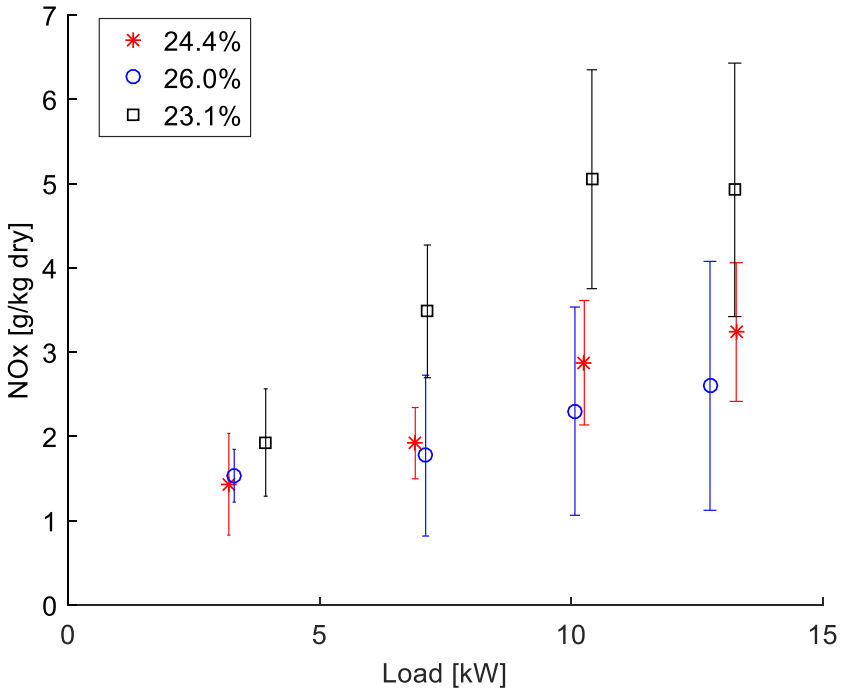

Figure 23: NO_x emissions on a per mass basis as a function of electrical load for different moisture content feedstocks

4.3 Thermal Efficiency Considerations

The thermal efficiency is one of the most important parameters to consider when looking at future renewable energy options. The thermal efficiency of the Power Pallet was found to be very dependent on the power output, as shown in Figure 24.

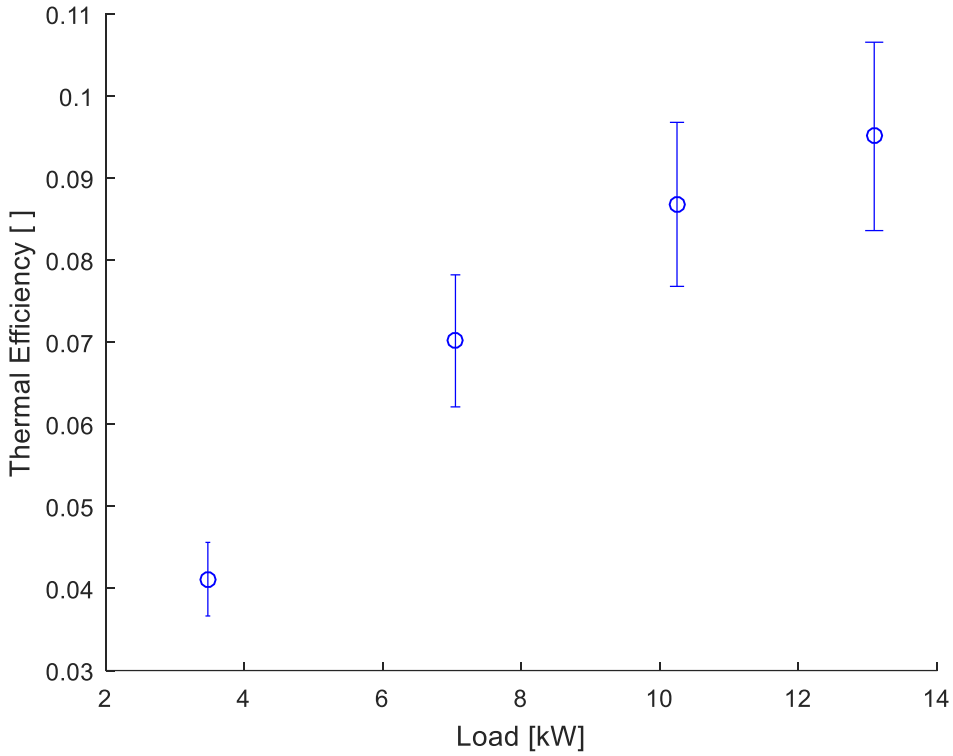

Figure 24: Power Pallet thermal efficiency as a function of load

The thermal efficiency rapidly increases with power, but starts to plateau at a maximum of 10-11%. This is significantly lower than largescale plants which fall between 25-45% for electrical output and even similarly sized gasoline and diesel generators (around 30%).

Several improvements could be made to increase the overall efficiency of the Power Pallet system. The easiest way that thermal efficiency could be increased in the future is through

mitigating heat losses. As the Power Pallet is designed, the heat losses in this system are not very optimized; the only well insulated component is the gasifier chamber itself while the rest of the components are thin sheet metal and/or corrugated pipes. Additionally, while corrugated pipe is ideal for easy adjustments, it has a very large surface area subject to heat transfer because of all the ridges. Other sources of heat loss include the engine oil, coolant, and exhaust – none of these have heat recovery systems currently in place.

The other source for efficiency improvements lie in the engine and generator. The Power Pallet's modified natural gas engine with a fixed speed (1500/1800 RPM for 50 Hz and 60 Hz systems respectively) and spark timing (38/42 degrees) is not optimized for use with producer gas. A natural gas engine is used because there is currently no commercially available engine that is optimized for use with this type of producer gas. One primary issue with the current engine is that the operating conditions of the engine were chosen to give good performance at standard operating conditions using estimated steady state fuel properties; there is no real-time optimization for actual fuel conditions (which can vary significantly throughout the operation of the system). Implementing a variable spark timing based on current fuel properties would allow for more efficient combustion, which would be expected to lead to both cleaner emissions and increased efficiency. The NPE32 generator used is also 85% efficient – there are more efficient generators on the market, but they are also larger and would not allow the Power Pallet to fit on a 4'x4' footprint.

A few efficiency improvements are already in the works on future iterations of All Power Labs' design, and things appear to be moving in the right direction. Since testing this gasifier system, APL has added another heat exchanger to their design to preheat engine

intake air using the hot producer gas entering the packed bed filter (which is expected to also reduce tars in the post-filter gas stream) and they're currently in the testing stages of an oil and coolant CHP system.

4.4 Lifecycle Analysis

The developed emissions factors presented in the last section allow the comparison with a range of methods for biomass transportation, use and destruction from literature using a lifecycle approach. Table 13 below is a combination of all the literature review and analysis done up to this point, but does not yet include collection, chipping, and transportation emissions. In Table 13, the total CO_2 equivalent is calculated using Equation 19.

$$CO_2e = CO_2 + \frac{44}{28} * CO + 25 * CH_4 + 298 * N_2O \quad (19)$$

Equation 19 assumes that all CO is converted to CO_2 in the atmosphere, but neglects the increase in atmospheric methane an increase in CO causes. The effects from NO_x, particulate, and nitrous oxide emission are also neglected unless N_2O concentrations were specifically reported, as is the case with decomposition. This is a simplification, and the actual greenhouse impact of each scenario will depend largely on the environment that it is being emitted into.

	CO_2 (kg/kg)	NO_x (g/kg)	CO (g/kg)	CH_4 (g/kg)	Soot/PM (g/kg)	N_2O (g/kg)	Total CO_2e (g/kg)
Open Burning	1.62	2.9	97.2	4.6	15.5	--	1888
Residential	1.56-1.62	0.05-2.7	19-154	6-10	1.2-10	--	1740-2112
Decomposition$_b$	1.74	--	--	33.3	--	0.04	2584
IGCC Turbine (GREET)	1.84	0.17	0.16	0.07	0.05	--	1841
Steam Turbine (GREET)	1.83	1.13	5.82	0.60	2.57	--	1854
Power Pallet$_a$	1.34 – 1.60	1.6 – 3.6	9.6 – 21.6	8.6 – 13.3	0 – 0.26*	--	1570 – 1966

a = Emissions based on a 3-run average at four different electrical loads. Individual run may fall outside of this range based primarily on feedstock/moisture content.
b = Calculated assuming 50% carbon, 0.1% nitrogen content
* = 0.26 g/kg assumes the engine is running poorly as described in Figure 21 at full load.
-- = no data

Table 13: Biomass emission factors on a per mass basis depending on method of use

As seen in Table 13, decomposition is the source that is most capable of releasing high amounts of greenhouse gases per mass of biomass, residential use is the highest emitting of harmful pollutants, and largescale plants are unsurprisingly the cleanest burning. All things considered, largescale plants are the cleanest burning use for biomass, followed by small-scale usage (the Power Pallet), open burning and finally residential use. Decomposition is heavily dependent on the environment, but storing large piles of poorly aerated feedstock should certainly be avoided whenever possible to reduce greenhouse gas emissions.

The Power Pallet has the potential for the lowest overall greenhouse gas emissions compared to the other biomass systems, mostly due to its high ratio of carbon storage in biochar. If this biochar were to be burned as well, then the emissions would look most like

the low emitting end of the residential use spectrum. There are also significant reductions in CO and soot compared to the open burning or residential use. Conversely, NO_x emissions have risen slightly (for dry feedstock cases), but that is more a product of drier feedstock being used in the Power Pallet than is normally subjected to open burning and/or decomposition. Surprisingly, the methane emissions are higher for the Power Pallet, although it would be good to get more data on the makeup the measured hydrocarbons to see if the methane emissions are actually that high – based on the reductions seen elsewhere, methane emissions would have been expected to also reduce.

When it comes to just electricity generation, the Power Pallet does not fare as well. Because of its low thermal efficiency compared to other technologies, emissions from distributed gasification (except soot) are significantly higher than the largescale counterparts on a per kWh basis as shown in Table 14.

	CO_2 (kg/kWh)	NO_x (g/kWh)	CO (g/kWh)	C_xH_y (g/kWh)	Soot (g/kWh)
IGCC Turbine (GREET)	0.83	0.08	0.07	0.03	0.02
Steam Turbine (GREET)	1.49	0.92	4.73	0.49	2.09
Power Pallet[a]	2.1 – 4.6	4.8 – 5.5	22.8 – 32.6	17.5 – 29.6	0 – 0.78*

a = Emissions based on four loads for a 3-run average. Individual runs may fall outside of this range based primarily on feedstock/moisture content.

* = 0.78 g/kWh assumes the engine is running poorly as described in Figure 21 at full load.

Table 14: Biomass emissions on a per kWh basis depending on method of use

When including emissions associated with feedstock preparation, the new emissions are shown in Table 15. Open burning, residential usage, and decomposition aren't included because they do not change from the previous data set.

	CO_2 (kg/kg)	NO_x (g/kg)	CO (g/kg)	CH_4 (g/kg)	Soot/PM (g/kg)	Total CO_2e (g/kg)
IGCC Turbine (100 mile)	1.90	0.37	0.24	0.07	0.054	1902
Steam Turbine (100 mile)	1.89	1.33	5.90	0.60	2.58	1914
Power Pallet (10 mile)	1.36 – 1.62	1.7 – 3.7	9.7 – 21.7	8.6 – 13.3	0.01 – 0.27*	1590 – 1987

* = 0.78 g/kWh assumes the engine is running poorly as described in Figure 21 at full load.

Table 15: Modified biomass emission factors on a per mass basis including feedstock preparation

The feedstock preparation emissions came primarily from transportation, and only significantly affect CO_2 and NO_x emissions. Even with the added processing emissions, the change in emissions is relatively small (40 g/kg extra CO_2 and 0.2 g/kg extra NO_x for largescale plants with 100-mile collection radius). While any larger of a collection area would be undesirable from a CO_2 perspective, it would have to be a very large collection radius (500+ miles) before CO, soot, or methane emissions begin to approach the open burning or residential usage emissions. The low emissions associated with transportation mean that, from an environmental standpoint, the biomass would be best disposed of by transporting it to a large plant with minimal regard given to the transportation distance.

The primary concern with transportation distance is whether it is economically worthwhile to transport material to largescale IGCC plants, and when it becomes too costly. There are significant costs associated with building a largescale plant as well as hiring loggers, drivers, and farmers to harvest biomass; if the costs aren't competitive or the supply isn't steady, then biomass is not a desirable source of fuel for these large stationary plants. Taking the costs of a stable feedstock supply into account, largescale plants are only truly

feasible when large quantities of sustainably grown, easily accessible biomass such as agricultural or logging residues are nearby and simultaneously need to have a demand for large amounts of electricity production.

The Power Pallet has the benefit of being mobile, which helps cut down on the transportation costs substantially and makes operation in remote, off-grid locations (such as a small village in Africa) a much more reasonable process (especially with the low capital cost).

5 Field Deployment

5.1 Site and Setup

As a final part of the project, the Power Pallet was deployed to a DNR facility in New Ulm, MN. This facility had a 70-kW solar array installed in 2013 that can provide much of the required power for day to day operations, but it cannot provide a stable supply because of solar power's inherent inconsistency; this means that power must be purchased from the grid overnight and in the mornings, or potentially all day on a cloudy day.

The gasifier was installed on site with the idea that it could reduce the amount of power purchased during these off-peak hours. For this experiment, the gasifier was run in the early mornings to reduce the spike in electrical demand caused by geothermal heat pumps as the building would begin to heat up for the work day. To help protect the gasifier from the elements, it was installed in a modified shipping container, which is shown in Figure 25.

Figure 25: Power Pallet at the DNR facility in New Ulm, MN

5.2 Impact

The gasifier could successfully reduce the amount of purchased power by about 10-15 kW for around 5 hours each day it was running. This is equivalent to an offset of roughly 15 kg of CO_2 per day if the electricity were generated from a modern natural gas power plant or as high as 30 kg of CO_2 if the electricity were generated from coal. The direct impact of the gasifier can be seen for a sunny day in Figure 26.

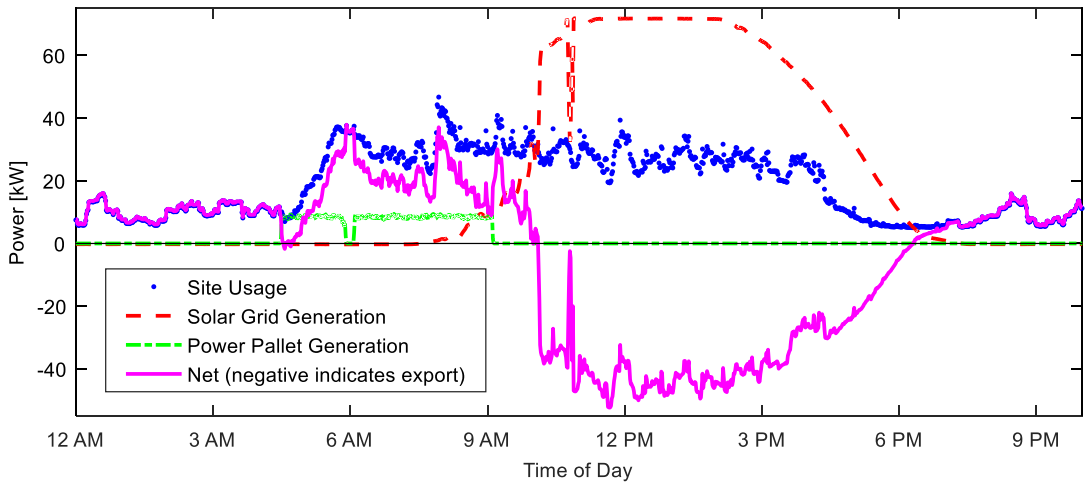

Figure 26: New Ulm DNR facilities power requirements and production on a sunny day in late March

Although the gasifier is undersized for a facility of this size, the effects on the net power can still be seen. The gasifier reduces the peak purchased power as intended, and can be run stably up until the solar array is ready to take over. Although the gasifier was only run for 5 hours per day throughout this experiment, the Power Pallet is capable of being run for longer periods if required.

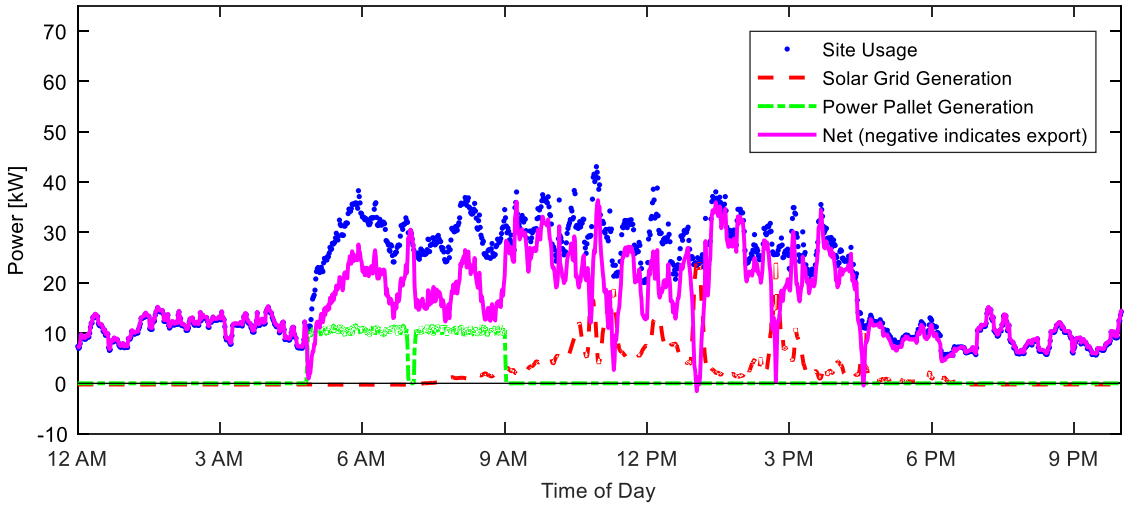

Figure 27: New Ulm DNR facilities power requirements and production on a cloudy day in late March

The impact of the gasifier on a cloudy day is more significant because of the solar array's inability to produce much power. Figure 27 shows an example of a day where it could be beneficial to have a gasifier on standby to run all day.

5.3 Operational Reliability

Throughout the course of operation and maintenance in the field, design defects in Power Pallet and the heavy time investment required of the operator became evident. Problems arose during daily operation, regular maintenance, and in several unanticipated component failures.

Daily startup was a complicated process. During every startup, the gasifier first needed to be ignited then allowed to heat up for up to 20 minutes before switching on the engine, although it could take even longer if the feedstock was wet or the pyrolysis chamber had been completely emptied on a previous run. The 88-gallon hopper lasted approximately 4 hours when running at full load and required refilling before running completely out or risk

having to do a lengthy process to re-establish the charcoal bed in the pyrolysis chamber. Accumulated ash, biochar, and water need to be removed after shutdown daily.

In addition to the daily startup/shutdown procedures, significant maintenance is required once every two weeks of running. The packed bed filter's media requires replacement and soot/tar buildup needs to be removed from all components leading up to the filter. Most notably, the additional engine air/packed bed filter heat exchanger that APL added after all of the emissions testing had been completed can become completely clogged if it's not regularly cleaned, as shown in Figure 28.

Figure 28: Clogged pre-filter heat exchanger after two weeks of heavy run time (left) compared to the clean heat exchanger (right)

Solidified tars, known as clinkers, can build up in the grate basket at the bottom of the reactor and need to be periodically broken up. This extended maintenance can take upwards of 4 hours, depending on the frequency of the maintenance and quality of the feedstock, and this high maintenance requirement is an important issue when comparing to similarly sized gas or diesel generators that require minimal maintenance.

Some unforeseen issues that cropped up over the time this machine was being run in New Ulm included the feed auger snapping, the engine air intake hose collapsing, a gas blower

shorting out, and ice buildup freezing components and causing feedstock bridging. These issues can be addressed through component redesign to ensure proper operation over a wider range of conditions.

6 Conclusions

Small-scale gasification using systems like the Power Pallet is an emerging technology that shows promise as a renewable energy source. The Power Pallet exhibits the potential benefits of small-scale gasification, both environmentally and economically.

From an environmental standpoint, small-scale gasification has the potential to simultaneously reduce harmful pollutants and slow the emission of greenhouse gases into the atmosphere. Controlled combustion conditions lead to significantly reduced harmful pollutants (notably CO and PM) when compared to current residential and open burning sources while the byproduct, biochar, represents a carbon sink that has the potential to make small-scale gasification a carbon-negative technology (if harvested biomass is always regrown). However, significant improvements are required before emissions factors of pollutants like CO, CH_4 and NO_x are competitive with large-scale plants.

From an economic standpoint, small-scale gasification has the potential to affordably bring electricity to off-grid locations but it is not currently competitive in developed areas where more user-friendly technologies exist (such as low maintenance solar, gas, or diesel generators). Its low capital cost and easy mobility allows the Power Pallet to operate in locations where largescale plants are not economically viable. Further, distributed gasification systems can use locally available resources without the requirement for long distance feedstock transportation. While the Power Pallet is simple enough operate and maintain by a single person, considerable time requirements for these tasks significantly increase the cost of electricity once hourly wages are taken into account. Despite the low

cost of biomass fuel, the high labor costs tend to make electricity generated from this system noticeably more expensive to operate than grid electricity or a similarly sized gas/diesel generator where those are available.

While the Power Pallet demonstrates that distributed gasifier-generators can reduce emissions of CO_2, CO, and PM compared to other biomass consumption processes and can be a carbon neutral source of electricity, there are several areas in which it could clearly benefit from further improvements. The engine is not optimized to run on producer gas alone, and would benefit from more research in the area to increase combustion efficiency by changing engine parameters (notably spark timing) to react to real time conditions, thereby increasing thermal efficiency and decreasing pollutants. Heat recovery is another point of further investigation because much of the system is poorly insulated and the corrugated piping provides a large surface area for heat loss. Furthermore, there is no exhaust treatment in place – a catalytic converter or similar technology would help to significantly reduce NO_x emissions. Lastly, the ease of operation could benefit from additional automation (particularly during initial startup) to reduce the need for an operator's time – this would help it better compete against simple gas and diesel generators where a flip of a switch and sufficient fuel is all that is required.

In the future, it would be beneficial to revisit the Power Pallet emissions and focus on trace emissions, including the distribution of hydrocarbons, nitrous oxide, and other small volume but potentially hazardous gases to get a clearer picture of the true impacts of this technology. It would also be helpful to try differing feedstock properties to get a better understanding of the device's operation over a wide range of conditions.

7 References

A. L. Westerling, H. G. Hidalgo, D. R. Cayan, T. W. S. (2006). Warming and Earlier Spring Increase Western U.S. Forest Wildfire Activity. *Science*, *313*, 940–943.

Akagi, S. K., Yokelson, R. J., Wiedinmyer, C., Alvarado, M. J., Reid, J. S., Karl, T., … Wennberg, P. O. (2011). Emission factors for open and domestic biomass burning for use in atmospheric models. *Atmospheric Chemistry and Physics*, *11*, 4039–4072. https://doi.org/10.5194/acp-11-4039-2011

ARI. (2017). Raman Spectroscopy and the Laser Gas Analyzer at work. Retrieved from http://www.atmrcv.com/technology.html

Aurell, J., Gullett, B. K., & Tabor, D. (2015). Emissions from southeastern U.S. Grasslands and pine savannas: Comparison of aerial and ground field measurements with laboratory burns. *Atmospheric Environment*, *111*, 170–178. https://doi.org/10.1016/j.atmosenv.2015.03.001

AVL. (2009). *AVL MICRO SOOT SENSOR Operating Manual/Product Guide*.

Ballard-Tremeer, G., & Jawurek, H. H. (1996). Comparison of five rural, wood-burning cooking devices: Efficiencies and emissions. *Biomass and Bioenergy*, *11*(5), 419–430. https://doi.org/10.1016/S0961-9534(96)00040-2

Bhattacharya, S. C., Albina, D. O., & Salam, P. A. (2002). Emission factors of wood and charcoal-fired cookstoves. *Biomass and Bioenergy*, *23*, 453–469.

Bridgwater, A. V. (1995). The technical and economic feasibility of biomass gasification for power generation. *Fuel*, *74*(5), 631–653. https://doi.org/10.1016/0016-2361(95)00001-L

CAI. (2017). 600 Series CLD NOx Analyzers. Retrieved from http://gasanalyzers.com/uploads/product/data_sheet/1/600_Series_CLD_Data_Sheet.pdf

Cai, H., Wang, M., Elgowainy, A., & Han, J. (2012). *Updated Greenhouse Gas and Criteria Air Pollutant Emission Factors and Their Probability Distribution Functions for Electric Generating Units*. https://doi.org/10.1007/s13398-014-0173-7.2

Christian, T. J., Kleiss, B., Yokelson, R. J., Holzinger, R., Crutzen, P. J., Hao, W. M., … Ward, D. E. (2003). Comprehensive laboratory measurements of biomass-burning emissions: 1. Emissions from Indonesian, African, and other fuels. *Journal of Geophysical Research-Atmospheres*, *108*(D23), 3-1-13. https://doi.org/10.1029/2003JD003704

Collard, F. X., & Blin, J. (2014). A review on pyrolysis of biomass constituents: Mechanisms and composition of the products obtained from the conversion of cellulose, hemicelluloses and lignin. *Renewable and Sustainable Energy Reviews*, *38*, 594–608. https://doi.org/10.1016/j.rser.2014.06.013

Cornwall, W. (2017). The Burning Question: Moves to designate wood as a carbon-neutral fuel have alarmed environmentalists and divided scientists. *Science*, *355*(6320), 18–21.

Donaldson, K., Tran, L., Jimenez, L. A., Duffin, R., Newby, D. E., Mills, N., … Stone, V. (2005). Combustion-derived nanoparticles : A review of their toxicology following inhalation exposure. *Particle and Fibre Toxicology*, 2–10. https://doi.org/10.1186/1743-8977-2-10

EIA. (2017). *Electric Power Monthly: with data for November 2016. U.S. Energy Information Administration*.

EPA. (2010). *BACKGROUND DOCUMENT 5TH EDITION AP-42 Wood Residue Combustion In Boilers*.

Evans, R. J., Knight, A. R., Onischak, M., Babu, S. P.: Development of biomass gasification to produce substitute fuels, Richland, Washington, USA, Pacific Northwest Laboratory (PNL), PNL--6518, 14 p. (1988).

Feldmann, H. F., Paisley, M. A., Appelbaum, H. R., Taylor, D. R.: Conversion of forest residues to a methane-rich gas in a high-throughput gasifier, Battelle, Columbus, OH (USA), DE88013138, 108 p. (1988).

Gaur, S., Reed, T. B.: Thermal data for natural and synthetic fuels, Marcel Dekker, New York, 259 p. (1998).

Glaser, B., Haumaier, L., Guggenberger, G., & Zech, W. (2001). The " Terra Preta " phenomenon : a model for sustainable agriculture in the humid tropics. *Naturwissenschaften*, *88*, 37–41. https://doi.org/10.1007/s001140000193

Goode, J. G., Yokelson, R. J., Ward, D. E., Susott, R. A., Babbitt, R. E., & Davies, M. A. (2000). Measurements of excess 03, CO2, CO, CH4, C2H4, C2H2, HCN, NO, NH3, HCOOH, CH3COOH, HCHO, and CH3OH in 1997 Alaskan biomass burning plumes by airborne Fourier transform infrared spectroscopy (AFTIR). *Journal of Geophysical Research*, *105*, 22147–22166.

Hamilton, J. (2013). *Characterization of Emissions from Small Scale Biomass Gasifier*. University of Minnesota.

Han, J., Elgowainy, A., Palou-Rivera, I., Dunn, J. B., & Wang, M. Q. (2013). *Well to Wheels Analysis of Fast Pyrolysis Pathways with GREET*. https://doi.org/10.1017/CBO9781107415324.004

Harrison, R. M., & Yin, J. (2000). Particulate matter in the atmosphere: Which particle properties are important for its effects on health? *Science of the Total Environment*, *249*, 85–101. https://doi.org/10.1016/S0048-9697(99)00513-6

Harter, J., Krause, H.-M., Schuettler, S., Ruser, R., Fromme, M., Scholten, T., … Behrens, S. (2014). Linking N2O emissions from biochar-amended soil to the structure and function of the N-cycling microbial community. *The ISME Journal*, *8*, 660–674. https://doi.org/10.1038/ismej.2013.160

Hayhurst, A.N. and Lawrence, A. D. (1992). Emissions of Nitrous Oxide from Combustion Sources. *Prog. Energy Combust. Sci.*, *18*, 529–552.

IPCC. (2007). *Climate Change 2007: The Physical Science Basis*. (S. Solomon, D. Qin, M. Manning, M. Marquis, K. Averyt, M. M. B. Tignor, … Z. Chen, Eds.). Cambridge, New York, Melbourne, Madrid, Cape Town, Singapore, Sao Paolo, Delhi: Cambridge University Press. https://doi.org/10.1017/CBO9781107415324.004

Johnson, D. W., Turner, J., & Kelly, J. M. (1982). The Effects of Acid Rain on Forest Nutrient Status. *Water Resources Research*, *18*(3), 449–461. https://doi.org/10.1029/WR018i003p00449

Kampa, M., & Castanas, E. (2008). Human health effects of air pollution. *Environmental Pollution*, *151*, 362–367. https://doi.org/10.1016/j.envpol.2007.06.012

Lashof, D. a, & Ahuja, D. R. (1990). Relative Contributions of Greenhouse Gas Emissions to Global Warming. *Nature*, *344*, 529–531. https://doi.org/10.1038/344529a0

Likens, G. E., & Bormann, F. H. (1974). Acid Rain: A Serious Regional Environmental Problem. *Science*, *184*, 1176–1179. https://doi.org/10.1126/science.184.4142.1176

Liu, Y., Goodrick, S., & Heilman, W. (2014). Wildland fire emissions, carbon, and climate: Wildfire-climate interactions. *Forest Ecology and Management*, *317*, 80–96. https://doi.org/10.1016/j.foreco.2013.02.020

Miles, T.R., Miles, T. R. Jr, Baxter, L., Bryers, R. W., Jenkins, M. B., Oden, L. L.: Alkali deposits found in biomass power plants. A preliminary investigation of their extend and nature, NREL/TP-433-8142, 82 p. (1995).

Miller, B. J. (2005). *Coal Energy Systems*. (R. C. Dorf, Ed.). Burlington, MA: Elsevier.

Milne, T. a, & Evans, R. J. (1998). *Biomass Gasifier " Tars ": Their Nature , Formation , and Conversion*. *NREL*. https://doi.org/10.2172/3726

Mohan, D., Pittman, C. U., & Steele, P. H. (2006). Pyrolysis of Wood / Biomass for Bio-oil : A Critical Review. *Energy & Fuesl*, *20*, 848–889. https://doi.org/10.1021/ef0502397

Mouillot, F., Narasimha, A., Balkanski, Y., Lamarque, J.-F., & Field, C. B. (2006). Global carbon emissions from biomass burning in the 20th century. *Geophysical Research Letters*, *33*(1), 2–5. https://doi.org/10.1029/2005GL024707

Ozgen, S., Caserini, S., Galante, S., Giugliano, M., Angelino, E., Marongiu, A., … Morreale, C. (2014). Emission factors from small scale appliances burning wood and pellets. *Atmospheric Environment*, *94*, 144–153. https://doi.org/10.1016/j.atmosenv.2014.05.032

Parikka, M. (2004). Global biomass fuel resources. *Biomass and Bioenergy*, *27*(6), 613–620. https://doi.org/10.1016/j.biombioe.2003.07.005

Pasangulapati, V., Ramachandriya, K. D., Kumar, A., Wilkins, M. R., Jones, C. L., & Huhnke, R. L. (2012). Effects of cellulose, hemicellulose and lignin on thermochemical conversion characteristics of the selected biomass. *Bioresource Technology*, *114*, 663–669. https://doi.org/10.1016/j.biortech.2012.03.036

Pöschl, U. (2005). Atmospheric aerosols: Composition, transformation, climate and health effects. *Angewandte Chemie - International Edition*, *44*, 7520–7540. https://doi.org/10.1002/anie.200501122

Rajvanshi, A. K. (1986). *Biomass gasification*. *Alternative Energy in Agriculture* (Vol. II).

Raub, J. A., Mathieu-Nolf, M., Hampson, N. B., & Thom, S. R. (2000). Carbon monoxide poisoning - A public health perspective. *Toxicology*, *145*(1), 1–14. https://doi.org/10.1016/S0300-483X(99)00217-6

Reid, J. S., Koppmann, R., Eck, T. F., & Eleuterio, D. P. (2005). A review of biomass burning emissions part II : Intensive physical properties of biomass burning particles. *Atmospheric Chemistry and Physics*, *5*, 799–825.

Sheth, P. N., & Babu, B. V. (2009). Experimental studies on producer gas generation from wood waste in a downdraft biomass gasifier. *Bioresource Technology*, *100*(12), 3127–3133. https://doi.org/10.1016/j.biortech.2009.01.024

Simoneit, B. R. T. (2002). Biomass burning — a review of organic tracers for smoke from incomplete combustion. *Applied Geochemistry*, *17*, 129–162.

Sinha, P., Hobbs, P. V., Yokelson, R. J., Blake, D. R., Gao, S., & Kirchstetter, T. W. (2004). Emissions from miombo woodland and dambo grassland savanna fires. *Journal of Geophysical Research*, *109*. https://doi.org/10.1029/2004JD004521

United States EPA. (2016). *Inventory of U . S . Greenhouse Gas Emissions and Sinks : 1990 – 2014*. https://doi.org/EPA 430-R-13-001

Wang, J., Xiong, Z., & Kuzyakov, Y. (2016). Biochar stability in soil: Meta-analysis of decomposition and priming effects. *GCB Bioenergy*, *8*, 512–523. https://doi.org/10.1111/gcbb.12266

Weimann, J. (2003). Toxicity of nitrous oxide. *Best Practice and Research: Clinical Anaesthesiology*, *17*(1), 47–61. https://doi.org/10.1053/bean.2002.0264

Wihersaari, M. (2005). Evaluation of greenhouse gas emission risks from storage of wood residue. *Biomass and Bioenergy*, *28*, 444–453. https://doi.org/10.1016/j.biombioe.2004.11.011

Wotawa, G. (2000). The Influence of Canadian Forest Fires on Pollutant Concentrations in the United States. *Science*, *288*, 324–328. https://doi.org/10.1126/science.288.5464.324

Yokelson, R. J., Burling, I. R., Urbanski, S. P., Atlas, E. L., Adachi, K., Buseck, P. R., … Wold, C. E. (2011). Trace gas and particle emissions from open biomass burning in Mexico. *Atmospheric Chemistry and Physics*, *11*, 6787–6808.

https://doi.org/10.5194/acp-11-6787-2011

Zanchi, G., Pena, N., & Bird, N. (2011). Is woody bioenergy carbon neutral? A comparative assessment of emissions from consumption of woody bioenergy and fossil fuel. *Global Change Biology: Bioenergy*, *4*(6), 761–772.

Appendices

Appendix A: Calibration Curves

Appendix A.1: Orifice Plate

This calibration was carried out at 70 F, 1 atm room air. The relationship was assumed to be dependent only on density and pressure drop, as all other variables in orifice plate theory remain unchanged. The square root relationship is linear, as expected.

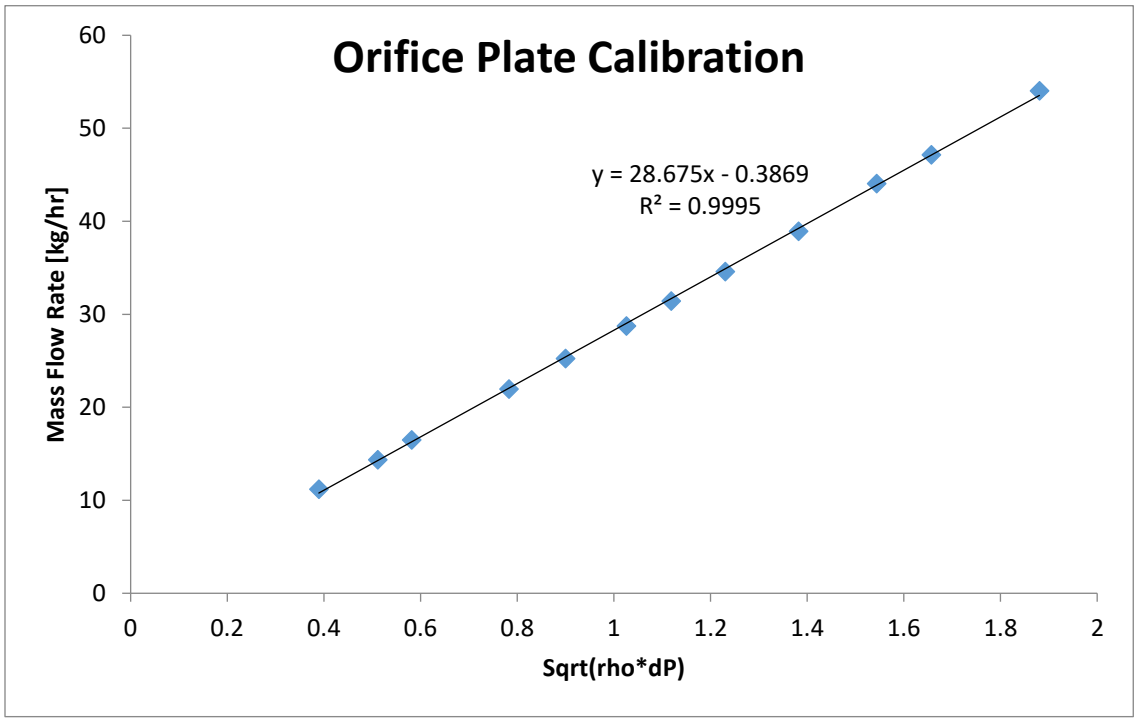

Figure 29: Orifice plate calibration curve

Appendix A.2: MAF Meters

The Ford MAF meters are not as nicely correlated. The MAF calibration curve was split up into two parts to get a better resolution: a low flow and a normal flow region. When the engine is running, both MAF sensors typically read in the normal flow region. The voltage was calibrated so it was voltage offset from a no flow condition, as battery load and voltage

seemed to influence the measured voltage. Both regions were found to be approximately a square root function.

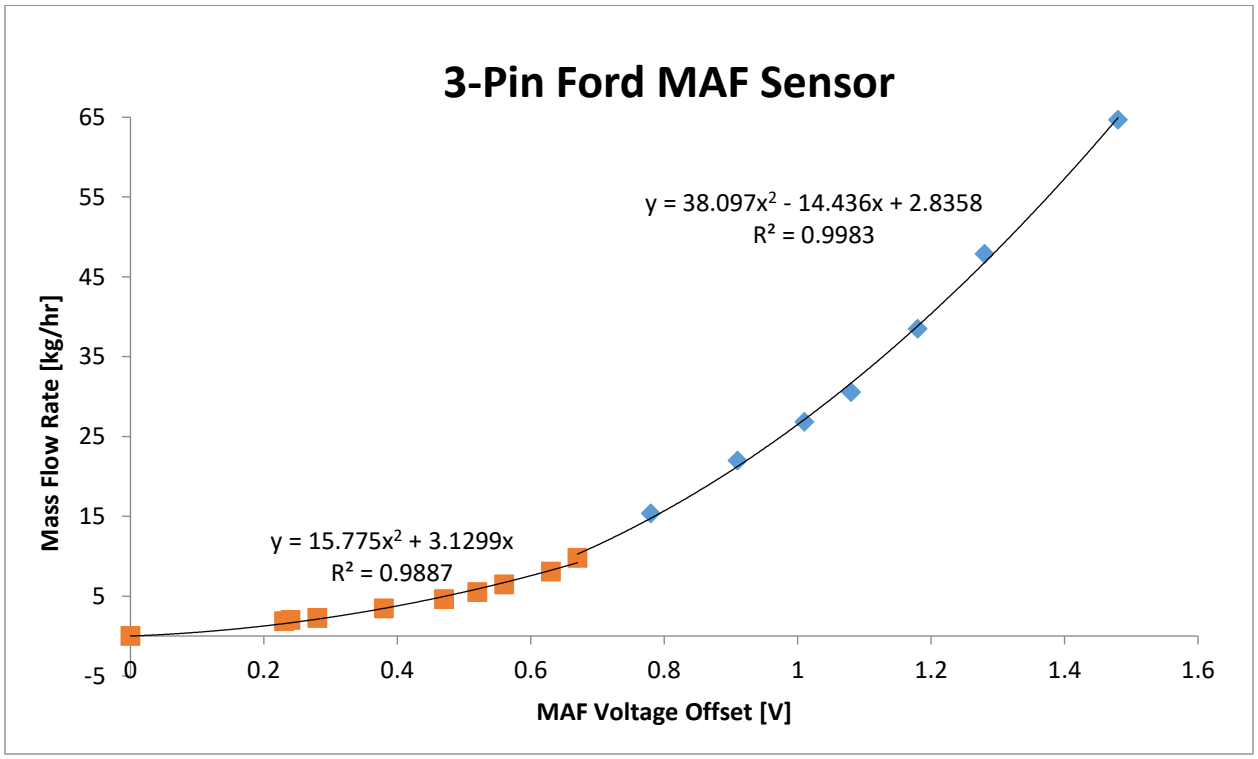

Figure 30: MAF sensor calibration curve for air

Appendix A.3: NO_x analyzer vs NO_x sensor

A secondary objective of this experiment was to compare the performance of the CAI NO_x analyzer to that of an automotive (NI-9755) NO_x sensor. When the CAI NO_x analyzer and NI 9755 NO_x sensor were both subjected to diluted samples of the 953.9 ppm NO calibration gas, the results can be seen in Figure 31.

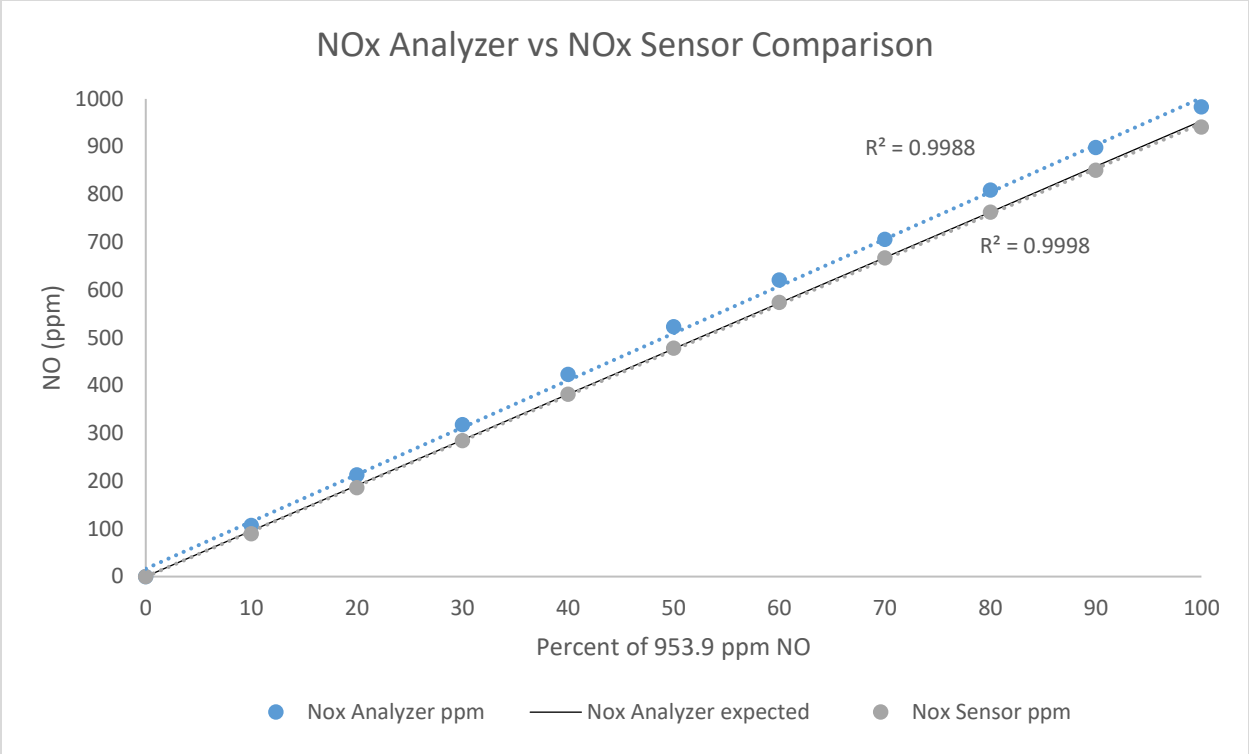

Figure 31: NO_x analyzer and NO_x sensor comparison

In this simple calibration scenario, both the sensor and the analyzer were both nearly perfectly straight lines and followed the expected NO very closely. The NO_x analyzer was overestimating the readings by a small amount, likely due to an offset caused by an incorrect span calibration.

Appendix B: MATLAB 2016 Code

Appendix B.1: Main Function

```
%% Data Import
% Error propagation done following http://ipl.physics.harvard.edu/wp-
uploads/2013/03/PS3_Error_Propagation_sp13.pdf
close all;
clear;
clc;
Date = 'Sep4';    % This will import all data for that day
LGATime = 263;    % Time at which LGA began recording
loops = 10000;    % Maximum number of loops when converging to H2O content
tolerance = 0.00001; % Tolerance of water content calculations
ash = 2.4279;    % kg produced for the whole run
```

```
%% Reading in cRIO text data as a matrix...
c1 = strcat('cRIO\cRIO-',Date,'.txt');
cRIO = dlmread(c1,'\t',1,0);
c3 = size(cRIO);
cRIOPoints = c3(1);

%% Reading in LGA text data as a matrix...
d1 = strcat('LGA\LGA-',Date,'.csv');
LGA = csvread(d1,1,0);
d3 = size(LGA);
LGAPoints = d3(1);

%% Sync Data
cRIOTime=cRIO(1,1); % Time at which cRIO began recording
offset=LGATime-cRIOTime;
% Note: Will always start cRIO first, then LGA

CompleteData(cRIOPoints,37)=0;
for n=1:cRIOPoints
 CompleteData(n,1:29) = cRIO(n,1:29);
end
for n=1:LGAPoints
 CompleteData((n+offset),30:37) = LGA(n,1:8);
end

%% MAF Voltage Correction (an updated calibration equation)
for n=1:cRIOPoints
 Pyr = CompleteData(n,12)-1.406;
 Eng = CompleteData(n,14)-1.407;
 CompleteData(n,13) = 38.097*Pyr^2-14.1436*Pyr+2.8358;
 CompleteData(n,15) = 38.097*Eng^2-14.1436*Eng+2.8358;
 if(Pyr < 0.67)
  CompleteData(n,13) = 15.775*Pyr^2+3.1299*Pyr;
 end
 if(Eng < 0.67)
  CompleteData(n,15) = 15.775*Eng^2+3.1299*Eng;
 end
 if(CompleteData(n,12) == 0)
  CompleteData(n,13) = 0;
  CompleteData(n,15) = 0;
 end
end

%% Plot Emissions
xmin = LGATime; % Minimum time on the plot
xmax = LGATime+LGAPoints; % Maximum time on the plot

% Definitions
length(xmax-xmin) = 0;
CO(xmax-xmin) = 0;
CO2(xmax-xmin) = 0;
O2(xmax-xmin) = 0;
H2(xmax-xmin) = 0;
N2(xmax-xmin) = 0;
CxHy(xmax-xmin) = 0;
LGAPower(xmax-xmin) = 0;

% Create arrays
for n = 1:LGAPoints
```

```
 length(n) = CompleteData(offset+n-1,1);
 CO(n) = CompleteData(offset+n-1,30);
 O2(n) = CompleteData(offset+n-1,33);
 H2(n) = CompleteData(offset+n-1,34);
 CO2(n) = CompleteData(offset+n-1,35);
 N2(n) = CompleteData(offset+n-1,36);
 CxHy(n) = CompleteData(offset+n-1,37);
 LGAPower(n) = CompleteData(offset+n-1,21);
end
figure(2);
yyaxis left
plot(length,CO,'r')
hold on;
plot(length,H2,'g')
plot(length,CO2,'b')
plot(length,CxHy,'m')
ylabel('Concentration [Vol %]')
yyaxis right
plot(length,LGAPower,'k')
ylabel('Power [kW]')
ylim([0, 20])
legend('CO','H2','CO2','CxHy','Power')
xlabel('Time [seconds]')
title('Emissions vs Time')
xlim([xmin, xmax])
hold off;

[gas] = ginput(16);

figure(3);
yyaxis left
plot(length,O2)
hold on;
ylabel('O2 Concentration [%]')
yyaxis right
plot(length,N2)
legend('O2','N2')
xlabel('Time [seconds]')
ylabel('N2 Concentration [%]')
title('Emissions vs Time')
xlim([xmin, xmax])
hold off;

%% Calculate average gas conditions over selected range
%********************** Load 1 **********************
syns = ceil(gas(1) - cRIO(1,1)); % Assuming 1 second per data point, this is
the index that will start
synl = floor(gas(2)) - ceil(gas(1)); % Floor and ceil are used to ensure data
stays within the selected range
exhs = ceil(gas(3) - cRIO(1,1)); % syn indicates syngas, exh indicates exhaust
exhl = floor(gas(4)) - ceil(gas(3));

% Returns average and std of syngas and exhaust for given load
[Syngas(1,:), SyngasStd(1,:)] = LGASample(CompleteData, syns, synl);
[Exhaust(1,:), ExhaustStd(1,:), T1(1), T2(1), T1s(1), T2s(1)] =
LGASample(CompleteData, exhs, exhl);

%********************** Load 2 **********************
syns = ceil(gas(5) - cRIO(1,1));
synl = floor(gas(6)) - ceil(gas(5));
```

```
exhs = ceil(gas(7) - cRIO(1,1));
exhl = floor(gas(8)) - ceil(gas(7));

% Returns average and std of syngas and exhaust for given load
[Syngas(2,:), SyngasStd(2,:)] = LGASample(CompleteData, syns, synl);
[Exhaust(2,:), ExhaustStd(2,:), T1(2), T2(2), T1s(2), T2s(2)] =
LGASample(CompleteData, exhs, exhl);

%********************** Load 3 **********************
syns = ceil(gas(9) - cRIO(1,1));
synl = floor(gas(10)) - ceil(gas(9));
exhs = ceil(gas(11) - cRIO(1,1));
exhl = floor(gas(12)) - ceil(gas(11));

% Returns average and std of syngas and exhaust for given load
[Syngas(3,:), SyngasStd(3,:)] = LGASample(CompleteData, syns, synl);
[Exhaust(3,:), ExhaustStd(3,:), T1(3), T2(3), T1s(3), T2s(3)] =
LGASample(CompleteData, exhs, exhl);

%********************** Load 4 **********************
syns = ceil(gas(13) - cRIO(1,1));
synl = floor(gas(14)) - ceil(gas(13));
exhs = ceil(gas(15) - cRIO(1,1));
exhl = floor(gas(16)) - ceil(gas(15));

% Returns average and std of syngas and exhaust for given load
[Syngas(4,:), SyngasStd(4,:)] = LGASample(CompleteData, syns, synl);
[Exhaust(4,:), ExhaustStd(4,:), T1(4), T2(4), T1s(4), T2s(4)] =
LGASample(CompleteData, exhs, exhl);

%% Plot NOx
xmin = CompleteData(1,1); % Minimum time on the plot
xmax = CompleteData(cRIOPoints,1); % Maximum time on the plot

c(xmax-xmin) = 0;
NO(xmax-xmin) = 0;
NO2(xmax-xmin) = 0;
NOx2(xmax-xmin) = 0;
NOx(xmax-xmin) = 0;
Power(xmax-xmin) = 0;

% Create arrays
for n = 1:cRIOPoints
 c(n) = CompleteData(n,1);
 NO(n) = CompleteData(n,17);
 NO2(n) = CompleteData(n,19);
 NOx2(n) = NO(n)+ NO2(n); % Analyzer NOx measurement
 NOx(n) = CompleteData(n,22); % Sensor NOx measurement
 Power(n) = CompleteData(n,21);
end
figure(4);
yyaxis left
plot(c,NO,'r')
hold on;
plot(c,NO2,'g')
plot(c,NOx,'b')
ylabel('Concentration [ppm]')
ylim([0,1000])
yyaxis right
plot(c,Power,'k')
```

```
legend('NO','NO2','NOx','Power')
xlabel('Time [seconds]')
ylabel('Power [kW]')
title('NOx vs Time')
ylim([0,20])
xlim([xmin, xmax])
hold off;

[NOin] = ginput(8);

%% Calculate average NOx conditions
%********************** Load 1 **********************
s = ceil(NOin(1) - CompleteData(1,1));
l = floor(NOin(2)) - ceil(NOin(1));

% Takes average and std for given range (Analyzer uses NO+NO2)
[Analyzer(1), Sensor(1), AnalyzerStd(1), SensorStd(1)] =
NOxSample(CompleteData, s, l);

%********************** Load 2 **********************
s = ceil(NOin(3) - CompleteData(1,1));
l = floor(NOin(4)) - ceil(NOin(3));

[Analyzer(2), Sensor(2), AnalyzerStd(2), SensorStd(2)] =
NOxSample(CompleteData, s, l);

%********************** Load 3 **********************
s = ceil(NOin(5) - CompleteData(1,1));
l = floor(NOin(6)) - ceil(NOin(5));

[Analyzer(3), Sensor(3), AnalyzerStd(3), SensorStd(3)] =
NOxSample(CompleteData, s, l);

%********************** Load 4 **********************
s = ceil(NOin(7) - CompleteData(1,1));
l = floor(NOin(8)) - ceil(NOin(7));

[Analyzer(4), Sensor(4), AnalyzerStd(4), SensorStd(4)] =
NOxSample(CompleteData, s, l);

%% Water Content and Corrected Flow Rate Calculation (Based on P, T and LGA at
orifice and uses same sample period as Syngas)
OrificeFlow(4) = 0;
CorrectedSyngas(4,8) = 0;
CorrectedExhaust(4,8) = 0;

%********************** Load 1 **********************
% Select range over which to take averages -- this is currently the same range
as
% syngas measurement
s = ceil(gas(1) - CompleteData(1,1));
l = floor(gas(2)) - ceil(gas(1));

% Iteratively calculate water content to get corrected syngas measurements
% based on nitrogen content (assuming 1% of fuel is converted to N2 as
% well)
[CorrectedSyngas(1,:), CorrectedExhaust(1,:), OrificeFlow(1), AvgPow(1),
AvgPyr(1), AvgEng(1), AvgP(1), AvgT(1), Finish(1,1), MW(1,1), MW(2,1),
StdPyr(1), StdEng(1), StdPow(1), StdOrifice(1), CorrectedSyngasStd(1,:),
CorrectedExhaustStd(1,:), StdMW(1,1), StdMW(2,1)] =
```

```
PercentWaterStd(CompleteData, s, l, Syngas(1,:), Exhaust(1,:), tolerance,
loops, SyngasStd(1,:), ExhaustStd(1,:));

%********************** Load 2 **********************
s = ceil(gas(5) - CompleteData(1,1));
l = floor(gas(6)) - ceil(gas(5));

[CorrectedSyngas(2,:), CorrectedExhaust(2,:), OrificeFlow(2), AvgPow(2),
AvgPyr(2), AvgEng(2), AvgP(2), AvgT(2), Finish(1,2), MW(1,2), MW(2,2),
StdPyr(2), StdEng(2), StdPow(2), StdOrifice(2), CorrectedSyngasStd(2,:),
CorrectedExhaustStd(2,:), StdMW(1,2), StdMW(2,2)] =
PercentWaterStd(CompleteData, s, l, Syngas(2,:), Exhaust(2,:), tolerance,
loops, SyngasStd(2,:), ExhaustStd(2,:));

%********************** Load 3 **********************
s = ceil(gas(9) - CompleteData(1,1));
l = floor(gas(10)) - ceil(gas(9));

[CorrectedSyngas(3,:), CorrectedExhaust(3,:), OrificeFlow(3), AvgPow(3),
AvgPyr(3), AvgEng(3), AvgP(3), AvgT(3), Finish(1,3), MW(1,3), MW(2,3),
StdPyr(3), StdEng(3), StdPow(3), StdOrifice(3), CorrectedSyngasStd(3,:),
CorrectedExhaustStd(3,:), StdMW(1,3), StdMW(2,3)] =
PercentWaterStd(CompleteData, s, l, Syngas(3,:), Exhaust(3,:), tolerance,
loops, SyngasStd(3,:), ExhaustStd(3,:));

%********************** Load 4 **********************
s = ceil(gas(13) - CompleteData(1,1));
l = floor(gas(14)) - ceil(gas(13));

[CorrectedSyngas(4,:), CorrectedExhaust(4,:), OrificeFlow(4), AvgPow(4),
AvgPyr(4), AvgEng(4), AvgP(4), AvgT(4), Finish(1,4), MW(1,4), MW(2,4),
StdPyr(4), StdEng(4), StdPow(4), StdOrifice(4), CorrectedSyngasStd(4,:),
CorrectedExhaustStd(4,:), StdMW(1,4), StdMW(2,4)] =
PercentWaterStd(CompleteData, s, l, Syngas(4,:), Exhaust(4,:), tolerance,
loops, SyngasStd(4,:), ExhaustStd(4,:));

[MCcalc, MCcalcStd, MassSyngas, MassExhaust, MassSyngasStd, MassExhaustStd] =
MoistureCalcStd(CorrectedSyngas, AvgPyr, OrificeFlow, AvgEng, Analyzer, Sensor,
CorrectedExhaust, CorrectedSyngasStd, CorrectedExhaustStd, StdOrifice, StdPyr,
AnalyzerStd, SensorStd);

%% Plot Microsoot
xmin = CompleteData(1,1); % CompleteData(1,1); % Minimum time on the plot
xmax = CompleteData(cRIOPoints,1); % CompleteData(cRIOPoints,1); % Maximum time
on the plot

% Create arrays
for n = 1:cRIOPoints
 c(n) = CompleteData(n,1);
 Soot(n) = CompleteData(n,25);
 MSSPower(n) = CompleteData(n,21);
end
figure(6);
yyaxis left
plot(c,Soot,'r')
hold on;
ylabel('Concentration [mg/m3 standard]')
ylim([0,1])
yyaxis right
plot(c,MSSPower,'k')
```

```
legend('Microsoot','Power')
xlabel('Time [seconds]')
ylabel('Power [kW]')
title('Soot vs Time')
ylim([0,20])
xlim([4500, 11000])
hold off;

[MSin] = ginput(8);

%% Calculate average MSS conditions
SootAvg(4) = 0;
SootStd(4) = 0;

%********************** Load 1 **********************
s = ceil(MSin(1) - CompleteData(1,1));
l = floor(MSin(2)) - ceil(MSin(1));

% Takes average and std for given range
[SootAvg(1), SootStd(1)] = MSSample(CompleteData, s, l);

%********************** Load 2 **********************
s = ceil(MSin(3) - CompleteData(1,1));
l = floor(MSin(4)) - ceil(MSin(3));

% Takes average and std for given range
[SootAvg(2), SootStd(2)] = MSSample(CompleteData, s, l);

%********************** Load 3 **********************
s = ceil(MSin(5) - CompleteData(1,1));
l = floor(MSin(6)) - ceil(MSin(5));

% Takes average and std for given range
[SootAvg(3), SootStd(3)] = MSSample(CompleteData, s, l);

%********************** Load 4 **********************
s = ceil(MSin(7) - CompleteData(1,1));
l = floor(MSin(8)) - ceil(MSin(7));

% Takes average and std for given range
[SootAvg(4), SootStd(4)] = MSSample(CompleteData, s, l);

%% Ash Fraction
a = 0;
for n = 1:cRIOPoints
 % For startup period, use the cRIO's estimate for flow rate
 if(CompleteData(n,21)<3 && CompleteData(n,11)>0)
  a = a + CompleteData(n,11)*1/3600;
 end
 % Flowrate from load 1
 if(CompleteData(n,21)>3 && CompleteData(n,21)<4)
  a = a + OrificeFlow(1)*1/3600;
 end
 % Flowrate from load 2
 if(CompleteData(n,21)>4 && CompleteData(n,21)<7.5)
  a = a + OrificeFlow(2)*1/3600;
 end
 % Flowrate from load 3
 if(CompleteData(n,21)>7.5 && CompleteData(n,21)<11.5)
  a = a + OrificeFlow(3)*1/3600;
```

```
 end
 % Flowrate from load 4
 if(CompleteData(n,21)>11.5)
  a = a + OrificeFlow(4)*1/3600;
 end
end

% Total fraction converted to ash -- assumed constant throughout operation
ashfrac = ash/a;

%% Converting Soot to g/kg dry...
% NOx in ppm
for i = 1:4
 Flow = 0.114; % m^3/hr, 1.9 L/min
 Pressure = 101.3; % kPa
 Temperature = 273.15; % Kelvin
 R = 8.314/MW(2,i); % kg/(kJ*K)
 rho = Pressure/(R*Temperature); % kg/m^3
 pholder = SootAvg(i)/rho; % mg soot/kg flow
 woodgas(i) = OrificeFlow(i)-AvgPyr(i);
 woodgasStd(i) = (StdOrifice(i)^2+StdPyr(i)^2)^(1/2);
 total = OrificeFlow(i)+AvgEng(i);
 Soot(i) = pholder*total/Flow*woodgas(i)/total*(1+ashfrac); % mg/kg wet biomass
 DrySoot(i) = Soot(i)/(1-MCcalc(i)); % dry soot mg/kg dry biomass
end

%% kg Emission/kg Fuel (wet and dry)
% Note: Analyzer is now gas 9 and Sensor is now gas 10
for i = 1:4
 % Flows (kg/hr)
 Woodgas = OrificeFlow(i)-AvgPyr(i);
 WoodgasStd = (StdOrifice(i)^2+StdPyr(i)^2)^(1/2);
 Total = AvgEng(i)+OrificeFlow(i);
 TotalStd = (StdEng(i)^2+StdOrifice(i)^2)^(1/2);
 for j = 1:10
  % mass fraction times total flow divided by woodgas flow (wet)
  WetSyngas(i,j) = MassSyngas(i,j)*Total/(Woodgas*(1+ashfrac));
  WetExhaust(i,j) = MassExhaust(i,j)*Total/(Woodgas*(1+ashfrac));
  WetSyngasStd(i,j) =
1/(1+ashfrac)*((MassSyngasStd(i,j)*Total/Woodgas)^2+(MassSyngas(i,j)*TotalStd/W
oodgas)^2+(MassSyngas(i,j)*Total/Woodgas^2*WoodgasStd)^2)^(1/2);
  WetExhaustStd(i,j) =
1/(1+ashfrac)*((MassExhaustStd(i,j)*Total/Woodgas)^2+(MassExhaust(i,j)*TotalStd
/Woodgas)^2+(MassExhaust(i,j)*Total/Woodgas^2*WoodgasStd)^2)^(1/2);

  % mass fraction times total flow divided by woodgas flow (dry corrected)
  DrySyngas(i,j) = WetSyngas(i,j)/(1-MCcalc(i));
  DryExhaust(i,j) = WetExhaust(i,j)/(1-MCcalc(i));
  DrySyngasStd(i,j) = ((WetSyngasStd(i,j)/(1-MCcalc(i)))^2+(WetSyngas(i,j)/(1-
MCcalc(i))^2*MCcalcStd(i))^2)^(1/2);
  DryExhaustStd(i,j) = ((WetExhaustStd(i,j)/(1-
MCcalc(i)))^2+(WetExhaust(i,j)/(1-MCcalc(i))^2*MCcalcStd(i))^2)^(1/2);
 end
end

%% kg/kWh Emissions
for i = 1:4
 % Flows (kg/hr)
 Total = AvgEng(i)+OrificeFlow(i);
 TotalStd = ((StdEng(i))^2+(StdOrifice(i))^2)^(1/2);
```

```
 for j = 1:10
  if(j ~= 3)
   % Mass fraction times Total Flow in kg/hr divided by Power in kW
   kWhSyngas(i,j) = MassSyngas(i,j)*Total/AvgPow(i);
   kWhExhaust(i,j) = MassExhaust(i,j)*Total/AvgPow(i);
   kWhSyngasStd(i,j) =
((MassSyngasStd(i,j)*Total/AvgPow(i))^2+(MassSyngas(i,j)*TotalStd/AvgPow(i))^2+
(MassSyngas(i,j)*Total*StdPow(i)/AvgPow(i)^2)^2)^(1/2);
   kWhExhaustStd(i,j) =
((MassExhaustStd(i,j)*Total/AvgPow(i))^2+(MassExhaust(i,j)*TotalStd/AvgPow(i))^
2+(MassExhaust(i,j)*Total*StdPow(i)/AvgPow(i)^2)^2)^(1/2);
  end
 end
end

%% Thermal Efficiency
[Eff, EffStd, HHV, HHVStd] = EfficiencyStd(AvgPow, MassSyngas, OrificeFlow,
AvgPyr, StdPow, StdPyr, StdOrifice, MassSyngasStd);
```

Appendix B.2: Water Content Correction (PercentWaterStd.m)

```
function [CorrectedSyngas, CorrectedExhaust, OrificeFlow, AvgPow, AvgPyr,
AvgEng, AvgP, AvgT, Finish, MW, MW2, StdPyr, StdEng, StdPow, StdOrifice,
CorrectedSyngasStd, CorrectedExhaustStd, StdMW, StdMW2] =
PercentWaterStd(CompleteData, s, l, Syngas, Exhaust, tolerance, loops,
SyngasStd, ExhaustStd)

count = 1;
a = 1;
Finish = 0;

for n = s:s+l-1
 T(a) = CompleteData(n,24)+273.15;     % Orifice Temp in K
 if(CompleteData(n,5)<-500)       % To ensure arduino is currently measuring
(it sometimes glitches on the arduino's end)
  P(count) = 101.3+(CompleteData(n,5)-34)/1000; % Pressure at top of filter in
kPa assuming 101.3 kPa atm
  count=count+1;
 end
 DP(a) = CompleteData(n,10);       % Orifice dP in " H2O
 Pyr(a) = CompleteData(n,13);      % Pyrolysis Air in kg/hr
 Eng(a) = CompleteData(n,15);      % Engine Air in kg/hr
 Pow(a) = CompleteData(n,21);      % Power in kW
 a = a+1;
end

% Takes mean and std
AvgT = mean(T);
AvgP = mean(P);
AvgDP = mean(DP);
AvgPyr = mean(Pyr);
AvgEng = mean(Eng);
AvgPow = mean(Pow);
StdT = std(T);
StdP = std(P);
StdDP = std(DP);
StdPyr = std(Pyr);
StdEng = std(Eng);
```

```
StdPow = std(Pow);

% Calculate MW, R, and Corrected orifice flow. NOTE: H2O LGA readings left out
on purpose
total = Syngas(1)+Syngas(3)+Syngas(4)+Syngas(5)+Syngas(6)+Syngas(7)+Syngas(8);
% Scaling factor
mtot =
Syngas(1)*28+Syngas(3)*46+Syngas(4)*32+Syngas(5)*2.016+Syngas(6)*44+Syngas(7)*2
8+Syngas(8)*16;
massfracN2 = Syngas(7)*28/mtot;
MWLGA = mtot/total;
R = 8.314/MWLGA;
rho = AvgP/(R*AvgT);
OrificeFlow = 28.675*(rho*AvgDP)^(1/2)-0.3869;    % Density and dP dependant
calibration curve for orifice

% Standard deviation calculations
Stdtotal =
(SyngasStd(1)^2+SyngasStd(3)^2+SyngasStd(4)^2+SyngasStd(5)^2+SyngasStd(6)^2+Syn
gasStd(7)^2+SyngasStd(8)^2)^(1/2);
Stdmtot =
((28*SyngasStd(1))^2+(46*SyngasStd(3))^2+(32*SyngasStd(4))^2+(2.016*SyngasStd(5
))^2+(44*SyngasStd(6))^2+(28*SyngasStd(7))^2+(16*SyngasStd(8))^2)^(1/2);
StdmassfracN2 =
((28/mtot*SyngasStd(7))^2+(28*Syngas(7)/mtot^2*Stdmtot)^2)^(1/2);
StdMWLGA = ((Stdmtot/total)^2+(mtot/total^2*Stdtotal)^2)^(1/2);
StdR = 8.314*StdMWLGA/MWLGA;
StdOrifice = 0;
StdLGAPercent = 0;

% My apologies in advance...
LGAPercent = 0.75; % starting estimate
MWH2O = 18.02;
for n=1:loops
 % Calculations
 massN2 = 0.755*AvgPyr+0.005*(OrificeFlow-AvgPyr);  % 75.5 wt% in air and 0.5
wt% in feedstock
 StdmassN2 = ((0.75*StdPyr)^2+(0.005*StdOrifice)^2)^(1/2);
 massN2LGA = OrificeFlow*LGAPercent*massfracN2;   % Mass of N2 based on LGA
with LGAPercent weighting
 LGAPercent = massN2/(OrificeFlow*massfracN2);   % Calculate 'new' LGAPercent
 StdLGAPercent =
((StdmassN2/(OrificeFlow*massfracN2))^2+(massN2/(OrificeFlow^2*massfracN2)*StdO
rifice)^2+(massN2/(OrificeFlow*massfracN2^2)*StdmassfracN2)^2)^(1/2);
 massfracH2O = 1-LGAPercent;
 StdmassH2O = StdLGAPercent;
 molefracH2O = massfracH2O/MWH2O/(massfracH2O/MWH2O+LGAPercent/MWLGA);
 StdmoleH2O =
((MWH2O*LGAPercent*MWLGA*StdmassH2O/(massfracH2O*MWLGA+MWH2O*LGAPercent)^2)^2+(
MWH2O*massfracH2O*MWLGA*StdLGAPercent/(massfracH2O*MWLGA+MWH2O*LGAPercent)^2)^2
+(MWH2O*massfracH2O*LGAPercent*StdMWLGA/(massfracH2O*MWLGA+MWH2O*LGAPercent)^2)
^2)^(1/2);
 MW = (1-molefracH2O)*MWLGA+molefracH2O*MWH2O;   % Calculate new MW with new
water content
 StdMW = (((-MWLGA+MWH2O)*StdmoleH2O)^2+((1-molefracH2O)*StdMWLGA)^2)^(1/2);
 R = 8.314/MW;           % Calculates new gas constant
 StdR = 8.314*StdMW/MW^2;
 rho = AvgP/(R*AvgT);         % Calculates new density
 StdRho =
((StdP/(R*AvgT))^2+(AvgP*StdR/(R^2*AvgT))^2+(AvgP*StdT/(R*AvgT^2))^2)^(1/2);
```

```
 OrificeFlow = 28.675*(rho*AvgDP)^(1/2)-0.3869;    % Recalculates orifice flow
for next iteration
 StdOrifice =
((14.3375*AvgDP*StdRho/(rho*AvgDP)^(1/2))^2+(14.3375*rho*StdDP/(rho*AvgDP)^(1/2
))^2)^(1/2);

 if(abs(massN2LGA-massN2) < tolerance)      % Checks if within tolerance
  Finish = n;
  break
 end
end
for i=1:8
 CorrectedSyngas(i) = Syngas(i)*LGAPercent;
 CorrectedSyngasStd(i) =
((SyngasStd(i)*LGAPercent)^2+(StdLGAPercent*Syngas(i))^2)^(1/2);
 if(i==2)
  CorrectedSyngas(i) = molefracH2O*100;
  CorrectedSyngasStd(i) = 100*StdmoleH2O;
 end
end

% Use similar mass balances of N2 and Ar
massN2 = 0.755*AvgPyr+0.005*(OrificeFlow-AvgPyr)+0.755*AvgEng;

% Calculate MW at Exhaust
total =
Exhaust(1)+Exhaust(3)+Exhaust(4)+Exhaust(5)+Exhaust(6)+Exhaust(7)+Exhaust(8); %
Scaling factor
mtot =
Exhaust(1)*28+Exhaust(3)*46+Exhaust(4)*32+Exhaust(5)*2.016+Exhaust(6)*44+Exhaus
t(7)*28+Exhaust(8)*16;
massfracN2 = Exhaust(7)*28/mtot;
MWLGA = mtot/total;

% Exhaust doesn't need to be iterative because all flows are known
LGAPercent = massN2/((OrificeFlow+AvgEng)*massfracN2);
massfracH2O = 1-LGAPercent;
molefracH2O = massfracH2O/MWH2O/(massfracH2O/MWH2O+LGAPercent/MWLGA);
MW2 = (1-molefracH2O)*MWLGA+molefracH2O*MWH2O;

% Standard deviations
StdmassN2 = ((0.75*StdPyr)^2+(0.005*StdOrifice)^2+(0.755*StdEng)^2)^(1/2);
Stdtotal =
(ExhaustStd(1)^2+ExhaustStd(3)^2+ExhaustStd(4)^2+ExhaustStd(5)^2+ExhaustStd(6)^
2+ExhaustStd(7)^2+ExhaustStd(8)^2)^(1/2);
Stdmtot =
((28*ExhaustStd(1))^2+(46*ExhaustStd(3))^2+(32*ExhaustStd(4))^2+(2.016*ExhaustS
td(5))^2+(44*ExhaustStd(6))^2+(28*ExhaustStd(7))^2+(16*ExhaustStd(8))^2)^(1/2);
StdmassfracN2 =
((28/mtot*ExhaustStd(7))^2+(28*Exhaust(7)/mtot^2*Stdmtot)^2)^(1/2);
StdMWLGA = ((Stdmtot/total)^2+(mtot/total^2*Stdtotal)^2)^(1/2);
StdLGAPercent =
((StdmassN2/((OrificeFlow+AvgEng)*massfracN2))^2+(StdOrifice*massN2/((OrificeFl
ow+AvgEng)^2*massfracN2))^2+(StdEng*massN2/((OrificeFlow+AvgEng)^2*massfracN2))
^2+(StdmassfracN2*massN2/((OrificeFlow+AvgEng)*massfracN2^2))^2)^(1/2);
StdmassH2O = StdLGAPercent;
StdmoleH2O =
((MWH2O*LGAPercent*MWLGA*StdmassH2O/(massfracH2O*MWLGA+MWH2O*LGAPercent)^2)^2+(
MWH2O*massfracH2O*MWLGA*StdLGAPercent/(massfracH2O*MWLGA+MWH2O*LGAPercent)^2)^2
```

```
+(MWH2O*massfracH2O*LGAPercent*StdMWLGA/(massfracH2O*MWLGA+MWH2O*LGAPercent)^2)
^2)^(1/2);
StdMW2 = (((-MWLGA+MWH2O)*StdmoleH2O)^2+((1-molefracH2O)*StdMWLGA)^2)^(1/2);

for i=1:8
 CorrectedExhaust(i) = Exhaust(i)*LGAPercent;
 CorrectedExhaustStd(i) =
((ExhaustStd(i)*LGAPercent)^2+(StdLGAPercent*Exhaust(i))^2)^(1/2);
 if(i==2)
  CorrectedExhaust(i) = molefracH2O*100;
  CorrectedExhaustStd(i) = 100*StdmoleH2O;
 end
end
```

Appendix B.3: Moisture Content Calculation (MoistureCalcStd.m)

```
function [MC, MCStd, SynMass, ExhMass, SynMassStd, ExhMassStd] =
MoistureCalcStd(Syngas, Pyrolysis, OrificeFlow, Engine, Ana, Sen, Exhaust,
SyngasStd, ExhaustStd, OrificeStd, PyrStd, AnaStd, SenStd)

[SynMass, ExhMass, SynMassStd, ExhMassStd] =
MoletoMassFrac(Syngas,Ana,Sen,Exhaust,SyngasStd,ExhaustStd,AnaStd,SenStd);

for i = 1:4
 H(i) =
(SynMass(i,2)*2.016/18.02+SynMass(i,5)+SynMass(i,8)*4.032/16)*OrificeFlow(i);
 HStd(i) =
((2.016/18.02*OrificeFlow(i)*SynMassStd(i,2))^2+((SynMass(i,2)*2.016/18.02+SynM
ass(i,5)+SynMass(i,8)*4.032/16)*OrificeStd(i))^2+(OrificeFlow(i)*SynMassStd(i,5
))^2+(4.032/16*OrificeFlow(i)*SynMassStd(i,8))^2)^(1/2);
 MC(i) = (H(i)-0.06*(OrificeFlow(i)-Pyrolysis(i)))*18.02/2.016/(OrificeFlow(i)-
Pyrolysis(i));
 MCStd(i) = 18.02/2.016*((1/(OrificeFlow(i)-
Pyrolysis(i))*HStd(i))^2+(H(i)/(OrificeFlow(i)-
Pyrolysis(i))^2*OrificeStd(i))^2+(H(i)/(OrificeFlow(i)-
Pyrolysis(i))^2*PyrStd(i))^2)^(1/2);
end
```

Appendix B.4: Mole Fraction to Mass Fraction Conversion (MoletoMassStd.m)

```
function [CorrectedSyngas, CorrectedExhaust, CorrectedSyngasStd,
CorrectedExhaustStd] = MoletoMass(Syngas, Ana, Sen, Exhaust, SyngasStd,
ExhaustStd)

% Molecular weights
MW = [28 16 46 32 2.008 44 28 16 30 30];

% Total mass at each load
for i = 1:4
 for j = 1:10
  if(j ~= 3)
   Synmass(i) = Synmass(i)+Syngas(i)*MW(j);
   Exhmass(i) = Exhmass(i)+Exhaust(i)*MW(j);
  end
 end
end

% Mass weighting
```

```
for i = 1:4
 for j = 1:8
  CorrectedSyngas(i,j) = Syngas(i,j)*MW(j)/Synmass(i);
  CorrectedExhaust(i,j) = Exhaust(i,j)*MW(j)/Exhmass(i);
 end
 CorrectedSyngas(i,9) = 0;
 CorrectedSyngas(i,10) = 0;
 CorrectedExhaust(i,9) = Ana(i)/1000000*100*MW(9)/Exhmass;
 CorrectedExhaust(i,10) = Sen(i)/1000000*100*MW(10)/Exhmass;
end
for i = 1:4
 for j = 1:10
  CorrectedSyngasStd(i,j) = SyngasStd(i,j)/Syngas(i,j)*CorrectedSyngas(i,j);
  CorrectedExhaustStd(i,j) =
ExhaustStd(i,j)/Exhaust(i,j)*CorrectedExhaust(i,j);
 end
end
```

Appendix B.5: LGA Sample Averages (LGASample.m)

```
function [Avg, Std, T1, T2, T1s, T2s] = LGASample(CompleteData, st, l)

% array definitions
temp(8,l) = 0;
Avg(1,8) = 0;
Std(1,8) = 0;

% read in all values in the given range (syns to synl)
for i = 1:8
 a = 1;
 for j = st:st+l-1
  temp(i,a) = CompleteData(j,29+i);
  if(CompleteData(j,2)>50)
   Trst(a) = CompleteData(j,2);
  end
  if(CompleteData(j,3)>50)
   Tred(a) = CompleteData(j,3);
  end
  a = a+1;
 end
end

% take mean and standard deviations
m = mean(temp,2);
s = std(temp,0,2);

T1 = mean(Trst);
T1s = std(Trst);
T2 = mean(Tred);
T2s = std(Tred);

% output mean and standard deviations
for i = 1:8
 Avg(i) = m(i);
 Std(i) = s(i);
end
```

Appendix B.6: NOx Averages (NOxSample.m)

```
function [Avg1, Avg2, Std1, Std2] = NOxSample(CompleteData, st, l)

% Definitions
temp1(l) = 0;
temp2(l) = 0;

% read in all values in the given range (syns to synl)
a = 1;
for j = st:st+l-1
 temp1(a) = CompleteData(j,17)+CompleteData(j,19); % Analyzer NO+NO2
 temp2(a) = CompleteData(j,22); % NOx Sensor
 a = a+1;
end

% take mean and standard deviations
Avg1 = mean(temp1);
Std1 = std(temp1);
Avg2 = mean(temp2);
Std2 = std(temp2);
```

Appendix B.7: Microsoot Sample Averages (MSSample.m)

```
function [Avg1, Std1] = MSSample(CompleteData, s, l)

% read in all values in the given range (syns to synl)
a = 1;
for j = s:s+l-1
 temp1(a) = CompleteData(j,25);
 a = a+1;
end

% take mean and standard deviations
Avg1 = mean(temp1);
Std1 = std(temp1);
```

Appendix B.8: Efficiency Calculation (EfficiencyStd.m)

```
function [Eff, EffStd, HHV, HHVStd] = Efficiency(Power, Syngas, OrificeFlow,
Pyr, PowStd, PyrStd, OrificeStd, SyngasStd)

for i = 1:4
 H2HHV = 141.88;
 H2LHV = 119.96;
 COHHV = 10.16;
 COLHV = 10.16;
 CH4HHV = 55.6;
 CH4LHV = 50;
 Biomass = 20; % Preliminary estimate in MJ/kg
(http://hydrogen.pnl.gov/tools/lower-and-higher-heating-values-fuels)

 total = 0;
 for j = 1:8
  total = Syngas(i,j)+total;
 end
```

```
 HHV(i) = Syngas(i,1)*COHHV+Syngas(i,5)*H2HHV+Syngas(i,8)*CH4HHV;
 HHVStd(i) =
((COHHV*SyngasStd(i,1))^2+(H2HHV*SyngasStd(i,5))^2+(CH4HHV*SyngasStd(i,8))^2)^(
1/2);
 Eff(i) = 3600*Power(i)/(1000*Biomass*(OrificeFlow(i)-Pyr(i)));
 EffStd(i) = 3.6/Biomass*((PowStd(i)/(OrificeFlow(i)-
Pyr(i)))^2+(Power(i)*OrificeStd(i)/(OrificeFlow(i)-
Pyr(i))^2)^2+(Power(i)*PyrStd(i)/(OrificeFlow(i)-Pyr(i))^2)^2)^(1/2);
end
```